UNIVERSITÀ
DEGLI STUDI
FIRENZE

DOTTORATO DI RICERCA
INTERNATIONAL DOCTORATE IN STRUCTURAL BIOLOGY

CICLO XXXVIII

COORDINATOR Prof. Roberta Pierattelli

Advanced structural and morphological characterization by NMR technologies of different biomolecules and biotechnological systems

Settore Scientifico Disciplinare CHEM-03/A

PhD student
Francesco Currò

Supervisor
Prof. Marco Fragai

Co-Supervisors
Dr. Daniela Stranges, Dr. Silvia Martini

Coordinator
Prof. Roberta Pierattelli

November 2022 – October 2025

This thesis has been approved by the University of Florence, the University of Frankfurt and the Utrecht University

Universiteit Utrecht

Abstract

This research work focuses on the advanced characterization of pharmaceutical systems which are used as delivery platforms for nucleic acids and proteins, using advanced Nuclear Magnetic Resonance (NMR) techniques. The delivery systems studied in this doctoral work are liposomes, Lipid Nanoparticles (LNPs) and Red Blood Cells (RBC). There is indeed an urgent need to enhance understanding of structural attributes that can be linked to functional variations, thereby guiding rational formulation design. Comprehensive characterization to increase product understanding of these systems is challenging due to their complexity (size, composition, dynamics). Additionally, the stability of these systems is often a concern, requiring thorough analytical investigations overtime and across different batches to ensure quality and consistency.

NMR presents distinct advantages for investigating delivery systems by integrating several unique capabilities. It provides atomic resolution that enables a detailed examination of individual components, within a complex architecture. It's a non-destructive technique allowing for the analysis of the encapsulated cargo in intact complexes. There is a wide set of experiments to gain insights into dynamics of systems, correlating structural attributes with activity. Furthermore, NMR allows to monitor stability over time under various storage and stress conditions, enabling the elucidation of degradation pathways. These comprehensive features make NMR an invaluable tool for advancing the design and optimization of delivery systems in pharmaceutical applications, ensuring their efficacy and reliability.

The first study of this doctoral work was focused on lipid quantification in liposomes. To optimize formulation and support large-scale production, precise and rapid analytical methods are necessary to monitor lipid content during formulation and follow degradation processes overtime. Two NMR methods were refined and applied for this scope: a conventional method employing an internal standard and the PULCON NMR method, in which the reference is external for streamlined reproducibility and accelerated processing, particularly beneficial for industrial-scale applications. Through comparison to Ultra-Performance Liquid Chromatography coupled with Evaporative Light Scattering Detection (UPLC-ELSD), this study demonstrates NMR as a viable and efficient alternative for lipid quantification, with rapid data acquisition and the need of only one reference standard.

Furthermore, we worked on the characterization of proteins encapsulated in Red Blood Cells, which are gaining interest as smart delivery systems, ensuring biocompatibility and long drug circulation. The research provided, utilizing NMR techniques, an in-depth structural analysis of the higher-order structure (HOS) of proteins encapsulated within erythrocytes, which is essential for maintaining

biological function and therapeutic effectiveness. A semi-quantitative analysis of the encapsulated enzymes was also performed using NMR, providing a tool for fast quantification which could guide optimization of the encapsulation protocol, applicable also to other cargos.
Finally, lipid nanoparticles (LNPs) were investigated, particularly focusing following the PEG shedding phenomenon using Pulsed Gradient Spin Echo (PGSE) NMR. PEG shedding rate affects the biodistribution of LNPs and should be considered carefully when designing the formulations for each specific application. Moreover, concern regarding the stability of PEG before injection is growing, making it necessary to develop a method as quality control and to guide a rational design of particles. For this purpose, the analysis assessed the release of PEG under different storage and stress conditions. In addition, a prediction of PEG shedding rate in vivo was performed by adding Bovine Serum Albumin (BSA) to the LNP solutions, highlighting variability among different formulations that should be considered in the design of particles.

Overall, this thesis contributes to the advancement of drug delivery system characterization by refining analytical methodologies to enhance quality controls of batches and to deepen our understanding of formulations. These findings will be instrumental for the rational design of delivery systems, ultimately improving their effectiveness.

This PhD project originates from a collaboration between GSK (Siena, IT) and the Magnetic Resonance Center (CERM) of the University of Florence (Florence, IT).

Table of Contents

1 Introduction

1.1 Delivery systems

1.1.1 Introduction to delivery systems

Although the active ingredient, whether a drug or an antigen in the case of vaccines, serves as the agent of therapeutic or prophylactic action in pharmaceuticals, effective delivery systems are essential to broaden their applications and capabilities[1,2]. Pharmacologically active molecules need to be administered within the human body, encountering numerous obstacles, primarily ensuring that the molecule reaches its intended site of action. In the case of biologics such as proteins and nucleic acids, active component(s) may quickly degrade due to environmental conditions like pH, temperature, and enzymatic activity. The proteases and nucleases that populate the gastrointestinal tract and bloodstream, would eliminate any unprotected biologics passing through[1,3].

Secondly, these molecules must be distributed and targeted precisely towards their intended site of action. Depending on the application, various cells, tissues, and organs represent the targets, each presenting distinct challenges and requiring specific properties of the carriers. After directing the drug to the target site, another crucial aspect is the duration of action. Conventional systems struggle to maintain drug concentrations within the therapeutic window over extended periods. This aspect requires frequent dosing, which can decrease patient compliance and increase the risk of side effects. Sustained release systems are employed to provide gradual, prolonged drug release, yet the duration of action should not exceed the necessary timeframe for the desired therapeutic effect, as this might lead to adverse outcomes[4,5].

Effective modulation and control of active ingredient action are fundamental to ensuring an optimal safety profile, avoiding fluctuations in plasma drug levels and unwanted targeting of non-specific sites. It's crucial to manage the biodistribution at precise rates and targeted locations, enhancing efficacy and safety. Additionally, the carrier must meet essential biocompatibility requirements to ensure safety and minimize adverse immune responses[6,7]. The selection of materials often plays a decisive role, as they must be biocompatible, biodegradable, and capable of responding to physical and chemical stimuli to modulate drug release. Innovations such as stimuli-responsive materials offer promising avenues for “smart” delivery systems that can react to environmental changes such as pH, temperature, or specific biological signals, enabling precise control over drug release[8–10].

Characterizing drug and vaccine delivery systems from a structural perspective is essential for optimizing their efficacy and safety, as the complex architecture of these systems directly impacts their performance in biological environments[11,12]. A detailed understanding of the structural components and interactions within these systems could guide the rational design of formulations to improve encapsulation efficiency, targeted delivery and cargo release. It is equally important to develop new analytical methods that accurately assess the quality attributes of these delivery systems, to ensure their consistency and reliability, particularly regarding stability under various conditions[11]. In conclusion, challenges arise from the complexity of these systems, which consist of an active biomolecule encapsulated within a multi-molecular envelope. Additionally, many delivery platforms are novel, lacking established protocols for structural characterization and quality assessment. This complexity necessitates innovative approaches and advanced technologies capable of capturing the properties of these delivery systems. As stability is a crucial concern, continuous efforts are required to develop reliable methods that can anticipate and measure potential degradation or loss of functionality. Overcoming these difficulties is pivotal in advancing the development and application of effective drug and vaccine delivery solutions[13–16].

1.1.2 Liposomes

Liposomes are a versatile and highly adaptable platform for drug delivery, offering opportunities to enhance therapeutic efficacy across a wide range of medical applications[17–20]. Initially discovered in the 1960s by Alec D. Bangham, liposomes have since evolved into a crucial tool in nanomedicine, largely due to their biocompatibility and ability to encapsulate both hydrophilic and hydrophobic drugs[21]. Liposomes are spherical vesicles characterized by one or more phospholipid bilayers that enclose an aqueous interior[22]. This unique amphiphilic nature allows them to mimic biological membranes, offering a model for cellular interaction and enabling the delivery of therapeutic agents directly to target cells[23].

Based on size and membrane lamellarity, liposomes can be classified into several categories: small unilamellar vesicles (SUVs), large unilamellar vesicles (LUVs), and multilamellar vesicles (MLVs). SUVs typically range from 20-100 nm in diameter, LUVs from 100 nm to 1 μm, and MLVs have multiple bilayers exceeding these dimensions. SUVs, due to their uniform drug encapsulation and extended circulation time, are most frequently utilized in drug delivery applications[17,24].

The composition of liposomal membranes is integral to their functionality and effectiveness as drug delivery vehicles. Natural and synthetic lipids, along with surfactants, are chosen based on desired therapeutic outcomes. The primary components are the phospholipids, which are natural constituents

of cellular membranes, contributing to their inherently biocompatible and biodegradable properties. Incorporating cholesterol enhances membrane rigidity and reduces leakiness, improving drug retention and prolonging circulation time. Polysaccharides and synthetic lipids offer avenues for specialized functionality, such as targeted delivery and stimuli responsiveness. Chitosan or PEGylation can modify liposomes to evade immune recognition, thus extending their half-life in systemic circulation[25]. Surfactants like sodium cholate can act as edge activators, increasing liposome deformability, enhancing skin penetration, or even enabling transdermal delivery[26].

Unique structural properties of liposomes make them ideal for various therapeutic applications, including cancer treatment, gene delivery, and vaccine administration[27]. They can encapsulate nucleic acids, proteins, and conventional drugs, offering improved delivery with reduced systemic toxicity. In cancer therapeutics, liposomes improve drug solubility and facilitate controlled distribution to tumor sites, taking advantage of the enhanced permeability and retention (EPR) effects in malignancies[28]. Notably, they are employed in anti-cancer treatments, with well-known examples for doxorubicin delivery, such as Myocet or Doxil which increased circulation time and reduced cardiotoxicity through pegylation of liposomes. Both are used for treating various types of cancer, including metastatic breast cancer[29–31]. In the realm of antifungal treatments, liposomal formulations are used for amphotericin B, with notable examples being Nomex® Liposome and AmBisome®[32–34]. Additionally, liposome application extends beyond pharmaceuticals to the field of vaccines. For example, the adjuvant AS01 is formulated with a lipid scaffold composed of DOPC and cholesterol, in conjunction with two immunostimulants: 3-O-desacyl-4'-monophosphoryl lipid A (MPL) and the saponin QS-21. This formulation is employed to enhance immune responses in vaccines for malaria and shingles[35–37].

Stimuli-responsive liposomes further advance therapy by enabling site-specific release triggered by pH changes, temperature variations, or enzymatic activity, making them a promising approach for biochemical and physicochemical targeted delivery. pH-sensitive liposomes, for instance, can destabilize in acidic environments found in tumors, releasing drugs directly at the site, while temperature-sensitive variants allow for controlled release upon external heating[38]. The field continues to explore enhancements in liposome technology, aiming to overcome challenges such as drug loading capacity, stability under biological conditions, and precise control over release dynamics. Future directions in liposome research focus on the integration of smart materials and advanced biomaterials, fostering innovation in personalized medicine[39]. Efforts are underway to utilize computational modeling for optimizing liposome composition and structure to predict *in vivo* interactions, thereby improving efficacy and patient outcomes[40].

In summary, liposomes present a robust and versatile platform for drug delivery, with continuous advancements promising to expand their utility across therapeutic areas. Their biocompatibility, capacity for targeted delivery and ability to address biologic degradation make them indispensable tools in modern medicine, paving the way for future breakthroughs in treatments.

1.1.3 Lipid Nanoparticles

Lipid nanoparticles (LNPs) are multilayer cores dispersed between lipid layers, with the insertion of a positively charged lipid to interact with the negatively charged nucleic acid cargo. LNPs offer high performance in terms of bioavailability, therapeutic efficacy, target-specificity, safety, and stability[1,2]. Initially developed for the delivery of small molecules, LNPs have become the main delivery system for nucleic acids. ONPATTRO (Patisiran) was the first approved LNP to deliver double-stranded small interfering RNA (siRNA) for treating polyneuropathies caused by transthyretin-mediated hereditary amyloidosis (hATTR)[41]. Their popularity grew when LNPs were successfully used to deliver mRNA-based vaccines against SARS-CoV-2, in particular Moderna's mRNA-1273 and Pfizer/BioNTech's BNT162b2[42,43].

Unlike liposomes, LNP composition includes a cationic or ionizable lipid, which interacts electrostatically with negatively charged nucleic acids to allow encapsulation. The shift from a cationic to an ionizable lipid, which become charged only under certain pH conditions, was a major advancement that addressed significant toxicity concerns associated with cationic lipids. These lipids acquire a positive charge within the acidic environment of endosomes, facilitating the release of the payload into the cytoplasm of target cells[44]. Other components of LNPs include phospholipids (such as DSPC, DOPC, DPPC…), which are essential structural elements that form the bilayer architecture of LNPs, stabilize the structure, and assist in fusing nanoparticles with cellular membranes to enhance payload delivery. Cholesterol is added to LNPs to improve structural integrity and fluidity, and it plays a crucial role in modulating interactions with membranes, essential for the entry and release of LNPs within cells[45]. Finally, PEG-lipids are used to enhance particle colloidal stability and prevent aggregation, ensuring therapeutic efficacy and regulating the circulation of LNPs in the bloodstream. PEG is known for its ability to reduce opsonization and the rapid elimination of nanoparticles by the immune system. The PEG coating creates a steric barrier that diminishes the adhesion of plasma proteins and immune cells to the surface of nanoparticles, the so-called "stealth effect". By doing so, it increases the circulation time of nanoparticles within the vascular system, enhancing the likelihood of reaching the target site before being sequestered by the mononuclear phagocyte system. This

property is particularly advantageous in treating complex diseases like solid tumors, where achieving sufficient therapeutic concentrations at the tumor site is crucial, or for targeting the brain which requires extended blood half-life to permeate the blood-brain barrier[46]. However, excessive PEG can hamper the efficacy of release, as it restricts the fusion of nanoparticles with cellular membranes, which is essential for releasing the therapeutic payload into the cytoplasm[47].

1.1.3.1 PEG shedding

"PEG shedding" refers to the detachment of PEG chains from the surface of lipid nanoparticles. Typically, PEG is anchored to the lipid nanoparticle via hydrophobic acyl chains. However, once the LNPs are injected, the PEG exposed on the surface interacts with serum proteins, leading to its release from the particles. PEG shedding thus facilitates the exposure of the underlying nanoparticle surface, promoting cellular uptake and membrane fusion, which are crucial for delivering the therapeutic payload into target cells. Research has underscored the relationship between PEG shedding rate and therapeutic efficacy. For instance, shorter acyl chain PEG-lipids are shown to shed more rapidly than longer chains, due to weaker hydrophobic interactions, facilitating quicker cellular uptake by target cells such as hepatocyte[48]. The choice of PEGylated lipid impacts the formation of the so-called protein corona, a collection of proteins that coat and interact with the surface of LNPs in the bloodstream. This corona effectively becomes the entry pass of particles when they are presenting to cells, affecting uptake. Research by Chen et al. demonstrated significant variations in cellular uptake and transfection efficiency across four types of LNP formulations, which differed in both polyethylene glycol lipid chain lengths (carbon 14 vs. carbon 18) and molar ratios (6% vs. 3%)[49]. This suggests that modulating the PEG shedding rate could optimize the balance between stability in circulation and efficient cellular delivery. Additionally, the level of PEG exposure also influences the immune response, leading to the production of anti-PEG IgM antibodies, which can cause rapid clearance of subsequent doses due to the ABC phenomenon. PEG-lipids that shed quicker are less likely to provoke this immunological reaction, thus sustaining therapeutic efficacy across multiple administrations[50,51].

The stability of formulations is also a concern, as it remains unclear whether PEG shedding can occur in vitro, during storage, or throughout all the manufacturing processes that involve handling, mixing, shaking, that might stress the particles. In a recent study it was observed that shaking with air entrainment leads to the formation of stable LNPs with larger sizes but reduced mRNA payloads. The authors hypothesized that air-liquid interfacial forces can strip away PEGylated lipids from the outer surface of LNPs. This reduction in steric hindrance among neighboring LNPs leads to the merging of

these unstable particles. During the merging process, the lipid layer surrounding the mRNA is temporarily disrupted, allowing some mRNA strands to be removed from the LNP, either completely or partially[52]. However, elucidating this mechanism necessitates the development of analytical methods to directly measure PEG shedding.

There is a clear need for analytical techniques to measure PEG shedding, as such methods would provide insights into the mechanisms behind the phenomenon, offer a tool for examining nanoparticle interactions across various biological environments, and monitor stability of formulations under various storage/stress conditions. PEG shedding from nanoparticles in biological fluids has been verified by separating particle-bound and shed PEG-lipid by chromatography techniques, quantified via LC/MS-MS[53] or radiolabeling[41], and by observing the fluorescence of profluorescent PEGs that initially show quenched fluorescence until shedding occurs[54]. These innovative techniques confirm PEG shedding but involve intricate sample handling and/or require PEG fluorescent labeling, which complicates real-time measurement and may alter PEG shedding behavior.

Pulsed gradient spin echo (PGSE) NMR can be an ideal tool to examine PEG shedding kinetics under conditions close to physiological environment. Since PEG associated with lipid nanoparticles diffuse much slower than free PEG, PGSE NMR can be used to distinguish the relative populations over time and quantify them, thereby determining the PEG shedding rate profile. The ability of ^{1}H NMR to differentiate analytes based on their unique chemical shifts allows for a specific molecular examination of the system, focusing on PEG in this context. Wilson et al. presented a simple, quantitative, label-free, and real-time approach for directly measuring PEG shedding using conventional NMR equipment with a high-resolution probe[55].

1.1.4 Erythrocytes as drug delivery systems

Erythrocytes, or red blood cells (RBCs), are the most abundant cells in the blood and possess significant potential as drug delivery system due to their biocompatibility and low immunogenicity[56]. RBCs are particularly suited for drug delivery due to their concave shape and lack of organelles, which allow for the encapsulation of a wide range of therapeutic agents, from small molecules to large multimeric proteins[57]. Additionally, erythrocytes offer the advantage of extended circulation times, roughly 120 days in humans. This prolonged circulation allows for sustained activity or release of therapeutic agents, reducing the frequency of dosage needed, especially beneficial for chronic conditions requiring long-term treatment. When drugs are encapsulated, they are isolated from the organism, interacting only with molecules that diffuse through the RBC membrane, greatly reducing

immune reactions towards both carrier and drug. RBCs can also be engineered for targeted delivery by modifying the cell surface to bind specific receptors or loading them with molecules responsive to environmental triggers, such as pH changes[58–61].

Several approaches are utilized for RBC drug loading[62]. One of the most common is hypotonic dialysis. This method leverages the RBC reversible swelling response to osmotic changes: placing them in a hypotonic solution induces the opening of membrane pores just large enough for various therapeutic agents to enter. After loading, erythrocytes return to an isotonic environment, resealing the membrane and entrapping the agents inside.

Therapeutic enzymes are promising candidates for RBC encapsulation, providing innovative solutions in enzyme replacement therapy by prolonging enzyme half-life. Notable examples include encapsulating asparaginase for acute lymphoblastic leukemia (ALL), adenosine deaminase (ADA) for immunodeficiency treatment and glutamine synthetase for ammonia detoxification[63–65]. L-asparaginase type-II (ANSII) is an enzyme that catalyzes the conversion of L-asparagine (L-Asn) into L-aspartate (L-Asp), as shown in Figure 1. Leukemic cells are deficient in asparagine synthetase (ASNS), preventing them from synthesizing L-asparagine. ANSII depletes the concentration of the metabolite leading selectively to the death of these cells. RBC encapsulation of asparaginase, targeting leukemic cells deficient in asparagine synthetase, is proposed to mitigate side effects associated with L-asparaginase treatment, such as hypersensitivity, hyperglycemia and coagulation disorders. L-Asparaginase, used to treat acute ALL and lymphoblastic lymphoma, has been evaluated in its erythrocyte-encapsulated form (GRASPA) in clinical trials for ALL and pancreatic cancer[66]. Despite the discontinuation of GRASPA's approval pursuit for ALL treatment, it remains a model for developing analytical tools to characterize this innovative class of biologics.

Another example of an enzyme encapsulated in RBCs is for ADA. Deficiency of this enzyme can result in the accumulation of 2-deoxyadenosine, which hampers lymphocyte differentiation, proliferation, and function, leading to severe immunodeficiency. Treatment using erythrocyte-encapsulated ADA has shown very promising outcomes in patients, providing a novel approach to address the challenges posed by this deficiency[67].

Similarly, glutamine synthetase, which plays a crucial role in the detoxification of ammonia. Elevated levels of ammonia can lead to functional disorders in the central nervous system. Encapsulating this enzyme within RBCs has proven to be effective, maintaining stability in most metabolites and metabolic parameters[68].

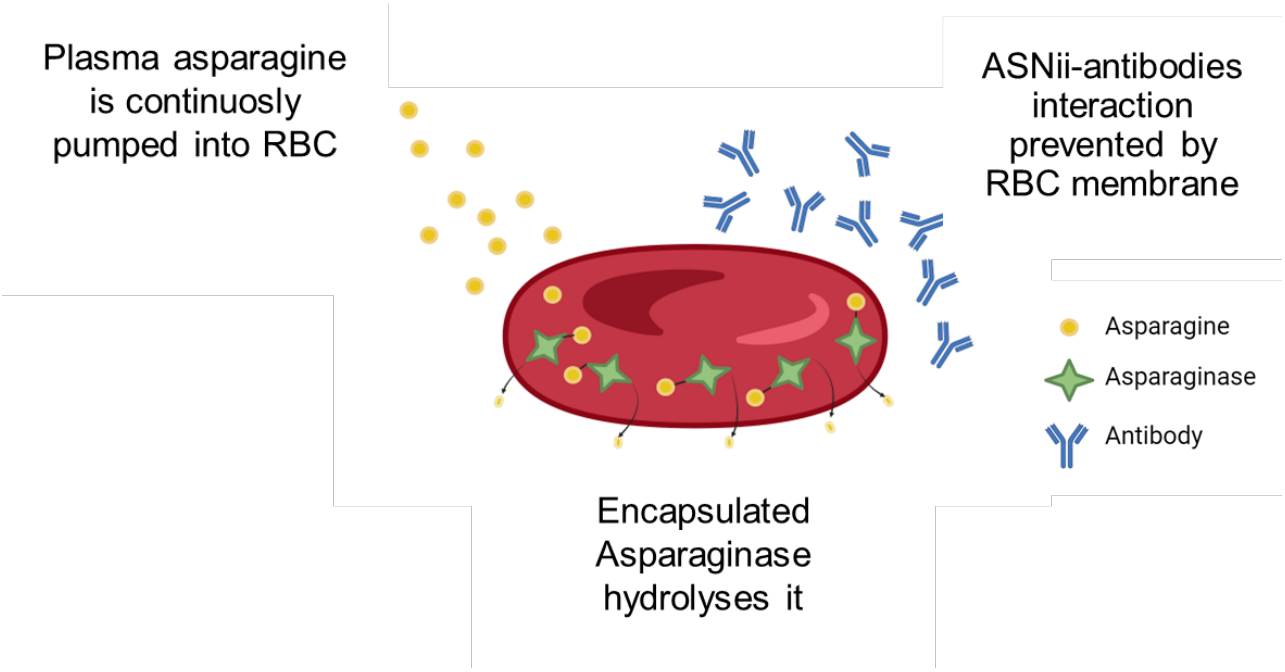

Figure 1. Schematic representation of the mechanism of action of erythrocyte-encapsulated L-asparaginase in the conversion of L-asparagine to L-aspartate for the treatment of acute lymphoblastic leukemia.

Effective characterization is crucial to guarantee the stability and functionality of biologics in pharmaceutical formulations. Various techniques have been employed to characterize enzymes into red blood cells. For instance, flow cytometry has been utilized to determine encapsulation efficiency by identifying the percentage of cells that have incorporated the enzyme[69]. Additionally, spectrophotometric and HPLC analysis are used to measure the concentration of the enzyme within the cells, while enzyme-specific assays evaluate the functionality of the enzyme post-encapsulation[64]. In terms of structure, current methods primarily focus on evaluating RBC integrity following encapsulation. Techniques such as Scanning Electron Microscopy (SEM) and Transmission Electron Microscopy (TEM) offer detailed visualization of structural modifications[70]. However, these methodologies do not address the characterization of higher-order structure (HOS) of the encapsulated enzyme, whose preservation is crucial to ensure functionality of the drug.

1.2 NMR as a tool for quantification of bioactive molecules in pharmaceutical products

1.2.1 NMR as a quantitative measurement

NMR spectroscopy has emerged as a pivotal quantitative tool in the realm of chemical analysis[71–74]. Unlike other spectroscopic techniques, NMR offers the valuable feature of being nondestructive, allowing researchers to analyze the sample without altering the organization of components. In addition, NMR offers a distinct advantage over chromatography and mass spectrometry by providing a direct correlation between signal intensity and the molar concentration of nuclei for each component. This correlation makes it unnecessary to use analyte calibration curves, as required in chromatography and mass spectrometry[75,76]. It is sufficient to utilize a reference standard of known concentration that does not interfere with the analyte and is miscible in the sample solution, thus enhancing both the speed and reproducibility of analyses. The possibility to use one single reference standard is particularly advantageous compared with chromatography or mass spectrometry when reference materials are scarce or expensive.

Quantification by NMR is based on the integration of spectral peaks. The following formula is used to calculate the molar concentration of the analytes, through the comparison to the reference.

$$C_{\text{analyte}} = \frac{I\text{analyte}\ n\text{std}}{n\text{analyte}\ I\text{std}}\, C_{\text{std}}$$

where

- I = integrated peak area,
- n = number of equivalent nuclei giving that peak,
- "std" = internal or external reference of known concentration Cstd.

The accuracy of NMR quantification is enhanced by instrument sensitivity and resolution capabilities, which have significantly improved over the years. Innovations such as cryoprobes and higher magnetic field strengths allow for better signal-to-noise ratios and resolution, facilitating quantification in samples with low concentrations up to micromolar range, even in complex mixtures. This level of detail allows to quantify subtle changes in molecular configurations, making it indispensable in the study of reaction mechanisms, the assessment of product purity, and the determination of kinetic parameters. Purity values obtained by qNMR (quantitativeNMR) have been shown to match classical primary methods in multi-lab studies[77]. Overall, the nondestructive nature

of NMR, combined with its quantitative accuracy and ability to provide structural elucidation, makes it an invaluable tool in both research and applied settings for determining molecular concentrations with a high degree of precision.

1.2.2 Pulse Length Based Concentration Determination (PULCON) method

The reference standard used for NMR quantification is commonly mixed with the analyte in the NMR tube. The use of an external reference for NMR quantification was introduced first by Wider G. *et al.* referring to the method as Pulse Length Based Concentration Determination (PULCON)[78].

The PULCON method is based on the principle of reciprocity, which states that the NMR signal strength is inversely related to the 90° pulse length required to achieve maximum magnetization. By leveraging this principle, PULCON allows for the determination of absolute concentration through direct comparison between a reference sample, whose concentration is known, and the sample of interest with unknown concentration, without necessitating any internal modifications. This approach involves initially acquiring the NMR spectrum of a reference sample, then obtaining a corresponding spectrum from the sample of interest. The ratio of these pulse lengths, alongside calculated integrals of signals, permits the estimation of unknown concentrations with remarkable precision. To ensure the fidelity of measurements, it is crucial to properly tune and match the NMR equipment so that the analysis of both the reference and sample tubes is consistent. Additionally, maintaining consistent sample volumes within the active coil region is essential for accurate concentration determination.

The sample concentration is determined using the equation below, which correlates the concentration (C) of the reference (r) and the sample of interest (x) with the integration of the specified resonance (I), the number of protons associated with that resonance (A), the sample temperature in Kelvin (T), the 90° pulse length (θ), and the number of scans (N).

$$Cx = Cr \frac{Ix\ Ar\ Tx\ \theta x\ Nr}{Ir\ Ax\ Tr\ \theta r\ Nx}$$

This method provides several advantages over traditional spectroscopic methods. First, the addition of an internal standard directly into the sample mixture is not required, which is advantageous when a standard may interfere with the sample or is impractical to be used. In addition, once a reference tube is prepared at exact concentration and analyzed to measure its integral, it is possible to quickly analyze multiple batches, eliminating the variability associated with adding a reference to each tube and saving considerable time[79,80]. PULCON has found diverse applications in analytical chemistry,

from the assessment of food quality to test of unstable intermediate synthesis products and purity of pharmaceutical samples in the context of official medicines control[81,82].

1.2.3 qNMR for small molecules

Nuclear Magnetic Resonance (NMR) spectroscopy's ability to face the complexity of mixtures, thanks to its atomic-level resolution and non-destructive nature, makes it highly attractive for quantifying small molecules in complex matrices such as pharmaceuticals, metabolomics, and materials science[83]. In the pharmaceutical industry, NMR serves as a cornerstone in drug development processes due to its ability to provide detailed characterization and quantification of a wide array of small molecules, including drug candidates, metabolites, and excipients[84–86]. The comprehensive nature of NMR to deliver multiple insights in a single analysis has proven to be a singular replacement for routine early development testing, which previously required the combination of identity testing, chromatographic assays, moisture analysis, residual solvent analysis, and elemental analysis.

This capability is crucial for quality control and regulatory compliance, where stringent evaluations of compound purity and concentration, forth by agencies such as the FDA and EMA, are mandatory to ensure a correct drug dosage. NMR also aids drug formulation and stability testing by providing quantitative data of the degradation products of active ingredients, which is vital for determining shelf life and storage conditions[74].

Beyond pharmaceuticals, NMR plays a significant role in metabolic research, where it is employed to quantify metabolites in biological samples, thus advancing our understanding of disease mechanisms and metabolic pathways. NMR quantification allows for the investigation of drug metabolism, enabling researchers to measure concentrations of metabolites and trace their pathways in biological systems. This application is particularly valuable in understanding the metabolic fate of drugs, identifying potential metabolites responsible for efficacy or adverse effects, and improving drug design to enhance patient safety[87,88].

Similarly, in environmental sciences, NMR assists in the analysis of pollutants and eco-friendly compounds, promoting sustainability measures by providing robust data on the concentrations of various environmental constituents[89]. Agriculture also benefits from NMR quantification through the precise monitoring of nutrient concentrations in soil and plant material, ultimately aiding in optimizing crop production[90]. Furthermore, NMR non-destructive nature makes it ideal for analyzing complex mixtures in food sciences, where issues of authenticity, safety, and quality are of paramount importance[91].

1.2.4 qNMR for lipid quantification

Lipid composition of liposomes is a key determinant in the effectiveness of cargo encapsulation and release, as well as in the stability and potency of the formulation, and is often being considered a critical quality attribute (CQA) under the Quality by Design Framework[92–94]. The initial concentration of lipids may differ from that of the final product due to potential losses during the multiple steps required for the formulation (such as mixing, filtration, centrifugation, etc.). Accurately quantifying these losses with a precise and rapid method can aid in formulation optimization and support large-scale process development[95–97]. Additionally, degradative processes such as hydrolysis and oxidation can significantly alter the phospholipid membrane properties (*e.g.*, permeability) and lead to the loss of encapsulated material[98–101]. Thus, implementing analytical methods that allow for accurate and rapid quantification of lipids in the final product is essential for both quality control and the optimization of preparation processes to minimize losses.

Nuclear Magnetic Resonance (NMR) is widely used for quantifying pharmaceutical components due to its atomic resolution, which allows to solve the complexity of mixtures, analyzing single components without overlap[102–104]. NMR offers a distinct advantage over chromatography and mass spectrometry by providing a direct correlation between signal intensity and the concentration of nuclei in each component, which can then be translated into molar concentration. Unlike chromatography and mass spectrometry, which typically require calibration curves, quantitative NMR can determine concentrations using only a single reference standard of known concentration, as long as it is miscible with the sample solution and does not interfere with the analyte. This approach enhances both the speed and reproducibility of analyses.

Solution NMR has been utilized to study liposomes, focusing on various key features, supported by well-established knowledge of the assignment of the spectra of lipids commonly used in formulations[105,106]. Lipid quantification in liposomes using NMR was already explored, with some studies focused on specific lipids or applications using ^{1}H and ^{31}P experiments[107–110]. The key to quantification lies in identifying which signals of the lipids under investigation are sufficiently intense and resolved to be integrated and used for calculating concentration. Despite the chemical similarity of lipids, primarily composed of a hydrocarbon backbone, small structural differences, such as the presence of heteroatoms or unsaturation, result in chemical shifts corresponding to higher frequencies. These shifts often allow for the identification of isolated signals suitable for quantification. Additionally, in the case of phospholipids, the ^{31}P NMR spectral window, which is quite broad, can be effectively exploited for quantification purposes. Endo et al. demonstrated, using

^{31}P detection, that the concentration ratios between lipids in intact liposomes can be still linearly estimated, particularly in liposomes with PEGylated lipids[108].

1.2.5 Possibilities and Limitations of quantifying concentrations for larger molecules

Solution NMR quantification is often impaired for large complexes due to the slower molecular tumbling associated with their size, which leads to broad spectral lines and reduced signal resolution, complicating the precise determination of molecular concentrations in solution. The difference between large complexes, like pharmaceutical delivery systems and small molecules, such as single biomolecules, lies in the duration of their transverse relaxation times (T_2). Small molecules exhibit rotational motion that is much faster than the precession frequency of the nucleus (spin orientation). This rapid motion leads to inefficient energy transfer, resulting in very slow relaxation processes. Consequently, the T_2 for small molecules can last several seconds, producing well-resolved and distinct peaks in NMR spectra. In contrast, large complexes have rotational speeds comparable to the precession frequency of their spins, facilitating more rapid energy transfer. This results in a much shorter T2, which causes broadened and less resolved signals[111,112].

An alternative to overcome the limits of solution NMR related to the size of samples is Solid-state nuclear magnetic resonance (ssNMR). Solid-state does not rely on molecular tumbling for spectral resolution. The dipolar interactions and chemical shift anisotropies which are averaged in solution by the molecular tumbling are addressed by the magic angle spinning (MAS) that simulates the averaging effect of molecular tumbling by physically rotating the sample at high speeds, at a particular angle 54.74° with respect to the direction of the magnetic field[113].
This makes solid-state NMR particularly valuable for studying high-molecular-weight assemblies such as membrane proteins, supramolecular polymers, virus-like particles, and nanoparticle–biomolecule conjugates. Notable applications include the analysis of the solid-state forms of Active Pharmaceutical Ingredients (APIs), like polymorphs, salts, and hydrate forms, which can significantly affect drug solubility and bioavailability, and can be quantified without requiring them to be dissolved, maintaining their native crystalline form[73,114]. In structural biology, it enables stoichiometric analysis of amyloid fibrils or oligomeric membrane protein complexes embedded in native-like lipid environments[115]. On the other hand, ssNMR relies on a complex hardware, commonly not available in industries, more demanding sample preparation, long acquisition times and sensitivity issues. These factors lead to a preference for solution NMR when solid-state analysis is not strictly necessary.

1.3 NMR to study HOS of proteins

Higher-order structure (HOS) is a crucial critical quality attribute (CQA) for protein biotherapeutics. It is monitored throughout the development and manufacturing processes because HOS serves as a fingerprint encompassing structural attributes that may be linked to the protein function. Understanding HOS is essential for elucidating the structure-function relationships of a molecule. HOS comprises secondary, tertiary, and quaternary structures. The secondary structure involves local folding patterns, such as alpha-helices and beta-sheets. The tertiary structure describes the overall three-dimensional folding of a single polypeptide chain, while the quaternary structure refers to the arrangement of multiple polypeptide chains into a functional unit when present[116]. Further folding levels support the protein's unique 3D structure, physicochemical properties, and function.

Characterizing HOS during drug development is complex and evolving, requiring various biophysical analyses. The main techniques to study HOS are X-ray crystallography, cryo-electron microscopy (cryo-EM), small-angle X-ray scattering (SAXS) and NMR spectroscopy[117]. NMR is a fundamental technique for the characterization of higher-order structures (HOS) in proteins, providing a depth of structural insight that is essential in the field of biotherapeutics. One of NMR's significant advantages is its ability to provide detailed information about protein dynamics, which complement static images obtained from other high-resolution techniques like X-ray crystallography or cryo-electron microscopy. While these techniques are limited to frozen or crystalline states and may miss dynamic processes crucial to biological function, NMR tracks the movement and interaction of atoms over time, in their native-like environment, thereby preserving their natural conformational landscape. This ability to capture dynamic equilibria makes NMR indispensable for exploring mechanisms of action and potential interactions with small molecules or other proteins, aspects that are central to drug design and optimization[118–120]. NMR provides a molecular fingerprint, capturing atomic-level details that make it highly effective for mapping secondary, tertiary, and quaternary structures of complex protein systems. Its ability to identify subtle structural variations is invaluable in drug development, where even minor shifts in protein conformation can significantly impact efficacy, specificity, and safety[116,121].

Innovations in NMR technology and methodologies, including improvements in sensitivity and resolution, are continually enhancing their applicability and accessibility in the field of biopharmaceutical development.

1.4 Diffusion NMR to study delivery systems

1.4.1 Diffusion NMR

Pulsed Gradient Spin Echo (PGSE) NMR is a powerful technique specifically designed to discriminate the signals of the sample molecules according to their diffusion properties. The fundamental principle of PGSE NMR relies on measuring molecular diffusion through the application of pulsed magnetic field gradients. These are essentially magnetic fields that vary in a specific spatial direction. Pulsed magnetic field gradients are applied to samples containing diffusing molecules, such as water in biological tissues. When a magnetic field gradient is applied, diffusing molecules move in such a way that their resonance frequencies vary slightly along the gradient direction. This phenomenon is called the "Doppler effect" and can be utilized to measure molecular diffusion. PGSE NMR employs a sequence of magnetic resonance pulses to generate a signal dependent on molecular diffusion. Specifically, a 90° pulse is applied to rotate the magnetic spins of molecules into the transverse plane of the magnetic field, followed by a magnetic field gradient. This gradient causes a variation in the resonance frequency of molecules along the gradient direction, which is then canceled out by a second equal and opposite gradient, referred to as the refocusing gradient. Following this refocusing gradient, a second 180° pulse is applied to reverse the magnetic spins of the molecules, followed by a third 90° pulse to read the NMR signal (Figure 2). The variation in NMR signal intensity is linked to molecular diffusion along the magnetic field gradient direction. By varying the duration and intensity of these gradients, it is possible to measure molecular diffusion in different spatial directions. This data can then be used to calculate the diffusion coefficient, which is a quantitative measure of molecular mobility.

Key Parameters Defining the Pulse Sequence for Measuring Molecular Diffusion are the "Big Delta" (Δ) and "Little Delta" (δ).

- Big Delta (Δ): it is the separation time between the application of the first and second magnetic field gradients. It is the "diffusion period" during which molecules in the sample move due to diffusion. This time interval is crucial because it determines how long molecules diffuse and impacts the experiment’s sensitivity to diffusion. Practically, Δ affects the temporal scale of diffusion being measured. A longer Δ allows observing diffusive movements over greater scales.
- Little Delta (δ): it is the duration of the pulsed magnetic field gradient. It refers to the time during which the gradient is effectively applied throughout the sequence. This gradient

encodes the spatial position of nuclei, creating an imprint on the NMR signal influenced by molecular motion. The length of δ directly affects the intensity of spatial contrast introduced by the gradient: a longer δ signifies a more intense gradient, increasing the experiment sensitivity to diffusion.

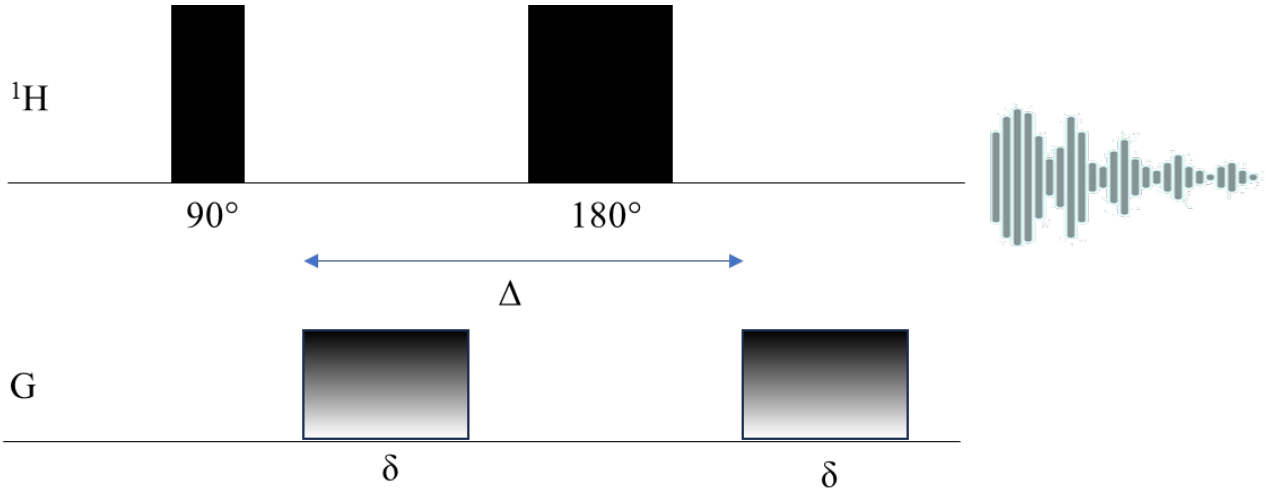

Figure 2: Pulse sequence for Pulsed Gradient Spin Echo (PGSE) NMR. After a first 90° pulse to flip the magnetic spins into the transverse plane of the magnetic field, a gradient pulse of specified strength (G) and duration (δ) is applied. A 180° pulse further reverses the spins, ensuring refocusing, After the end of diffusion time (Δ), a second gradient pulse of equal strength is applied, serving as the refocusing gradient to attempt cancellation of the positional phase shifts. A third 90° pulse reads the NMR signal, capturing diffusion behavior and allowing for diffusion coefficient calculations.

The relationship between big delta, little delta, and the magnetic field gradient (G) is used to calculate the diffusion coefficient (D). Spin echo signal attenuation depends on these parameters and can be described by the Stejskal-Tanner equation:

$$I/I_0 = \exp[-\gamma^2 G^2 \delta^2 D(\Delta - \delta/3)]$$

where:

- I = signal intensity with a gradient
- I_0 = signal intensity without a gradient
- γ = gyromagnetic ratio of the nucleus
- G = gradient strength
- δ = duration of the gradient pulse (little delta)
- Δ = the diffusion time (big delta)

Both Δ and δ are crucial in determining how much of the diffusion effect will be highlighted and quantifiable in the NMR signal, allowing to extrapolate the diffusion coefficient of the studied

molecules. Therefore, the choice of these parameters depends on the system under analysis and the experiment sensitivity requirements[122].

PGSE NMR is particularly useful for isolating signals of interest from a complex matrix, such as a full pharmaceutical formulation[123]. By filtering out excipient signals, typically small molecules, from the spectra, potential overlap with signals from active pharmaceutical ingredients can be eliminated. The determination of the diffusion coefficients of molecules is functional also to gain insights into molecular size, shape, and interaction dynamics[124]. The interaction between a ligand and a target can be demonstrated by the fact that the intermolecular complex formed diffuses more slowly than the individual free molecules in solution. The technique is particularly valuable in heterogeneous samples, revealing how molecules interact and migrate despite varied viscosities or binding conditions. This capability makes PGSE NMR invaluable for research targeting complex biological systems, such as cellular environments, where diffusion is influenced by compartmentalization and binding events. Similarly, PGSE NMR aids materials science by uncovering molecular mobility in polymers and porous structures, guiding the design of substances with tailored mechanical or optical properties[125,126]. By connecting diffusion measurements to molecular characteristics, PGSE NMR not only offers a window into dynamic processes but also drives innovation across multiple domains, underscoring its importance as a versatile and indispensable analytical tool.

1.4.2 Application to other systems to study interaction with delivery system

Diffusion NMR experiments are powerfully and quantitatively applied to investigate encapsulation, transport, release, structural characterization, and exchange kinetics in a wide range of biologically relevant delivery systems.

A key application of diffusion NMR is monitoring drug encapsulation. By comparing the diffusion coefficients of free versus encapsulated drug molecules, NMR can distinguish between carrier bound and released drug fractions, providing insight into loading efficiency and potential leakage. This has been demonstrated on several delivery systems such as hydrogels, liposomes and polymeric nanoparticles, under different relevant conditions like pH, temperatures, or formulation composition[127–129].

Furthermore, NMR diffusion techniques determine nanoparticle size distributions by exploiting the inverse relationship between diffusion coefficients (D) and hydrodynamic radii (r_H) expressed with Stokes-Einstein equation:

$$r_H = \frac{kBT}{6\pi\eta D}$$

where kB is the Boltzmann constant, T is the temperature expressed in Kelvin, and η is the viscosity of the solution. NMR is particularly advantageous for monitoring size changes in polydisperse samples, especially in complex biological matrices, where chemically different species contemporarily present in a sample may be individually studied or opaque suspensions, where techniques like Dynamic Light Scattering (DLS) fall short[130–132].

The use of PGSE NMR also provides direct structural insights into the carrier, which are directly linked to the release profile of the encapsulated therapeutics and ultimately inform the performance criteria for drug or therapeutic delivery. For example, NMR studies have shown that drugs encapsulated in liposomes prepared via extrusion exhibit more homogeneous diffusion profiles compared to those prepared by sonication, reflecting differences in vesicle size distribution and lamellarity[133]. Moreover, in stimuli-responsive systems such as pH-sensitive micelles or temperature-responsive hydrogels, structure–property–function analysis enables the direct observation of morphological transitions (e.g., micelle-to-vesicle conversion, gel swelling) in response to external cues, as well as the resulting changes in molecular mobility and release kinetics[134–136]. These insights are critical for rational design, allowing to engineer carrier structures that are fine-tuned for specific therapeutic goals.

Overall, the ability of NMR diffusion measurements to be conducted under physiological conditions offers translationally relevant data on delivery system behavior. This, coupled with the technique precision in distinguishing signals based on diffusivity, makes NMR an indispensable tool for rational design and quality control in modern delivery system development.

2 Aim of the project

Overall, this project aims to deepen the understanding of these delivery system properties, paving the way for enhanced therapeutic delivery solutions and to develop new analytical methodologies to test the quality attributes of formulations. Specifically, in the context of liposomes, lipid quantification is an essential area of study. This study aims to refine NMR methods for lipid quantification suitable for industrial applications, testing formulations that are prepared by mimicking the commercial products. The method presented herein aims to be versatile across various lipid delivery systems, where the lipids investigated form the scaffold of a typical lipid particle used for delivery. The refinement of a quick and accurate method to quantify lipid concentration at all stages of manufacturing allows to assess potential losses during the formulation process and can also aid in optimizing the production process to ensure the preservation of the expected concentration levels of the components within the formulations. We demonstrated applicability and highlighted the benefits of PULCON quantification for this purpose, in comparison to the NMR method with internal standard. Finally, the proposed method has been compared to a protocol optimized for lipid quantification using Ultra-Performance Liquid Chromatography coupled with Evaporative Light Scattering Detection (UPLC-ELSD). Comparing NMR methods to UPLC, which is commonly used and well-established in the industry for similar applications, affords a comprehensive exploration of the advantages and limitations of each technique, aiding in the determination of their suitability for specific applications.

In addition to liposomes, lipid nanoparticles constitute another important field of interest, in particular we focused on PEG shedding which plays an important role in the activity promoted by the LNP delivery system. Our work aims to refine a method for PEG shedding evaluation with NMR, to be applied to several LNP formulations under various storage/stress conditions. This approach will enhance the understanding of formulation stability, enabling testing of different batches for quality control purposes. Furthermore, we aim to identify the factors influencing this phenomenon by simulating post-injection conditions, such as adding proteins to the solution that are known to contribute to PEG release in the human body. This simulation allows us to predict LNP behavior in vivo, providing new insights that can inform and improve the rational design of LNP formulations.

The last aspect of this work involves Red Blood Cells, where an effective method to monitor the functionality and stability of the enzymes encapsulated in red blood cells is required as quality control for pharmaceutical development. The assessment of the preservation of the high order structure is crucial for a thorough understanding of these formulations and for optimizing encapsulation protocols, sample handling, and storage. Our initial goal was to refine a protocol for the effective encapsulation of enzymes within red blood cells, and to demonstrate encapsulation with NMR. After

that, we conducted NMR characterization of the complex to examine the preservation of the HOS of the encapsulated enzyme. Additionally, peak re-assignment was performed to identify which residues were most affected by encapsulation and to evaluate whether all the secondary structure motifs were preserved. The study also involved conducting a semi-quantitative analysis of encapsulated enzymes, comparing the intensity of signals from both free standard solutions and encapsulated proteins. This approach could serve as an important analytical tool for rapid determination of encapsulation efficiency of cargo in red blood cells, aiding in the optimization of the encapsulation protocol.

3 Materials and methods

The present chapter describes all the experimental procedures organized by papers.

3.1 Fast and straightforward lipid quantification in pharmaceutical compositions using NMR

The materials and methods described in this paragraph are reproduced from the paper: Currò, F., Eguskiza, A., Cerofolini, L., Martini, S., Biagini, M., Stranges, D., Fragai, M., & Denis, M. Fast and Straightforward Lipid Quantification in Pharmaceutical Compositions Using NMR. *ACS Omega*. (2025) and reported in section 4.1.

3.1.1 Materials

All reagents were purchased from common commercial sources and were used without additional purification. Distearoylphosphatidylcholine (DSPC), cholesterol, 1,2-dioleoyl-*sn*-glycero-3-phosphocholine (DOPC) and Chloroform-d 99.8% atom enrichment were purchased from Sigma Aldrich. DMPE-PEG2K was purchased from Avanti Polar. Ethanol was purchased from Merck. HyPure WFI quality water was purchased from Cytiva. N,N-Dimethylformamide anhydrous 99.8% (DMF) and trifluoroacetic acid (TFA) were purchased from Sigma Aldrich. Isopropanol was purchased from Carlo Erba.

All the volumes with $CDCl_3$ as solvent were handled with glass Hamilton precision syringes of 1 mL, 500 µL and 100 µL capacity. Plastic pipette tips were not used because of potential plasticizer leaks.

3.1.2 Lipid standards preparation

Solutions of each lipid at a known concentration were prepared in $CDCl_3$. DOPC was not considered in this step, since the functional group used for the integration of its signal is the same as that of DSPC, without differences in chemical shift and intensity. Solutions were vortexed to ensure complete dissolution of lipids. Each lipid was analyzed at three concentrations: (i) the concentration of the stock solution, (ii) after 1:10 and (iii) 1:100 dilutions. The intermediate concentration for each lipid was of the same order of magnitude as the lipid concentration in the final liposome formulation. Lipid mix solutions were prepared aiming to prepare mixtures representative of the composition and concentration of each liposome formulation analyzed. Refer to tables S1-5 for detailed preparation.

3.1.3 Liposome solutions preparation

Liposomes were prepared using microfluidic mixing with the NanoAssemblr Ignite nanoparticle formulation system. For each liposome formulation, the organic and aqueous phases were prepared as detailed in Table 1. Lipids were dissolved in ethanol for the organic phase while PBS pH 7.4 was used for the aqueous phase.

Table 1. Lipid composition of liposome formulations and mixing parameters.

Liposome	Lipid composition (w:w)	DSPC or DOPC concentration (mg/mL)	Cholesterol concentration (mg/mL)	DMPE-PEG2K concentration (mg/mL)	Flow Rate Ratio (AP:OP[1])	Total Flow rate (mL/min)
(A)	DSPC : Cholesterol (2:1)	1.20	0.60	N/A	3:1	10
(B)	DSPC : Cholesterol : DMPE-PEG2k (10.9 : 14.6 : 1)	1.09	1.46	0.1	2:1	10
(C)	DOPC : Cholesterol (4:1)	3.18	0.79	N/A	2:1	2

[1] AP = Aqueous Phase OP = Organic Phase

The resulting mixtures appeared as clear solutions, with the liposome (C) exhibiting a more opaque, whitish appearance, likely due to its higher concentration. Each formulation was exchanged with Hypure WFI quality water using PD10 columns to remove ethanol.

Liposomes must be disrupted to enable accurate NMR quantification, free from proton relaxation issues caused by their large size. For each liposome solution, 800 µL were placed into glass vials, prepared in four replicates, two for NMR and the other pair for UPLC analysis. The resulting 12 vials, along with two additional vials each containing 800 µL of H_2O as controls, were placed in a SpeedVac set to 45°C at a pressure of 1 mTorr for 3 hours. At the end of this process, all water had evaporated, leaving only the dried lipid residue in the liposome vials. Finally, the content of each vial was resuspended in 800 µL of $CDCl_3$ for NMR analysis.

3.1.4 NMR sample preparation

DMF was chosen as internal reference due to its inertness, miscibility in organic solvents, and the fact that its chemical shift occurs in a spectral region where no other proton resonates. A pure (>99.5%) DMF solution was diluted to achieve a concentration in the tube comparable to that of lipids, aiming for a similar signal-to-noise ratio. The dilution process was designed to ensure that the addition of DMF constituted roughly 10% of the total volume in the NMR tube and avoiding many dilution steps to reduce the risk of imprecision. Specifically, 40 µL of DMF solution (MW = 73.09, density = 0.944 g/mL) was diluted to a total volume of 1.040 mL in $CDCl_3$ to achieve a final concentration of 497 mM. Each NMR tube (Wilmad, 5 mm, 500 MHz precision) was filled with 500 µL of the analyzed solution and 40 µL of a 497 mM DMF solution, resulting in a final DMF concentration of 36.796 mM. In contrast, for the PULCON method, the analyte tubes were prepared by adding 540 µL of the sample solution in CDCl3, while the reference tubes were prepared by adding 40 µL of the DMF solution and 500 µL of CDCl3, to achieve the same DMF concentration of 36.796 mM.

3.1.5 NMR measurements

All NMR experiments were recorded at 298 K on a Bruker Avance NEO spectrometer, operating at 500 MHz, 1H Larmor frequency, 11.7 T, equipped with quadrupole resonance QCI H/P/C/N Cryoprobe. For each sample, the following procedures were applied: locking to CDCl3, manual matching and tuning, shimming, optimization of the 1H pulse, and automatic receiver gain optimization. 1D 1H zg experiments were acquired using 16 scans, 64K data points, an offset of 4.674 ppm and acquisition time of 4.2 s. To correctly evaluate the interscan delay, 1D 1H experiments were performed gradually increasing such delay. An interscan delay of 35 s was found sufficient to allow complete spin relaxation, since no increase in signal intensity was observed for longer delays.

3.1.6 NMR spectra analysis

All the spectra were processed with a Bruker Topspin 3.5pl6 software package. Fourier transformation with exponential function with line broadening equal to 5.00 Hz was used to process all the spectra, followed by manual phase optimization and baseline correction. Integration of the signals of interest was performed in manual mode. For each lipid, one well-solved specific signal, was identified recording the spectra of the single lipids (Fig. S1) and integrated for the quantification

while the well-solved aldehyde proton peak of DMF was chosen for the integration of the reference (Fig. 1). Equation 1 was applied for lipid quantification using the method with internal standard:

$$\text{Equation 1: [Lipid]} = \left(\frac{Ilipid}{IDMF}\right)/n\ Hlipid * 36.796 * (540/500)$$

The unknown concentration of the lipid is calculated from the ratio of the specific integral of the lipid ($Ilipid$) and the integral of the aldehyde proton of DMF ($IDMF$) divided by the number of protons contributing to the lipid signal ($n\ Hlipid$). This ratio is then multiplied by the molar concentration of DMF (36.796 mM) and further adjusted by the dilution factor of the sample (from 500 µL to 540 µL)

The PULCON method consisted of recording the spectra of both the reference and the sample on the same spectrometer, using the same pulse sequence, the same delay (d1) to ensure complete proton relaxation, and the same receiver gain. Sample concentration was determined using Equation 2 below, which correlates the concentration (C) of the reference (r) and the sample of interest (x) with the integration of the specified resonance (I), the number of protons associated with that resonance (A), the sample temperature in Kelvin (T), the 90° pulse length (θ), and the number of scans (N).

$$\text{Equation 2:} \quad Cx = Cr\ \frac{Ix\ Ar\ Tx\ \theta x\ Nr}{Ir\ Ax\ Tr\ \theta r\ Nx}$$

The molar concentrations calculated from NMR integrals were converted into mg/mL concentrations using the molecular weight (g/mol) of each component.

3.1.7 UPLC-ELSD analysis

UPLC analysis was performed using a Waters Acquity CSH C18 column (2.1 x 50 mm, 1.7 µm) maintained at 55°C, with samples held at 20°C. 5 µL injection volume and consistent flow rate of 0.6 mL/min were employed over a run time of 13 minutes. The mobile phase consisted of 0.1% v/v trifluoroacetic acid (TFA) in water (Phase A) and 0.1% v/v TFA in isopropanol (IPA), (Phase B), with a gradient of solvent compositions spanning throughout the run. Evaporative Light Scattering (ELS) detection was configured with evaporation temperature set at 50°C, data collection rate of 2 Hz, and a filter setting of 3.6.

Standard solutions containing DSPC, DOPC, cholesterol and DMPE-PEG2K were prepared, showing good resolution of the components (Fig. S2). Calibration curves for each lipid were generated in triplicates, originating from the standard solution across the concentration ranges relevant for liposome analysis, taking into account a 1:5 dilution factor applied to the initial liposome solutions

(Fig. S3). A lipid mix solution containing DSPC, cholesterol and DMPE-PEG2K dissolved in CDCl3 at known concentrations (Table S6) was analyzed to test the accuracy and precision of the method.

The liposome solutions were first analyzed in their formulation buffer and subsequently after drying, as described for NMR analysis, followed by resuspension in 800 µL of ethanol. In both cases, the solutions were diluted at a 1:5 ratio in absolute ethanol and thoroughly vortexed to ensure homogeneity. Each sample was prepared and analyzed in triplicate.

3.2 NMR Assessment of the High Order Structure of Biological Therapeutics in Erythrocytes Provides a Tool for Drug Delivery Design

The materials and methods described in this paragraph are reproduced from the paper: Padilla-Cortés L, Gheorghita GR, Currò F, Calamandrei R, Susini B, Callozzo S, Crivello G, Russomanno P, Ravera E, Cerofolini L, Fragai M. NMR Assessment of the High Order Structure of Biological Therapeutics in Erythrocytes Provides a Tool for Drug Delivery Design. *J Am Chem Soc.* (2025) and reported in section 4.2.

3.2.1 Materials

Luria−Bertani (LB) medium, ampicillin, kanamycin, Dglucose, sodium chloride (NaCl), sodium phosphate dibasic (Na_2HPO_4), potassium phosphate monobasic (KH_2PO_4), magnesium sulfate ($MgSO_4$), calcium chloride ($CaCl_2$), ^{15}N-amonium sulfate $(NH_4)_2SO_4$, zinc sulfate ($ZnSO_4$), Tris sulfate (Tris-SO4), isopropilβ-D-1-tiogalattopiranoside (IPTG), sodium phosphate dibasic heptahydrate ($Na_2HPO_4 \cdot 7H_2O$), sodium phosphate monobasic monohydrate ($NaH_2PO_4 \cdot H_2O$), Tris hydrochloride (Tris-HCl), dithiothreitol (DTT), hydrochloric acid (HCl), sodium hydroxide (NaOH), ^{2}H–^{13}C-^{15}N-enriched medium, Coomassie blue, ethylenediaminetetraacetic acid (EDTA), sucrose, reduced glutathione and ATP were purchased from Sigma-Aldrich. Plasmids were obtained from Twist Bioscience, San Francisco, CA.

3.2.2 Expression and Purification of Uniformly Isotopically Enriched Carbonic Anhydrase II [U−^{15}N]

The gene encoding α-CAII into the pCAM vector was transformed into Escherichia coli BL21(DE3) cells, which were subsequently precultured overnight in LB medium containing ampicillin (0.1 mg

cm^{-3}) and 1% glucose at 37 °C and 160 rpm. The main culture (1 dm^3) was then incubated at 37 °C, 160 rpm until it reached the optical density at 600 nm (OD600) ~0.6 and harvested for 15 min at 4000 rpm to proceed with the isotopic enrichment according to the Marley method. The cell pellet was resuspended in 1 dm^3 of M9 minimal medium (3 g dm^{-3} KH_2PO_4, 0.5 g dm^{-3} NaCl, 6.8 g dm^{-3} Na_2HPO_4) supplemented with 2 mmol dm^{-3} $MgSO_4$, 0.2 mmol dm^{-3} $CaCl_2$, 3 g dm−3 glucose, 1.2 g dm−3 ^{15}N-ammonium sulfate, 0.5 mmol dm−3 $ZnSO_4$ and ampicillin. The new culture was further incubated for 30 min at 37 °C and 160 rpm, before inducing with 1 mmol dm^{-3} IPTG and incubating overnight at 25 °C and 160 rpm. The cell culture was harvested at 7500 rpm for 20 min (JA-10 Beckman Coulter). The cell pellet was resuspended in 70 cm^3 of 20 mmol dm^{-3} Tris-SO_4, 500 μmol·dm^{-3} $ZnSO_4$ pH 8 and underwent 10 cycles of sonication for 30 s with a resting period of 3 min on ice, 60% power (sonicator Vibra-cell of Sonics & Materials Inc.). The lysate was ultracentrifuged at 40,000 rpm for 40 min (Beckman Optima LE-80K Ultracentrifuge, rotor F15−6 × 100y from Thermo Scientific) and the supernatant recovered is filtered with a 0.45 μm filter. The supernatant, containing crude α-CAII protein, was purified by Nickel affinity chromatography using a linear 0−0.5 mol dm^{-3} Imidazole gradient on a HisTrap 5 cm^3 (GE Healthcare). Finally, the α-CAII was subjected to a size-exclusion chromatography on a Superdex 75pg 26/60 column (Amersham Biosciences) in 50 mmol dm^{-3} sodium phosphate buffer at pH 7 (7.744 g dm^{-3} of $Na_2HPO_4·7H_2O$, 2.913 g dm^{-3} of $NaH_2PO_4·H_2O$, pH adjusted with HCl and NaOH).

3.2.3 Expression and Purification of Uniformly Isotopically Enriched TTR [U−^{15}N]

E. coli BL21(DE3) RIPL cells were transformed with pET-28a (+) plasmid coding for TTR gene. The cells were cultured in ^{15}N-enriched M9 minimal medium supplemented with kanamycin at 37 °C until OD600 reached 0.6− 0.8 and then 1 mmol dm^{-3} IPTG was added for induction. The cells were incubated overnight at 37 °C and then harvested by centrifugation (JA-10 Beckman Coulter) at 7500 rpm for 15 min at 4 °C. The pellet was suspended in 20 mmol dm^{-3} Tris-HCl, pH 8.6 buffer supplied with 5 mmol dm^{-3} DTT (80 cm^3 per liter of culture) and sonicated at 4 °C for 10 cycles of 30 s ON and 3 min OFF, at 60% power. The suspension was centrifuged at 40,000 rpm (Beckman Optima LE-80K Ultracentrifuge, rotor F15−6 × 100y Thermo Scientific) for 40 min and the pellet was discarded. The protein was purified by anionic-exchange chromatography using a HiPrep Q FF 16/10 column (GE Healthcare Life Science), previously equilibrated with 20 mmol dm^{-3} Tris-HCl, pH 8.6. The protein was eluted in 20 mmol dm^{-3} Tris-HCl, pH 8.6 with a linear 0−1 mol dm^{-3} NaCl gradient. Fractions containing pure TTR were joined and purified by Size Exclusion Chromatography using HiLoad Superdex 75pg 26/60 in 50 mmol dm^{-3} phosphate buffer, pH 7.5.

3.2.4 Expression and Purification of Uniformly Isotopically Enriched L-Asparaginase II [U-^{2}D-^{13}C–^{15}N]

E. coli (DE3) C41 cells were transformed with pET-21a (+) plasmid with ANSII insert. The cells were cultured at 37 °C in ^{2}H–^{13}C-^{15}N-enriched medium (*E. coli*-OD2 rich growth media, Silantes) supplemented with ampicillin until OD600 0.6 was reached, then 1 mmol dm^{-3} IPTG was added for induction. All reagents were previously dissolved in H_2O. The culture was incubated at 37 °C overnight and then harvested by centrifugation at 6500 rpm (JA-10 Beckman Coulter) for 15 min at 4 °C. The pellet was suspended in 10 mmol dm^{-3} Tris-HCl, pH 8.0, 15 mmol dm^{-3} EDTA, 20% sucrose buffer (60 cm^3 per liter of culture) and incubated at 4 °C for 20 min under magnetic stirring. The suspension was centrifuged at 10,000 rpm (Beckman Optima LE80K Ultracentrifuge, rotor F15−6 × 100y, Thermo Scientific) for 30 min and the supernatant was discarded. The recovered pellet was resuspended in H_2O milli-Q (60 cm^3 per liter of culture) and incubated at 4 °C for 20 min under magnetic stirring. Again, the suspension was centrifuged at 10,000 rpm for 30 min and the pellet was discarded. The supernatant was treated with ammonium sulfate to trigger the precipitation of ANSII. Under magnetic stirring, solid ammonium sulfate was added in aliquots up to 50% saturation. The precipitate was removed by centrifugation and discarded, then additional ammonium sulfate was added up to 90% saturation to trigger the precipitation of ANSII. The precipitated ANSII was redissolved in a minimal amount of 20 mmol dm^{-3} Tris-HCl, pH 8.6, and dialyzed extensively against the same buffer. ANSII was purified by anionic-exchange chromatography using a HiPrep Q FF 16/10 column (GE Healthcare Life Science). The protein was eluted in 20 mmol dm^{-3} Tris-HCl, pH 8.6 with a linear 0−1 mol dm^{-3} NaCl gradient. Fractions containing pure ANSII were identified by Coomassie staining SDS-PAGE gels, then joined and dialyzed extensively against the final buffer.

3.2.5 Encapsulation of ^{15}N-Labeled Proteins in Red Blood Cells

Commercially available Bovine red blood cells Packed 100% from Innovative Research were used. RBCs were washed by diluting 5 cm^3 of 100% packed RBC in 5 cm^3 of cold PBS. The sample was centrifuged at 2305 rpm (Heraeus Megafuge 16R Centrifuge, TX-400 Swinging Bucket Rotor, Thermo Scientific) for 1 min at 4 °C and the supernatant was removed. The process was repeated two more times. ^{15}N-labeled CAII, TTR and ANSII were encapsulated using a previously reported hypotonic dialysis method of encapsulation. Seven parts (700 mm^3) of washed packed RBC were mixed with 3 parts (300 mm^3) of a concentrated solution of the protein (3 mmol dm^{-3} solution of CAII, 1 mmol dm^{-3} solution of TTR and 236 μmol dm^{-3} solution of ANSII). One cm^3 of this

suspension was placed on a dialysis tube (12 kDa MWCO) and dialyzed against 150 cm^3 of hypotonic buffer (5 mmol dm^{-3} KH_2PO_4, 5 mmol dm^{-3} K_2HPO_4, pH 7.4) at 4 °C with a rotation of ∼20 rev/min for 180 min. The erythrocytes were then resealed by transferring the dialysis tube into a container holding 150 cm^3 of isotonic buffer (PBS 1×, 5 mmol dm^{-3} glucose, 5 mmol dm^{-3} $MgCl_2$) at 37 °C under continuous stirring for 60 min. The addition of reduced glutathione (3 mmol dm^{-3}) and ATP (2 mmol dm^{-3}) in the buffer was also evaluated (see Figure S6). An aliquot of CAII was also titrated with the active-site ligand furosemide. Then 1.95 cm^3 of a solution of free CAII at the concentration of 330 μmol dm^{-3} was mixed with 1.89 cm^3 of a solution of inhibited CAII at the concentration of 330 μmol dm^{-3}. The volume of the resulting solution was reduced to 340 mm^3. The same procedure for protein encapsulation was also performed on this sample. To wash away nonencapsulated ^{15}N isotopically enriched protein or released components from the erythrocytes, the sample was transferred into a dialysis tube of 1000 kDa MWCO and dialyzed against 1 dm^3 of isotonic buffer at 4 °C for 12 h. This dialysis was repeated 2 times. The dialyzed erythrocytes were then washed with an equal volume of cold PBS three times. A first FID of 2D ^1H ^{15}N SOFAST-HMQC spectrum of a sample from the last wash was acquired to confirm the absence of any ^{15}N-labeled protein outside of the red blood cells. Two distinct control experiments were conducted using CAII, the first protein to be studied and used to verify the efficacy of the protocol. These experiments aimed to rule out the possibility of protein adsorption on the surface of the red blood cells and to confirm the efficacy of the washing procedure. In Control 1, the erythrocytes were subjected to hypotonic dialysis in the absence of proteins. The samples were prepared by mixing 7 parts of washed packed RBC with 3 parts of cold PBS, then 1 cm^3 of cell suspension was placed on a dialysis tube (12 kDa MWCO). The sample was dialyzed against 150 cm^3 of hypotonic buffer at 4 °C with a rotation of around ∼20 rev/min for 180 min. The dialysis tube was then transferred to a container holding 150 cm3 of isotonic buffer at 37 °C under continuous stirring for 60 min. To wash away the released components from the erythrocytes, the sample was transferred into a dialysis tube of 1000 kDa MWCO and dialyzed against 1 dm^3 of isotonic buffer at 4 °C for 12 h. This dialysis was repeated two times. The dialyzed erythrocytes were then washed with an equal volume of cold PBS three times. In Control 2, proteins were added but not encapsulated. The samples were prepared by mixing 7 parts of washed packed RBC with 3 parts of a 3 mmol dm^{-3} solution of the ^{15}N-labeled CAII, then 1 cm^3 of cell suspension was placed on a dialysis tube (12 kDa MWCO). The sample was dialyzed against 150 cm^3 of isotonic buffer at 4 °C with a rotation of around ∼20 rev/min for 180 min. The sample was then dialyzed against the same isotonic buffer at 37 °C under continuous stirring for 60 min. To wash away the nonencapsulated ^{15}N isotopically enriched protein, the sample was transferred into a dialysis tube of 1000 kDa MWCO and dialyzed against 1 dm^3 of isotonic buffer at 4 °C for 12 h. This dialysis was

repeated two times. The dialyzed erythrocytes were then washed with an equal volume of cold PBS three times.

3.2.6 Sample Preparation and NMR Measurements

All NMR experiments were recorded at 310 K on Bruker Avance NEO spectrometers, operating at 900 (CAII and ANSII) and 1200 (TTR) MHz, ^{1}H Larmor frequency (21.1 and 28.2 T, respectively), equipped with triple resonance cryoprobes. Experiments on encapsulated CAII were also performed on a Bruker Avance NEO spectrometer operating at 600 MHz, ^{1}H Larmor frequency (14.1 T), and equipped with a CPQCI cryoprobe. The NMR samples of the encapsulated proteins were prepared with 540 mm^3 of RBC suspension (in PBS buffer, pH 7.4) and 60 mm^3 of H_2O, for field frequency lock purposes. The spectra of the free proteins were recorded using the same parameters and buffer composition for comparison purposes. 2D ^{1}H–^{15}N SOFAST-HMQC experiments[58] were acquired with an HN offset of 8.1 ppm and an excitation HN bandwidth of 4 ppm, acquisition times of 35 ms (ANSII and CAII) or 20 ms (TTR) and 14 ms (ANSII and CAII) or 10 ms (TTR) for the direct and indirect dimensions, respectively, 256 scans (for the spectra recorded at 900 and 1200 MHz) and 1024 scans (for the spectra recorded at 600 MHz), and interscan delay of 0.2 s. The lower acquisition times used to record the spectra of TTR are related to its shorter transverse relaxation time, due to its high molecular weight and absence of deuteration. The experiments for the determination of ^{15}N transverse relaxation rates were recorded at 310 K and 600 MHz on ^{15}N-enriched samples of free CAII in PBS and CAII encapsulated in RBCs. ^{15}N transverse relaxation rates (R2) were measured using a Carr−Purcell− Meiboom−Gill (CPMG) sequence with delays of 8.48, 16.96, 25.2, 33.92, 42.4, 50.88, 67.84, 84.8, 101.76, 118.72, 144.16, 169.6 ms for the free protein and 8.48, 16.96, 42.4,84.8 and 144.16 ms for the encapsulated protein, with a refocusing delay of 450 μs. Because of the low signal-to-noise ratio, the spectra for the evaluation of ^{15}N transverse relaxation rates of the encapsulated protein were acquired using 1024 scans. Transverse relaxation rates were determined by fitting the signal intensities as a function of the delay to a single-exponential decay using Dynamics Center (Bruker) software. All the spectra were processed on a Bruker TopSpin 4.0 software package and analyzed with CARA program (ETH Zürich).

3.3 Monitoring PEG Shedding with NMR: Molecular Insight into LNP Stability

3.3.1 Materials

All reagents were purchased from common commercial sources and were used without additional purification. Dlin-MC3-DMA was purchased from Cayman Chemical. Distearoylphosphatidylcholine (DSPC), cholesterol and sucrose were purchased from Sigma Aldrich. DMPE-PEG2K was purchased from Avanti Polar. Ethanol was purchased from Merck. HyPure WFI quality water was purchased from Cytiva. Tris-HCl 1 M pH 8 and 10x PBS buffer pH 7.4 were purchased from Invitrogen. PD-10 desalting columns were purchased from Cytiva (cat. 17085101). Float-A-Lyzer G2 Dialysis Devices, Spectra/Por, MWCO: 100kDa were purchased from Repligen. 5 mm NMR tubes were purchased from Bruker. Anotop 25 filters 0.02 um were purchased from Whatman.

3.3.2 Formulation

Lipid nanoparticles were prepared through microfluidics using NanoAssemblr Ignite. The lipid compositions of the formulations analyzed, detailed in Table 1, were selected to replicate the formulation of Onpattro, the first approved RNA-LNP based drug, with slight modifications in lipid ratio due to further optimizations. The lipid solution was prepared by dissolving the lipids in ethanol, which was then mixed with the aqueous phase containing eGFP mRNA in a 75 mM citrate buffer at pH 4 to form the LNPs. A total flow rate of 12 mL/min and an organic to aqueous phase flow rate ratio of 1:2 was applied for the mixing. The resulting solutions were exchanged in the final formulation buffer that was either Tris-HCl 20 mM pH 8 with variable sucrose concentrations as cryoprotectant and PBS1x pH 7.4 through PD-10 desalting columns.

Preliminary analyses were performed in each sample to assess particle size distribution using Dynamic Light Scattering as the evaluation of the average particle size and their homogeneity is an indicator of a successful formulation.

Table 1: Lipid composition of tested LNP formulations	
Lipid	**% mol**
Dlin-MC3-DMA	40%
DSPC	10%
Cholesterol	48%
Pegylated Lipid*	2%

*Specified for each experiment

1% (w/w) DMPE-PEG2K solutions were prepared dissolving the powder in Tris-HCl 20 mM pH 8 buffer.

Dialysis of the LNP formulation was conducted to exchange the buffer from 20 mM Tris-HCl at pH 8 with 7.5% sucrose to PBS 1x at pH 7.4. This was achieved using a Float-A-Lyzer G2 Dialysis Device (Spectra/Por) with a molecular weight cut-off (MWCO) of 100 kDa. The process involved placing 1 mL of the formulation within the dialysis membrane and allowing it to float in 500 mL of PBS 1x at pH 7.4, agitated for 24 hours, with the buffer being exchanged three times.

For lyophilization, 600 µL of the LNP solution was loaded into 3 mL lyophilization vials (Muller) and dried using an Epsilon Martin Christ 2-10d LSC Plus lyophilizer. The lyophilized samples were then resuspended in the initial volume of 600 µL per vial with 20 mM Tris and varying amounts of sucrose.

3.3.3 PGSE NMR

^{1}H diffusion experiments were employed to monitor real time PEG forms in LNP formulations, exploiting the different diffusion rate of free PEG and LNP linked PEG. The method was based on the work of Wilson et al.[8] and refined for our purposes. The technique employed in our study is based on pulsed gradient spin-echo NMR, which enables the differentiation of signals from different species based on their diffusion coefficients. As shown in Figure 1, ranging from the minimum strength of gradient (2%) to the maximum (98%) signals are filtered according to their

diffusion rate. The signals close to the one arising from the PEG chain (3.60 ppm), indeed, disappeared because they belong to the fast diffusion excipients.

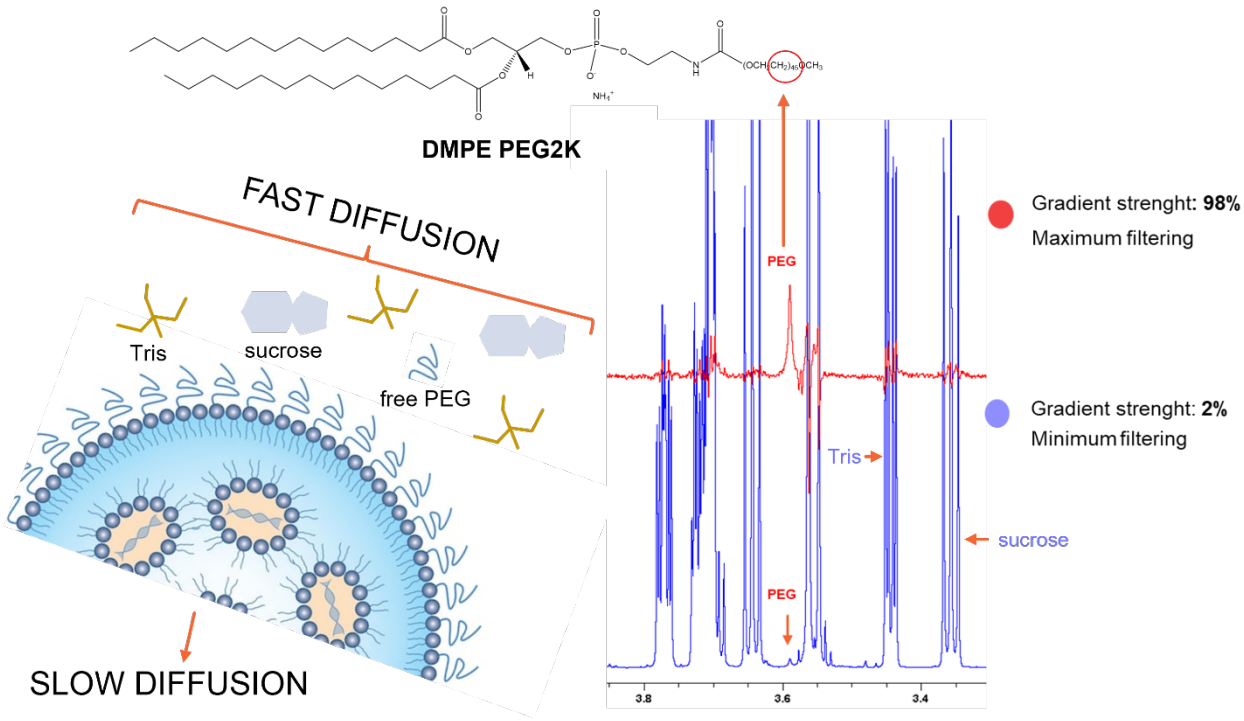

Figure 1. Application of diffusion filter to LNP full formulation. The signals associated with the small excipients are filtered out using the maximum gradient strength due to their rapid diffusion. The signals related to the slow-diffusing LNP, such as the PEG chain signal at 3.60 ppm, are minimally affected by the diffusion filter.

Specifically, the PEG signal is a combination of PEG linked to the LNP and potential freely dissociated PEG in solution. By applying selective pseudo 2D DOSY on this signal, we calibrated the diffusion pulse length and the gradient strength to obtain a decay of PEG integral signal at least up to 10% of the initial value to be representative of the whole population. Elaboration of data with Dynamics Center software provided the integral of PEG signal at each point of the gradient acquired (TD = 32, from 2% to 98%). Then GraphPad Prism software was employed to fit the curves depicting the decay of the integral of the signal, using Stejskal-Tanner equation[9] (Figure 2).

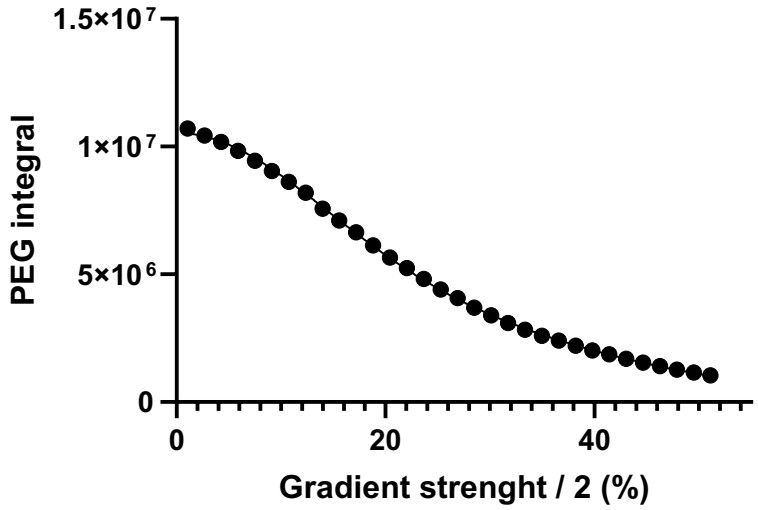

Figure 2. PEG integral curve decay under gradient diffusion filtering. For each sample, the acquisition parameters were set to reduce the PEG signal to at least 10% of its initial value, ensuring a complete decay profile. The integrals from 32 gradient points were calculated using Dynamics Center, and the resulting curves were plotted in GraphPad Prism for fitting.

Each sample was first analyzed using a one-component equation to verify if all the PEG was still linked to LNP, with a unique diffusion coefficient describing effectively the system. If the fitting resulted incomplete, two-component equation was employed. The two-component equation takes in account the PEG bound to PEG and the free PEG fraction.

Stejskal-Tanner equation (one-component):

$$I = I_0 \exp(-\gamma^2 G^2 \delta^2 D(\Delta - \delta/3))$$

Stejskal-Tanner equation (two-components):

$$I = I_0 [w1\exp(-\gamma^2 G^2 \delta^2 D1(\Delta - \delta/3)) + w2\exp(-\gamma^2 G^2 \delta^2 D2(\Delta - \delta/3))]$$

where:

- I = signal intensity with a gradient
- I_0 = signal intensity without a gradient
- γ = gyromagnetic ratio of the nucleus
- G = gradient strength
- δ = duration of the gradient pulse (little delta)
- D = diffusion coefficient

- Δ = the diffusion time (big delta)
- w = PEG form fraction

In this way it's possible to calculate the proportions of various PEG species, along with their corresponding diffusion coefficients, according to the best curve fit.

NMR experiments were recorded on a Bruker Avance III spectrometer operating at 900 MHz 1H Larmor frequency at 298 K. 50 µL of D_2O were added to 500 µL of each sample for the preparation of NMR tubes for field frequency lock purposes. To induce PEG shedding, an additional 50 µL of a BSA solution at 4.4 mM, prepared by dissolving 60 mg in 200 µL (MW = 68,000), was added to achieve a final concentration of 366 µM in the tube, comparable to serum levels.

Pseudo2D NMR experiments were acquired with the following parameters:

ledbpgppr2s; B° = 900 MHz; NS = 32 TD (F2) = 32768; TD (F1) = 32; P1 = 7.10 us; D1 = 3.75 s; RG = 101; T = 298 K Δ = 700 ms; δ = 4 ms

Processing with QSINE function, SSB = 3 to minimize line width and consequently PEG signal overlap.

3.3.4 DLS analysis

Free DMPE-PEG2K solutions were prepared at different concentrations to assess if PEG micelles were detectable and assess the size of free PEG. Solutions of DMPE-PEG2K 1% (w/w) and DMPE-PEG2K 10% (w/w) were prepared by dissolving the powder in water. The exact Critical Micellar Concentration for this lipid was not found in literature but for the homologous DSPE-PEG 2000 is reported to be between 0.5–1 µM, way far below a concentration of 1% (w/w) which corresponds to 3.5 mM (MW = 2790 Da)[10]. So, we believe it's reasonable that the pegylated lipid forms micelle at the analyzed concentration.

Then an LNP formulation containing DMPE-PEG2K was analyzed before and after 13 hours since the addition of BSA, reproducing the NMR conditions, with a final concentration of BSA 366 µM. LNP samples were diluted 100x in HyPure WFI quality water previously filtered with Anotop 25 filters 0.02 µm for analysis. Experiments were recorded using DLS Zetasizer ULTRA Malvern,

loading 80µL of each sample in the BRAND™ UV Disposable Cuvettes. Measurements were performed in triplicate, with a controlled temperature of 25°C and equilibration time of 120 s.

3.3.5 NTA analysis

The same 1% PEG solution and LNP formulations before and after addition of BSA tested with DLS were analyzed.

LNP samples were diluted 1:5000 with HyPure WFI quality water previously filtered with Anotop 25 filters 0.02 µm for analysis.

The analysis was performed in three replicates on NanoSight NS300. The samples were measured for 60 s at 20 °C (RT) using a blue laser (488 nm), sCMOS camera and under a constant syringe pump speed of 50 (arbitrary units). Data were analyzed using NTA 3.4 Build 3.4.4 software, with a detection threshold of 5 or 6 depending on the sample. The capillary was cleaned after each sample by injecting 1 mL of HyPure WFI-quality water and removing any bubbles by introducing air.

3.3.6 Cryo-EM analysis

The same LNP formulations were analyzed before and after 13 hours from the addition of BSA as done with the other techniques, using 4 µL of samples for each analysis.

A solution of 4 uL of LNPs (total lipid concentration = 2 mg/mL) was applied on Quantifoil Cu R2/2 300 mesh carbon grids (Quantifoil) previously glow discharged at 15 mA for 10 seconds using a PELCO easiGlow™ system (Ted Pella Inc.). Excess of LNP solution was blotted out for 5 seconds and grid was plunged-frozen in liquid ethane at -180°C using EM-GP (Leica Microsystems). Subsequentially, grids were transferred to a Simple Origins Dual Grid Cryo Transfer Holder Model 205 (Simple Origins) maintained at -180°C and inserted into a Talos L120C (ThermoFisher Scientific) with an accelerating voltage of 120 kV. Images were recorded at 22,000X and 45,000X magnification using a Ceta M 4k camera (ThermoFisher Scientific) with a dose rate of ~22 e-/A^2 under a defocus ranging from -4 to -7 µm.

4 Results and Discussion

4.1 Enhancing Lipid Quantification in Liposomes with NMR methods

In this work we aimed to enhance lipid quantification in liposome using NMR methods, as crucial quality control for batches and as a tool for improvement of drug product manufacturing. The study demonstrated the accuracy and reproducibility of NMR methods using both internal or external standard (PULCON), by testing lipid mixtures at known concentration. Various liposome formulations were analyzed to identify potential losses during microfluidic formulation. By performing this analysis using a UPLC-ELSD method, the study highlights the advantages of NMR, including faster acquisition times and the possibility to use only one reference, without the need for calibration curves for all tested molecules.

I contributed by designing the methods, performing all the experimental activities (except for the UPLC-ELSD analysis, for which I provided support), and writing the paper.

The study was published in *Omega ACS* and is reported in this section.

Currò, F., Eguskiza, A., Cerofolini, L., Martini, S., Biagini, M., Stranges, D., Fragai, M., & Denis, M. Fast and Straightforward Lipid Quantification in Pharmaceutical Compositions Using NMR. *ACS Omega*. (2025) DOI: 10.1021/acsomega.5c09329

ACS OMEGA

Open Access

http://pubs.acs.org/journal/acsodf

Article

Fast and Straightforward Lipid Quantification in Pharmaceutical Compositions Using NMR

Francesco Currò, Ander Eguskiza, Linda Cerofolini, Silvia Martini, Massimiliano Biagini, Daniela Stranges, Marco Fragai, and Maxime Denis*

Cite This: https://doi.org/10.1021/acsomega.5c09329

Read Online

ACCESS | Metrics & More | Article Recommendations | Supporting Information

ABSTRACT: Liposomes are versatile nanoscale delivery systems used extensively in pharmaceuticals. Accurate quantification of lipids in liposome formulations is critical for ensuring the product quality and efficacy. This study evaluates the use of NMR spectroscopy applied to lipid quantification within liposomes. The investigation focused on lipids commonly found in liposomal products and other lipid-based delivery systems, such as DSPC, DOPC, cholesterol, and DMPE-PEG2K. Lipid quantification was performed using both an internal reference and an external standard through PULCON (pulse length-based concentration determination) methods. Both methods showed high accuracy, precision, and reproducibility. Additionally, the PULCON NMR technique offered enhanced consistency and faster analyses, making it particularly suitable for industrial needs involving rapid analysis across numerous samples. The quantification of liposome solutions was also conducted using a UPLC-ELSD method for a comparison of the two techniques. These findings support the refinement of rapid, accurate lipid quantification methods, essential for quality control in large-scale manufacturing processes and optimizing the drug product formulation process.

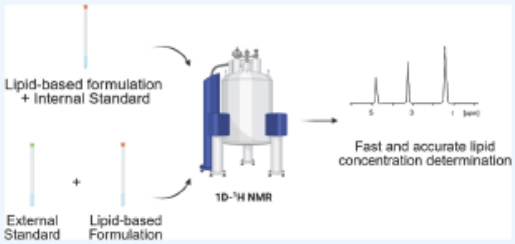

INTRODUCTION

Liposomes are spherical vesicles composed of one or more phospholipid bilayers that allow the encapsulation of both hydrophilic and hydrophobic substances. Over the years, liposomes have found numerous applications in the fields of drug delivery, cosmetics, and medical diagnostics.[1−4] Their versatility, tunable physicochemical properties, and ability to mimic biological membranes make them ideal vehicles for targeted therapeutic delivery, enhancing the efficacy, and reducing the side effects of drugs. Notably, they are employed in anticancer treatments, with marketed examples such as Doxil (liposomal doxorubicin) and Myocet (nonpegylated liposomal doxorubicin), both used for treating various types of cancer, including metastatic breast cancer.[5−7] In the realm of antifungal treatments, liposomal formulations are used for amphotericin B delivery, with notable examples being Nomex Liposome and AmBisome.[8−10] Additionally, liposome application extends beyond pharmaceuticals to the field of vaccines. For instance, AS01 is used as an adjuvant to boost immune responses in vaccines for malaria and shingles.[11−13]

Lipid composition in liposomes is a key determinant in the effectiveness of cargo encapsulation and release, as well as in the stability and potency of the formulation, and is often considered a critical quality attribute (CQA) under the Quality by Design Framework.[14−16] The initial concentration of lipids may differ from that of the final product due to potential losses during the multiple steps required for the formulation (such as mixing, filtration, centrifugation, etc.). Accurately quantifying these losses with a precise and rapid method can aid in formulation optimization and support large-scale process development.[17−19] Additionally, degradative processes such as hydrolysis and oxidation can significantly alter the phospholipid membrane properties (e.g., permeability) and lead to the loss of encapsulated material.[20−23] Thus, implementing analytical methods that allow for accurate and rapid quantification of lipids in the final product is essential for both quality control and optimization of preparation processes to minimize losses.

Lipid-based systems have historically posed analytical challenges due to the limited presence of functional groups that differentiate individual lipids, which primarily share a hydrocarbon backbone. The traditional colorimetric molybdate method to quantify phospholipids is still frequently used. Despite its high sensitivity, the method is error-prone and naturally cannot be applied to nonphosphorus lipids.[24,25] In recent years, alongside the development of mass spectrometry

Received: September 15, 2025
Revised: October 16, 2025
Accepted: October 20, 2025

https://doi.org/10.1021/acsomega.5c09329
ACS Omega XXXX, XXX, XXX−XXX

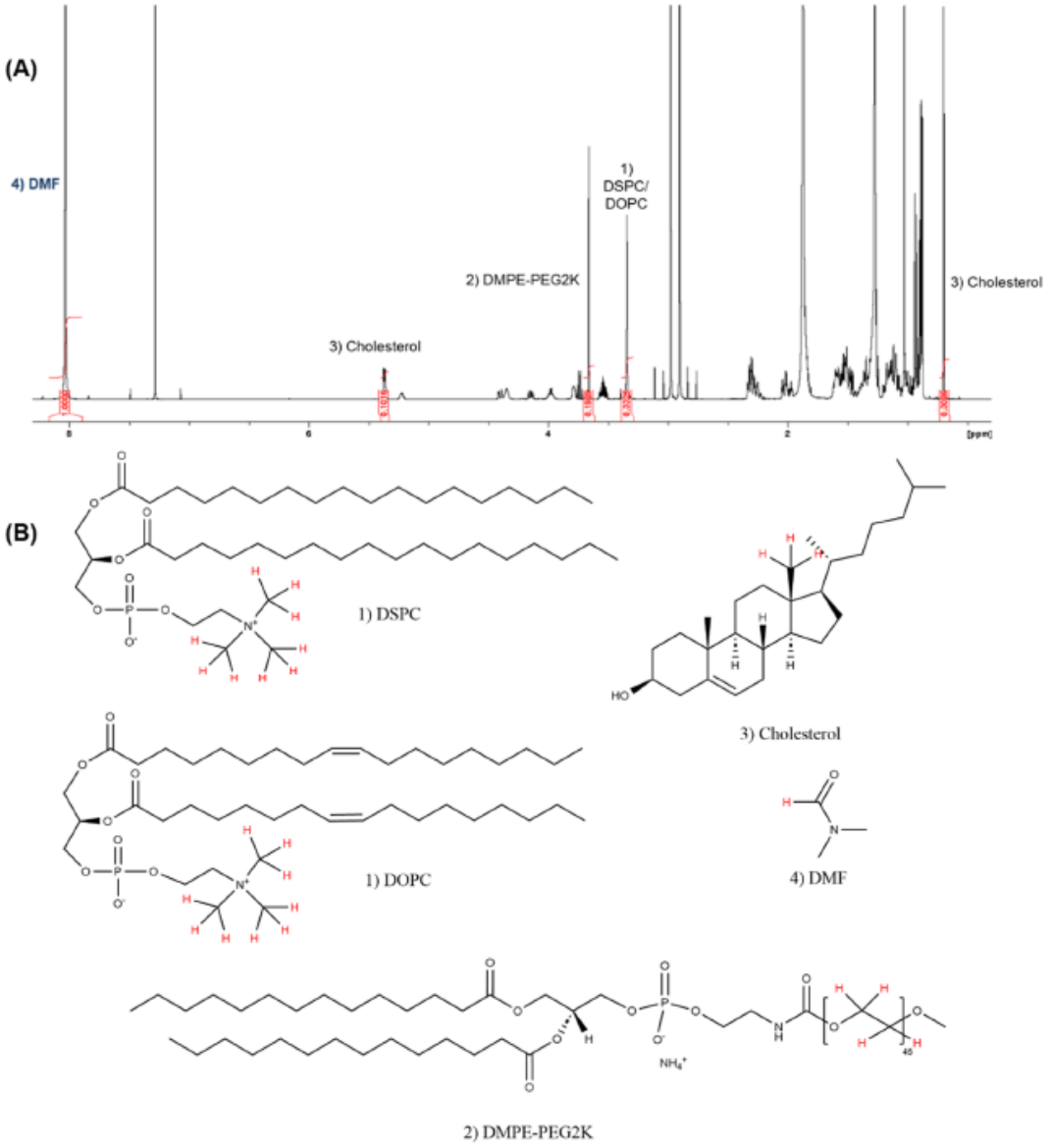

Figure 1. NMR signals of lipids used for the integration. (A) 1D ^{1}H NMR spectrum of a standard lipid mix solution, containing DSPC, cholesterol, and DMPE-PEG2K; the integrals of the signals used for quantification across all tested samples are displayed in red. Each signal was identified based on individual lipid spectrum recordings and chemical shift predictions using ChemDraw Professional software and literature refs 45 and 46. (B) The signals used for the integration of each component are highlighted in the molecular structures: (1) the 9 *N*-methyl protons for DSPC, which share the same chemical shift as DOPC when present, resonating at 3.35 ppm; (2) the 180 protons from the repeating units of PEG (–[–O–CH_2–CH_2–]–) in DMPE-PEG2K at 3.66 ppm; (3) the 3 protons of the methyl group at 0.69 ppm for cholesterol; and (4) the aldehydic proton of the standard reference DMF, integrated at 8.03 ppm.

methods, chromatography techniques have gained importance, particularly those using charged aerosol detection (CAD) and evaporative light scattering detection (ELSD).[28−29] These techniques do not require a chromophore, which is typically absent in lipids, as occurs for UV−vis detection.

Nuclear magnetic resonance (NMR) is widely used for quantifying pharmaceutical components due to its atomic resolution, which allows us to solve the complexity of mixtures, analyzing single components without overlaps.[30−32] Solution NMR has been utilized to study liposomes, focusing on various

https://doi.org/10.1021/acsomega.5c09329
ACS Omega XXXX, XXX, XXX−XXX

Table 1. Summary of NMR Results for DSPC, Cholesterol, and DMPE-PEG2K Standard Solutions across Different Concentrations

lipid	theoretical (mg/mL)	experimental (mg/mL)	recovery %[a]	% RSD replicates (%)[b]
DSPC	10.28	10.15	98.8	2.6
DSPC	1.03	1.00	97.5	5.2
DSPC (PULCON)	1.03	1.02	99.2	0.6
DSPC	0.100	0.095[c]	95.0	8.0
cholesterol	5.56	5.40	97.1	3.0
cholesterol	0.56	0.53	94.9	2.8
cholesterol (PULCON)	0.56	0.53	95.0	1.6
cholesterol	0.054	0.031[c]	52.4	6.2
DMPE-PEG2K	2.34	2.15	92.0	2.1
DMPE-PEG2K	0.23	0.22	95.6	1.9
DMPE-PEG2K (PULCON)	0.23	0.22	95.6	3.0
DMPE-PEG2K	0.023	0.021[c]	91.3	0.2

[a]The ratio of experimental to theoretical concentrations, expressed as a percentage. [b]The ratio between the standard deviation and the mean, expressed as a percentage, calculated from the three replicates of each sample. [c]An additional decimal is retained because omitting it would have yielded excessive approximations for the lowest concentrations, inconsistent with the uncertainty of the method.

key features, supported by well-established knowledge of the assignment of lipids commonly used in formulations.[33−38] Franz et al. already showed the feasibility of using NMR for lipid quantification in liposomes through ^{1}H and ^{31}P experiments using triphenyl phosphate (Ph_3PO_4), tritolyl phosphate (Tol_3PO_4), and triphenylphosphine oxide (Ph_3PO) as references.[33] This study aims to refine NMR methods for lipid quantification tailored for industrial applications, seeking faster and reproducible analyses through the comparison with a more standard ultraperformance liquid chromatography coupled with the evaporative light scattering detection (UPLC-ELSD) method. The method presented herein aims to be versatile across various lipid delivery systems, testing formulations that are prepared by mimicking commercial products. The investigated lipids are typical lipids found in liposome formulations. Specifically, it involves phospholipids (e.g., DSPC, DOPC), which facilitate the interface between lipid and aqueous phases; cholesterol, which modulates interaction with cellular membranes; and PEGylated lipids (e.g., DMPE-PEG2K), which control particle size and circulation via the "stealth effect", thereby preventing premature clearance by the immune system.[1,2,39,40] Liposomes were prepared using microfluidics, a method that has gained popularity for its practicality, high encapsulation efficiency, and applications in the formulation of liposomes and lipid nanoparticles (LNPs).[40−43] Developing a fast and precise method to measure lipid concentrations throughout the manufacturing process enables the evaluation of potential losses during formulation. Additionally, it supports the optimization of production processes to maintain the expected concentration levels of components in the formulations. NMR offers a distinct advantage over chromatography and mass spectrometry by providing a direct correlation between the signal intensity and the molar concentration of nuclei for each component. This eliminates the need for analyte calibration curves, which are essential for chromatography and mass spectrometry. It is sufficient to utilize a reference standard compound of known concentration that does not interfere with the analyte and is miscible in the solution under analysis, enhancing both the speed and reproducibility of analyses. The reference standard can be internal (mixed with the analyte in the NMR tube) or external (in a separate NMR tube). The use of an external reference compound for NMR quantification was explained first by Wider et al., referring to the method as pulse length-based concentration determination (PULCON).[41] This technique does not require the addition of an internal standard directly into the sample mixture, which is advantageous when a standard may interfere with the sample or is impractical to use. In addition, once a reference tube is prepared at an exact concentration and analyzed to measure its proton signal integral, it is possible to quickly analyze multiple batches, eliminating the variability associated with the addition of a reference to each tube and saving considerable time. To the best of our knowledge, this method has not been tested for lipid quantification in complex mixtures so far.[42−44] In our study, we demonstrated its applicability and highlighted its benefits for this purpose in comparison to the NMR analytical method, which uses an internal standard.

Finally, the proposed method has been compared to a protocol optimized for lipid quantification using UPLC-ELSD. Comparing NMR to UPLC methods, which are commonly used and well-established in the industry for similar applications, provides a comprehensive evaluation of the advantages and limitations of each technique, enabling more informed decision-making about their suitability for specific applications.

RESULTS AND DISCUSSION

NMR Quantification of Single Lipid Solutions. A well-resolved specific signal for each lipid that could be used for integral analysis also in the spectrum of liposomes was selected. The chosen signals and the corresponding assigned proton are indicated in Figure 1. Three tubes from the same stock were analyzed to assess the variability of the NMR tube preparation and the analysis itself. Additionally, investigating three different concentrations allowed us to identify the range in which the method responds linearly and to determine the detection limit for accurate analysis. The intermediate concentration analyzed for each lipid is on the same order of magnitude as the one the lipid has in the prepared liposomes. Standard single lipid solutions were analyzed by performing triplicate measurements of each of the investigated concentrations, always adding the same quantity of DMF reference in each tube. The same analysis was also performed using the PULCON method to compare the two techniques for this application. The PULCON method is based on the reproducibility of the NMR signal as a function of analyte concentration to quantify an analyte in an NMR tube using a separate NMR tube for reference. All the parameters

https://doi.org/10.1021/acsomega.5c09329
ACS Omega XXXX, XXX, XXX−XXX

Table 2. Summary of NMR Results for Lipid Mixtures Tested with the Internal Standard Method

lipid mix	lipid	theoretical (mg/mL)	experimental (mg/mL)	recovery %[a]	% RSD replicates[b] (%)
(A) DSPC/Chol (2:1)	DSPC	1.11	1.08	97.3	8.0
	cholesterol	0.56	0.54	96.4	6.0
(B) DSPC/Chol/DMPE-PEG2K (10.5:14.2:1)	DSPC	1.05	1.03	98.1	6.7
	cholesterol	1.42	1.39	97.9	3.9
	DMPE-PEG2K	0.100	0.098[c]	94.2	9.1
(C) DOPC/Chol (4:1)	DOPC	2.96	2.98	100.7	8.0
	cholesterol	0.76	0.72	94.7	6.0

[a]The ratio of experimental to theoretical concentrations, expressed as a percentage. [b]The ratio between the standard deviation and the mean, expressed as a percentage, calculated from the three replicates of each sample. [c]An additional decimal is retained because omitting it would have yielded excessive approximations for the lowest concentrations, inconsistent with the uncertainty of the method.

Table 3. Summary of NMR Results for Lipid Mix (D) Obtained with the PULCON Method

lipid mix	lipid	theoretical (mg/mL)	experimental (mg/mL)	recovery %[a]	% RSD replicates (%)[b]
(D) DSPC/Chol/DMPE-PEG2K (54.6:83.5:1)	DSPC	3.71	3.73	99.7	2.0
	cholesterol	5.67	5.78	98.2	0.3
	DMPE-PEG2K	0.0679	0.0677[c]	99.4	1.7

[a]The ratio of experimental to theoretical concentrations, expressed as a percentage. [b]The ratio between the standard deviation and the mean, expressed as a percentage, calculated from the three replicates of each sample. [c]An additional decimal is retained because omitting it would have yielded excessive approximations for the lowest concentrations, inconsistent with the uncertainty of the method.

such as temperature, pulse calibration, and relaxation delay that directly influence the signal intensity and integration accuracy are taken into account for concentration determination by comparing integrals of analyte and reference in two separate tubes, allowing for the use of an external standard (refer to the "Methods" section for the equation). The reference integral of DMF was determined by averaging the measurements from three tubes, each prepared at a concentration of 36.796 mM.

Table 1 summarizes the results, showing the concentration calculated from the mean of three replicates and the corresponding percentage of relative standard deviation (% RSD) to express the variability of the method among replicates. Additionally, the recovery value, expressed as the percentage of the experimental concentration relative to the theoretical concentration, serves as an indicator of the method accuracy in each case.

For each lipid, a different level of accuracy and precision was obtained, and it has been summarized as follows:

- DSPC: the experimental concentrations were in good agreement with the theoretical values throughout the tested range. As expected, variability among replicates increases with decreasing concentration. Determination with PULCON at 1.03 mg/mL concentration demonstrated excellent accuracy as well, accompanied by even lower variability among replicates, highlighting the advantage of this method in terms of consistency.
- Cholesterol: experimental values close to the theoretical ones, with low variability between replicates, were obtained at concentrations of 5.56 and 0.56 mg/mL. These results were consistent across both internal and external standard methods. However, for the solution with the largest dilution of cholesterol (0.054 mg/mL), a value nearly half of what was expected was obtained. The discrepancy between the experimentally calculated concentration and the theoretical one is likely due to the weak signal intensity. However, it is possible to proceed to liposome analysis with sample concentrations higher than 0.56 mg/mL, which is typically the case for pharmaceutically relevant liposomes. Sufficiently accurate and precise results were, indeed, obtained above this concentration without needing to increase the number of scans or the acquisition times, which would have improved the signal-to-noise ratio and the accuracy for low concentrations.
- DMPE-PEG2K: the method exhibited good linearity even at the concentration of 0.023 mg/mL, thanks to the high number of protons (180) composing the polymeric repeating unit, which led to an intense NMR signal. Recovery values ranged from 91% to 95%, slightly lower than those observed for other lipids. However, considering the minimal absolute differences in concentration between theoretical and experimental values, these discrepancies do not impact the purpose of the analysis. It is important to note that the molecular weight of commercial pegylated lipids provided by the supplier is an average value due to the polydispersity of PEG. Therefore, calculating molarity concentrations requires careful consideration.

Overall, the experimental concentrations closely matched the theoretical values, though they tended to be slightly lower, possibly due to the purity of the materials.

NMR Quantification of Lipid Mixtures. Quantification of lipid concentrations was also performed on lipid mixtures with the same lipid composition used for liposome preparation to further confirm that the lipids can be analyzed simultaneously. The results are reported in Table 2. The recovery values for all lipids in the investigated mixtures range from 94.2% to 100.7% with an average % RSD equal to 6.8%, indicating accurate and precise quantification. This demonstrates that the simultaneous presence in solution of different lipids, mimicking liposome composition, does not impair the efficiency of the analysis.

With the aim of comparing the quantification using an internal or external standard compound, the lipid mix (D) was prepared to test the PULCON method. The same signals used for lipid integration with the method of an internal standard were employed here. As shown in Table 3, the experimental concentrations are in agreement with the theoretical values. Moreover, the variability among the replicates is very low,

https://doi.org/10.1021/acsomega.5c09329
ACS Omega XXXX, XXX, XXX−XXX

Table 4. Analysis of Liposome (A−C) Solutions with NMR

liposomes	lipid	theoretical concentration (mg/mL)	experimental concentration (mg/mL)	recovery %[a]	NMR mass ratio[c]
(A) DSPC/Chol (2:1)	DSPC	1.20	1.13	94.2	1.9
	cholesterol	0.60	0.62	103.3	1.0
(B) DSPC/Chol/DMPE-PEG2K (10.9:14.6:1)	DSPC	1.09	1.00	91.7	10.5
	cholesterol	1.46	1.31	89.7	13.6
	DMPE-PEG2K	0.100	0.0096[b]	96.0	1.0
(C) DOPC/Chol (4:1)	DOPC	3.18	2.98	93.7	3.9
	cholesterol	0.79	0.76	95.9	1.0

[a]The ratio of experimental to theoretical concentrations, expressed as a percentage. [b]An additional decimal is retained because omitting it would have yielded excessive approximations for the lowest concentrations, inconsistent with the uncertainty of the method. [c]The experimental NMR mass ratio of the lipids in each formulation.

demonstrating the advantageous reproducibility of this method. Overall, the outcome matched that of the standard method, demonstrating that both approaches are fit-for-purpose for accurate quantification.

NMR Quantification of Liposomes. Liposomes with the same lipid composition analyzed in the previous section were formulated. Successful liposome formulation was confirmed by using dynamic light scattering (DLS) analysis (Table S1). To avoid quantification inaccuracies due to the rapid relaxation of high molecular weight liposomes or lipid micelles in water, liposome solutions were dried and resuspended in $CDCl_3$ for liposome disruption prior to analysis. The experimental concentrations obtained with NMR are compared to the theoretical concentrations of the formulation and are presented in Table 4. Theoretical liposome concentrations are calculated under the assumption that no losses occurred during preparation. The experimental analysis aimed to evaluate whether such losses happened. For all formulations, the experimental concentrations were below the theoretical values, indicating losses during the formulation steps. However, the recovery ranges between 89% and 99%, suggesting that the extent of the losses was low, demonstrating good efficiency of the manufacturing process.

Comparison of NMR and UPLC Performance in Lipid Quantification. UPLC analysis of a lipid mixture containing DSPC, cholesterol, and DMPE-PEG2K, at concentrations on the same order of magnitude as those tested with NMR, was first performed to assess the accuracy of the method using known concentrations. Experimental concentrations were in good agreement with theoretical values with deviations within 5% of the total (Table S2).

Lipid quantification of liposomes was conducted both on the solutions immediately after formulation and following the drying and resuspension steps required for NMR analysis. No significant variations were observed between the two conditions, indicating that no loss of material occurred during the drying and resuspension processes (Table S3).

The results obtained by UPLC-ELSD were compared with those of NMR on the same samples, and the recovery values are shown in Figure 2. The theoretical concentrations were calculated under the assumption that no lipid losses occurred throughout all formulation steps. The experimental concentrations derived from both NMR and UPLC-ELSD showed notable but slight differences, within a 7% variance, except for DSPC in liposomes (A), which shows a 10% difference. For liposomes (A) and DSPC in liposomes (B), the experimental values range between values near to 100% of the recovery. For the other components in liposome formulations (B) and (C), there is a good agreement between the two techniques with experimental concentrations being lower than theoretical values, confirming potential modest losses during the formulation process.

Overall, both NMR and UPLC-ELSD methods have demonstrated high accuracy and precision, yielding experimental concentration values close to theoretical values in standard solutions with low variability among replicates. However, there are differences between the methods that should guide the choice of technique on a case-by-case basis. The main advantages of NMR lie in the use of a single reference compound as opposed to the time-consuming UPLC requirement of the calibration curve construction with each lipid of interest. NMR signal integrals are intrinsically proportional to the concentration of the nucleus under examination and rely on a standard (DMF in this work), which can be changed as long as it ensures a high degree of purity, chemical compatibility, and an isolated chemical shift and is paired with a sufficiently long interscan delay to ensure complete relaxation of the protons in both the reference and the samples. The advantage of using a single standard potentially applicable to the analysis of all lipids eliminates the need for highly pure certified standards for each lipid analyzed, which can be demanding in terms of both cost and effort, especially in early development phases. Additionally, as we have demonstrated, the use of an external reference with the PULCON method presents significant benefits; indeed, using an external standard abrogates the manipulation and variability associated with the introduction of an internal standard. Moreover, a single NMR tube containing the reference can be used for the quantification of lipids across different formulations in a single session. On the other hand, UPLC-ELSD offers advantages primarily related to sensitivity. Indeed, we observed a decrease in NMR accuracy for cholesterol concentrations close to 0.05 mg/mL, although this issue could be partially mitigated by increasing the number of scans at the cost of longer acquisition times. However, the sensitivity issue does not affect the pegylated lipid using NMR due to the enhanced signal from the repeating protons along the polymer. UPLC faces challenges when approaching the detection limit at the tested concentration of 0.10 mg/mL. Moreover, although UPLC-ELSD does not necessarily require liposomes to be disintegrated prior to injection into the column, drying and dissolving them in an organic solvent such as $CDCl_3$ was essential for NMR analysis. This step ensured that no supramolecular lipid structures formed, which could otherwise lead to quantification inaccuracies due to fast relaxation of protons and broadening of signals.

https://doi.org/10.1021/acsomega.5c09329
ACS Omega XXXX, XXX, XXX−XXX

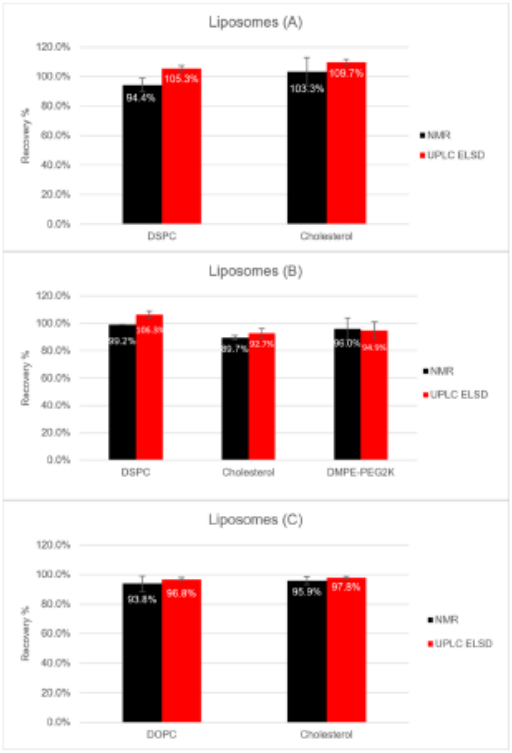

Figure 2. NMR vs UPLC-ELSD lipid recovery. The percentage recovery of each component of liposome formulations is shown, indicating the experimental concentration as a percentage of the theoretical concentration (i.e., the expected lipid concentration in the absence of loss). The results obtained using NMR (displayed with black bars) and UPLC-ELSD (displayed with red bars) are compared. Error bars represent the relative standard deviation among the replicates. For liposomes (A), DPSC showed the highest difference between NMR and UPLC-ELSD results, with values close to theoretical concentrations, while for cholesterol, the experimental concentration was slightly higher than the theoretical value with both techniques. Overall, the findings suggest no significant losses over the formulation. DSPC in liposomes (B) is close to theoretical values with both techniques. For the other components in liposome formulations (B) and (C), the two techniques show a good agreement, with experimental concentrations being lower than the theoretical values. This suggests that there may be modest losses occurring during the formulation process.

CONCLUSIONS

We demonstrated the successful application of NMR spectroscopy for lipid quantification in liposomal formulations. By using DMF as an internal standard, the method exhibited high levels of accuracy, precision, and reproducibility. Concurrently, the PULCON NMR method delivered results consistent with the standard approach, demonstrating enhanced reproducibility due to the use of a single common external reference. This streamlined approach is particularly advantageous for industrial applications that require rapid analysis of numerous batches. Notably, quantitative NMR benefits from the ease of access to commercially available standards. Only a single compound can be employed as a universal standard to quantify all lipid species, simplifying the analytical workflow in comparison to chromatographic methods.

This study focused on DSPC, DOPC, cholesterol, and DMPE-PEG2K as model lipids, which represent typical components of liposomal formulations. However, the developed methodologies are adaptable to other lipids by identifying isolated representative peaks for integration during quantification. The compatibility of the method with other classes of biomolecules present in the formulations, such as cargo, should be verified by ensuring that there is no significant overlap between the signals of these molecules and those used for the integration of lipids.

Comparative analyses with UPLC-ELSD revealed that both techniques are highly effective and accurate for lipid quantification in liposomes, with each method offering distinct advantages. The choice between NMR and UPLC-ELSD should be guided by the specific composition and concentration of the lipids being analyzed. When feasible, the combination of these techniques provides a more comprehensive and robust analytical framework.

Additionally, this method, optimized here for liposomes, can be readily applied to other lipid-based delivery systems, such as lipid nanoparticles. These nanoparticles, which often contain similar lipid compositions, are gaining significant attention as vehicles for mRNA-based vaccine delivery, further underscoring the versatility and relevance of the methods described for the broader pharmaceutical industry.

METHODS

Materials. All reagents were purchased from common commercial sources and were used without additional purification. Distearoylphosphatidylcholine (DSPC), cholesterol, 1,2-dioleoyl-*sn*-glycero-3-phosphocholine (DOPC), and chloroform-d 99.8% atom enrichment were purchased from Sigma-Aldrich. DMPE-PEG2K was purchased from Avanti Polar. Ethanol was purchased from Merck. HyPure WFI quality water was purchased from Cytiva. *N*,*N*-Dimethylformamide anhydrous 99.8% (DMF) and trifluoroacetic acid (TFA) were purchased from Sigma-Aldrich. Isopropanol was purchased from Carlo Erba.

All the volumes with $CDCl_3$ as a solvent were handled with glass Hamilton precision syringes of 1 mL, 500 μL, and 100 μL capacity. Plastic pipet tips were not used because of potential plasticizer leaks.

Caution! $CDCl_3$ is a volatile halogenated solvent that is recognized as potentially carcinogenic and poses significant health risks upon inhalation or skin contact in addition to potential environmental impacts. Similarly, DMF is a polar aprotic solvent known for its reproductive toxicity and other health hazards. Both chemicals must be handled in a well-ventilated fume hood with appropriate personal protective equipment.

Lipid Standard Preparation. Solutions of each lipid at a known concentration were prepared in $CDCl_3$. DOPC was not considered in this step since the functional group used for the integration of its signal is the same as that of DSPC, without differences in chemical shift and intensity. Solutions were vortexed to ensure the complete dissolution of lipids. Each lipid was analyzed at three concentrations: (i) the concentration of the stock solution and (ii) after 1:10 and (iii) 1:100 dilutions. The intermediate concentration for each lipid was on the same order of magnitude as the lipid concentration in the final liposome formulation. Lipid mix solutions were prepared,

https://doi.org/10.1021/acsomega.5c09329
ACS Omega XXXX, XXX, XXX−XXX

Table 5. Lipid Composition of Liposome Formulations and Mixing Parameters

liposome	lipid composition (w/w)	DSPC or DOPC concentration (mg/mL)	cholesterol concentration (mg/mL)	DMPE-PEG2Kconcentration (mg/mL)	flow rate ratio (AP/OP)[a]	total flow rate (mL/min)
(A)	DSPC/cholesterol (2:1)	1.20	0.60	N/A	3:1	10
(B)	DSPC/cholesterol/DMPE-PEG2k (10.9:14.6:1)	1.09	1.46	0.1	2:1	10
(C)	DOPC/cholesterol (4:1)	3.18	0.79	N/A	2:1	2

[a]AP = aqueous phase and OP = organic phase.

aiming to prepare mixtures representative of the composition and concentration of each liposome formulation analyzed. Refer to Tables S5−S8 for detailed preparation.

Liposome Solution Preparation. Liposomes were prepared by using microfluidic mixing with the NanoAssemblr Ignite nanoparticle formulation system. For each liposome formulation, the organic and aqueous phases were prepared as detailed in Table 5. Lipids were dissolved in ethanol for the organic phase, while PBS pH 7.4 was used for the aqueous phase.

The resulting mixtures appeared as clear solutions, with the liposome (C) exhibiting a more opaque, whitish appearance likely due to its higher concentration. Each formulation was exchanged with Hypure WFI quality water using PD10 columns to remove ethanol.

Liposomes must be disrupted to enable accurate NMR quantification, free from proton relaxation issues caused by their large size. For each liposome solution, 800 μL was placed into glass vials, prepared in four replicates, two for NMR and the other pair for UPLC analysis. The resulting 12 vials, along with two additional vials each containing 800 μL of H_2O as controls, were placed in a SpeedVac set to 45 °C at a pressure of 1 mTorr for 3 h. At the end of this process, all water had evaporated, leaving only the dried lipid residue in the liposome vials. Finally, the content of each vial was resuspended in 800 μL of $CDCl_3$ for NMR analysis.

NMR Sample Preparation. DMF was chosen as an internal reference due to its inertness, miscibility in organic solvents, and the fact that its chemical shift occurs in a spectral region where no other proton resonates. A pure (>99.5%) DMF solution was diluted to achieve a concentration in the tube comparable to that of lipids, aiming for a similar signal-to-noise ratio. The dilution process was designed to ensure that the addition of DMF constituted roughly 10% of the total volume in the NMR tube and to avoid many dilution steps to reduce the risk of imprecision. Specifically, 40 μL of DMF solution (MW = 73.09, density = 0.944 g/mL) was diluted to a total volume of 1.040 mL in $CDCl_3$ to achieve a final concentration of 497 mM. Each NMR tube (Wilmad, 5 mm, 500 MHz precision) was filled with 500 μL of the analyzed solution and 40 μL of a 497 mM DMF solution, resulting in a final DMF concentration of 36.796 mM. In contrast, for the PULCON method, the analyte tubes were prepared by adding 540 μL of the sample solution in $CDCl_3$, while the reference tubes were prepared by adding 40 μL of the DMF solution and 500 μL of $CDCl_3$ to achieve the same DMF concentration of 36.796 mM.

NMR Measurements. All NMR experiments were recorded at 298 K on a Bruker AVANCE NEO spectrometer, operating at 500 MHz, ^{1}H Larmor frequency, and 11.7 T, equipped with a quadrupole resonance QCI H/P/C/N Cryoprobe. For each sample, the following procedures were applied: locking to $CDCl_3$, manual matching and tuning, shimming, optimization of the ^{1}H pulse, and automatic receiver gain optimization. 1D ^{1}H zg experiments were acquired using 16 scans, 64 K data points, an offset of 4.674 ppm, and an acquisition time of 4.2 s. To correctly evaluate the interscan delay, 1D ^{1}H experiments were performed, gradually increasing such a delay. An interscan delay of 35 s was found sufficient to allow complete spin relaxation, since no increase in signal intensity was observed for longer delays.

NMR Spectra Analysis. All of the spectra were processed with a Bruker Topspin 3.5pl6 software package. Fourier transformation with an exponential function with line broadening equal to 5.00 Hz was used to process all of the spectra, followed by manual phase optimization and baseline correction. Integration of the signals of interest was performed in manual mode. For each lipid, one well-solved specific signal was identified recording the spectra of the single lipids (Figure S1) and integrated for the quantification, while the well-solved aldehyde proton peak of DMF was chosen for the integration of the reference (Figure 1). Equation 1 was applied for lipid quantification using the method with an internal standard:

$$[\text{Lipid}] = \left(\frac{\text{Ilipid}}{\text{IDMF}}\right)/n\text{Hlipid} \times 36.796 \times (540/500) \quad (1)$$

The unknown concentration of the lipid is calculated from the ratio of the specific integral of the lipid (Ilipid) and the integral of the aldehyde proton of DMF (IDMF) divided by the number of protons contributing to the lipid signal (nHlipid). This ratio is then multiplied by the molar concentration of DMF (36.796 mM) and further adjusted by the dilution factor of the sample (from 500 to 540 μL).

The PULCON method consisted of recording the spectra of both the reference and the sample on the same spectrometer using the same pulse sequence, the same delay (d_1) to ensure complete proton relaxation, and the same receiver gain. Sample concentration was determined using eq 2 below, which correlates the concentration (C) of the reference (r) and the sample of interest (x) with the integration of the specified resonance (I), the number of protons associated with that resonance (A), the sample temperature in Kelvin (T), the 90° pulse length (θ), and the number of scans (N).

$$Cx = Cr\frac{Ix\ Ar\ Tx\ \theta x\ Nr}{Ir\ Ax\ Tr\ \theta r\ Nx} \quad (2)$$

The molar concentrations calculated from NMR integrals were converted into milligrams per milliliter concentrations using the molecular weight (g/mol) of each component.

UPLC-ELSD Analysis. UPLC analysis was performed using a Waters Acquity CSH C18 column (2.1 mm × 50 mm, 1.7 μm) maintained at 55 °C with samples held at 20 °C. A 5 μL injection volume and consistent flow rate of 0.6 mL/min were employed over a run time of 13 min. The mobile phase consisted of 0.1% v/v trifluoroacetic acid (TFA) in water (phase A) and 0.1% v/v TFA in isopropyl alcohol (IPA) (phase B), with a gradient of solvent compositions spanning throughout the run. Evaporative

https://doi.org/10.1021/acsomega.5c09329
ACS Omega XXXX, XXX, XXX−XXX

Light Scattering (ELS) detection was configured with an evaporation temperature set at 50 °C, a data collection rate of 2 Hz, and a filter setting of 3.6.

Standard solutions containing DSPC, DOPC, cholesterol, and DMPE-PEG2K were prepared, showing good resolution of the components (Figure S2). Calibration curves for each lipid were generated in triplicate, originating from the standard solution across the concentration ranges relevant for lipid mixtures and liposome analysis, taking into account a 1:5 dilution factor applied to samples (Figure S3). A lipid mix solution containing DSPC, cholesterol, and DMPE-PEG2K dissolved in $CDCl_3$ at known concentrations (Table S9) was analyzed to test the accuracy and precision of the method. The solution was analyzed in triplicate after dilution 1:5 in absolute ethanol.

The liposome solutions were first analyzed in their formulation buffer and subsequently after drying, as described for NMR analysis, followed by resuspension in 800 μL of ethanol. In both cases, the solutions were diluted to a 1:5 ratio in absolute ethanol and thoroughly vortexed to ensure homogeneity. Each sample was prepared and analyzed in triplicate.

■ ASSOCIATED CONTENT

Supporting Information

The Supporting Information is available free of charge at https://pubs.acs.org/doi/10.1021/acsomega.5c09329.

Standard lipid solution preparation, dynamic light scattering data for liposome formulations, NMR spectra of individual lipid solutions, UPLC-ELSD elution profile, calibration curves, and results for both lipid mix and liposome samples (PDF)

■ AUTHOR INFORMATION

Corresponding Author

Maxime Denis − *GSK, 53100 Siena, Italy;* orcid.org/0009-0005-1081-6614; Email: maxime.x.denis@gsk.com

Authors

Francesco Currò − *Department of Chemistry Ugo Schiff (DICUS), University of Florence, 50019 Sesto Fiorentino, Italy; Centro di Risonanze Magnetiche (CERM), University of Florence, 50019 Sesto Fiorentino, Italy; GSK, 53100 Siena, Italy*

Ander Eguskiza − *GSK, 53100 Siena, Italy;* Present Address: Asparia Glycomics, Paseo Miramón 170, Donostia-San Sebastián, Gipuzkoa, 20014, Spain

Linda Cerofolini − *Department of Chemistry Ugo Schiff (DICUS), University of Florence, 50019 Sesto Fiorentino, Italy; Centro di Risonanze Magnetiche (CERM), University of Florence, 50019 Sesto Fiorentino, Italy; Consorzio Interuniversitario di Risonanze Magnetiche di Metalloproteine (CIRMMP), 50019 Sesto Fiorentino, Italy*

Silvia Martini − *GSK, 53100 Siena, Italy*

Massimiliano Biagini − *GSK, 53100 Siena, Italy*

Daniela Stranges − *GSK, 53100 Siena, Italy*

Marco Fragai − *Department of Chemistry Ugo Schiff (DICUS), University of Florence, 50019 Sesto Fiorentino, Italy; Centro di Risonanze Magnetiche (CERM), University of Florence, 50019 Sesto Fiorentino, Italy; Consorzio Interuniversitario di Risonanze Magnetiche di Metalloproteine (CIRMMP), 50019 Sesto Fiorentino, Italy;* orcid.org/0000-0002-8440-1690

Complete contact information is available at: https://pubs.acs.org/10.1021/acsomega.5c09329

Author Contributions

The manuscript was written through contributions of all authors. All authors have given approval to the final version of the manuscript.

Notes

The authors declare the following competing financial interest(s): This work was sponsored by GlaxoSmithKline Biologicals SA. Francesco Curr is a student at the University of Florence and participates in a post graduate studentship program at GSK. Silvia Martini, Massimiliano Biagini, Daniela Stranges and Maxime Denis are employed by the GSK group of companies. Ander Eguskiza Bilbao was employed by the GSK group of companies at the time the experimental work was performed, while he was employed by Asparia Glycomics during writing and review processes.

■ ACKNOWLEDGMENTS

This work was sponsored by GlaxoSmithKline Biologicals SA. The authors acknowledge the support and the use of resources of Instruct-ERIC, a landmark ESFRI project, and specifically the CERM/CIRMMP Italy centre, the Res4Priopath Joint Research Activities Consortium (ID Number: ISID_JRA_s8mf), the "Progetto Dipartimenti di Eccellenza 2023−2027" to the Department of Chemistry "Ugo Schiff" of the University of Florence, the Recombinant Proteins JOYNLAB laboratory, and the project "Potentiating the Italian Capacity for Structural Biology Services in Instruct Eric (ITACA)" (Project no. IR0000009) within the call MUR 3264/2021 PNRR M4/C2/L3.1.1, funded by the European Union NextGenerationEU. This study was also supported by the European Union—NextGenerationEU programme in the context of the National Recovery and Resilience Plan, Mission 4, Component 2, Investment 1.4, CN00000041, CN3 "National Center for Gene Therapy and Drugs based on RNA Technology"—Spoke 5 "Inflammatory and Infectious Diseases", CUP: B13C22001010001, and by the Italian Ministry of Health project "Hub multidisciplinare e interregionale di ricerca e sperimentazione clinica per il contrasto alle pandemie ed all'antibiotico resistanza" (PAN-HUB 2021-T4-AN-07). During the preparation of this work, the authors used a large language model for editorial assistance. After using this tool, the authors reviewed and edited the content as needed and take full responsibility for the content of the published article. In conclusion, we sincerely acknowledge Inge Van Dyck and Huijuan Li for their contribution to the revision of the manuscript.

■ REFERENCES

(1) Nsairat, H.; Khater, D.; Sayed, U.; Odeh, F.; Al Bawab, A.; Alshaer, W. Liposomes: Structure, Composition, Types, and Clinical Applications. *Heliyon* **2022**, *8* (5), No. e09394.

(2) Large, D. E.; Abdelmessih, R. G.; Fink, E. A.; Auguste, D. T. Liposome Composition in Drug Delivery Design, Synthesis, Characterization, and Clinical Application. *Adv. Drug Delivery Rev.* **2021**, *176*, 113851.

(3) Jash, A.; Ubeyitogullari, A.; Rizvi, S. S. H. Liposomes for Oral Delivery of Protein and Peptide-Based Therapeutics: Challenges, Formulation Strategies, and Advances. *J. Mater. Chem. B* **2021**, *9* (24), 4773−4792.

(4) Bulbake, U.; Doppalapudi, S.; Kommineni, N.; Khan, W. Liposomal Formulations in Clinical Use: An Updated Review. *Pharmaceutics* **2017**, *9* (2), 12.

(5) Barenholz, Y. Doxil-The First FDA-Approved Nano-Drug: Lessons Learned. *J. Controlled Release* **2012**, *160* (2), 117−134.

(6) Zhang, K. P.; Fang, X.; Zhang, Y.; Chao, M. The Prognosis of Cancer Patients Undergoing Liposomal Doxorubicin-Based Chemotherapy A Systematic Review and Meta-Analysis. *Medicine* **2021**, *100* (34), No. E26690.
(7) Rivankar, S. An Overview of Doxorubicin Formulations in Cancer Therapy. *J. Cancer Res. Ther.* **2014**, *10* (4), 853−858.
(8) Hamill, R. J. Amphotericin B Formulations: A Comparative Review of Efficacy and Toxicity. *Drugs* **2013**, *73* (9), 919−934.
(9) Pemán, J.; Quindos, G. Liposomal Amphotericin B: Thirty Years of a Highly Effective Therapy for the Treatment of Invasive Mycoses. *Rev. Iberoam. Micol.* **2021**, *38* (2), 39−41.
(10) Herrada, J.; Gamal, A.; Long, L.; Sanchez, S. P.; McCormick, T. S.; Ghannoum, M. A. In Vitro and in Vivo Antifungal Activity of Ambisome Compared to Conventional Amphotericin B and Fluconazole against Candida Auris. *Antimicrob. Agents Chemother.* **2021**, *65* (6), No. e00306-21.
(11) Roman, F.; Burny, W.; Ceregido, M. A.; Laupèze, B.; Temmerman, S. T.; Warter, L.; Coccia, M. Adjuvant System AS01: From Mode of Action to Effective Vaccines. *Expert Rev. Vaccines* **2024**, *23* (1), 715−729.
(12) Didierlaurent, A. M.; Berger, A.; Heineman, T. C.; Hendericksx, V.; Tavares Da Silva, F.; Vekemans, J.; Voss, G.; Garçon, N. The Development of the Adjuvant System AS01: A Combination of Two Immunostimulants MPL and QS-21 in Liposomes. *Immunopotentiators in Modern Vaccines*, 2nd ed.; Academic Press, 2017; pp 265−285.
(13) Syed, Y. Y. R. T. S. RTS,S/AS01 malaria vaccine (Mosquirix): a profile of its use. *Drugs Ther. Perspect.* **2022**, *38* (9), 373−381.
(14) Buya, A. B.; Mahlangu, P.; Witika, B. A. From Lab to Industrial Development of Lipid Nanocarriers Using Quality by Design Approach. *Int. J. Pharm. X* **2024**, 8 (July), 100266.
(15) Alshaer, W.; Nsairat, H.; Lafi, Z.; Hourani, O. M.; Al-Kadash, A.; Esawi, E.; Alkilany, A. M. Quality by Design Approach in Liposomal Formulations: Robust Product Development. *Molecules* **2023**, *28* (1), 10.
(16) Giordani, S.; Marassi, V.; Zattoni, A.; Roda, B.; Reschiglian, P. Liposomes Characterization for Market Approval as Pharmaceutical Products: Analytical Methods, Guidelines and Standardized Protocols. *J. Pharm. Biomed. Anal.* **2023**, *236* (October), 115751.
(17) Sercombe, L.; Veerati, T.; Moheimani, F.; Wu, S. Y.; Sood, A. K.; Hua, S. Advances and Challenges of Liposome Assisted Drug Delivery. *Front. Pharmacol.* **2015**, *6* (DEC), 1−13.
(18) Fan, Y.; Marioli, M.; Zhang, K. Analytical Characterization of Liposomes and Other Lipid Nanoparticles for Drug Delivery. *J. Pharm. Biomed. Anal.* **2021**, *192*, 113642.
(19) Yan, Q.; Trabulo, S.; Wolk, S.; Bridwell, H.; Burgers, P.; Throyk, E.; Hamill, P.; Joest, E.; Ward, R.; Srinivasan, S.; Rayaprolu, B.; Carr, C.; Wang, S.; Peters, E.; Pach, R.; Hajjami, N. E. *Defining the Required Critical Quality Attributes (CQAs) and Phase Requirements for MRNA/LNP Product Development and Manufacture*; Biophorum, 2023.
(20) Mosca, M.; Ceglie, A.; Ambrosone, L. Effect of Membrane Composition on Lipid Oxidation in Liposomes. *Chem. Phys. Lipids* **2011**, *164* (2), 158−165.
(21) Wang, C.; Gamage, P. L.; Jiang, W.; Mudalige, T. Excipient-Related Impurities in Liposome Drug Products. *Int. J. Pharm.* **2024**, *657* (May), 124164.
(22) Zuidam, N. J.; Gouw, H. K. M. E.; Barenholz, Y.; Crommelin, D. J. A. Physical (in) Stability of Liposomes upon Chemical Hydrolysis: The Role of Lysophospholipids and Fatty Acids. *Biochim. Biophys. Acta Biomembr.* **1995**, *1240* (1), 101−110.
(23) Ickenstein, L. M.; Sandström, M. C.; Mayer, L. D.; Edwards, K. Effects of Phospholipid Hydrolysis on the Aggregate Structure in DPPC/DSPE-PEG2000 Liposome Preparations after Gel to Liquid Crystalline Phase Transition. *Biochim. Biophys. Acta Biomembr.* **2006**, *1758* (2), 171−180.
(24) Bartlett, G. R. Phosphorus Assay in Column Chromatography. *J. Biol. Chem.* **1959**, *234* (3), 466−468.
(25) Itoh, Y. H.; Itoh, T.; Kaneko, H. Modified Bartlett Assay for Microscale Lipid Phosphorus Analysis. *Anal. Biochem.* **1986**, *154* (1), 200−204.
(26) Roces, C. B.; Kastner, E.; Stone, P.; Lowry, D.; Perrie, Y. Rapid Quantification and Validation of Lipid Concentrations within Liposomes. *Pharmaceutics* **2016**, *8* (3), 29.
(27) Bender, V.; Fuchs, L.; Süss, R. RP-HPLC-CAD Method for the Rapid Analysis of Lipids Used in Lipid Nanoparticles Derived from Dual Centrifugation. *Int. J. Pharm. X* **2024**, *7* (March), 100255.
(28) Yang, H.; Fei, C.; Wang, S.; Shen, X.; Yang, L.; Yang, H.; Li, G. Validation of an HPLC-CAD Method for Measuring the Lipid Content of Novel LNP-Encapsulated COVID-19 MRNA Vaccines. *J. Virol. Methods* **2024**, *330* (October), 115040.
(29) Beckert, N.; Dietrich, A.; Hubbuch, J. RP-CAD for Lipid Quantification: Systematic Method Development and Intensified LNP Process Characterization. *Pharmaceuticals* **2024**, *17* (9), 1217.
(30) Simmler, C.; Napolitano, J. G.; McAlpine, J. B.; Chen, S. N.; Pauli, G. F. Universal Quantitative NMR Analysis of Complex Natural Samples. *Curr. Opin. Biotechnol.* **2014**, *25* (May), 51−59.
(31) Li, M.; Xu, W.; Su, Y. Solid-State NMR Spectroscopy in Pharmaceutical Sciences. *TrAC, Trends Anal. Chem.* **2021**, *135*, 116152.
(32) Malet-Martino, M.; Holzgrabe, U. NMR Techniques in Biomedical and Pharmaceutical Analysis. *J. Pharm. Biomed. Anal.* **2011**, *55* (1), 1−15.
(33) Franz, A. H.; Samoshina, N. M.; Samoshin, V. V. A Convenient Method for the Relative and Absolute Quantification of Lipid Components in Liposomes by 1H- and 31P NMR-Spectroscopy. *Chem. Phys. Lipids* **2024**, *261* (March), 105395.
(34) Endo, N.; Aoki, C.; Sugiki, T.; Sakai-Kato, K. Quantitative Lipid Composition Characterization of Intact Liposomes via 31P Nuclear Magnetic Resonance Spectroscopy. *Anal. Sci.* **2024**, *40* (5), 871−879.
(35) Farhadi, F.; Nayebzadeh, N.; Badiee, A.; Arabsalmani, M.; Hatamipour, M.; Iranshahi, M. Journal of Pharmaceutical and Biomedical Analysis A Validated 1 H-NMR Method for Quantitative Analysis of DOTAP Lipid in Nanoliposomes Containing Soluble Leishmania Antigen. *J. Pharm. Biomed. Anal.* **2021**, *194*, 113809.
(36) Cansell, M.; Bardeau, T.; Morvan, E.; Grélard, A.; Buré, C.; Subra-Paternault, P. Phospholipid Profiles of Oleaginous Pressed Cakes Using NMR and Gas Chromatography. *J. Am. Oil Chem. Soc.* **2017**, *94* (9), 1219−1223.
(37) Schlattmann, D.; Weber, B.; Wyszynski, L.; Schönhoff, M.; Haas, H. Molecular Localization and Exchange Kinetics in Pharmaceutical Liposome and mRNA Lipoplex Nanoparticle Products Determined by Small Angle X-Ray Scattering and Pulsed Field Gradient NMR Diffusion Measurements. *Eur. J. Pharm. Biopharm.* **2024**, *201* (July), 114380.
(38) Froehlich, M.; Brecht, V.; Peschka-Suess, R. Parameters Influencing the Determination of Liposome Lamellarity by 31 P-NMR. *Chem. Phys. Lipids* **2001**, *109*, 103−112.
(39) Hald Albertsen, C.; Kulkarni, A. J.; Witzigmann, D.; Lind, M.; Pertersson, K.; Simonsen, B. J. The Role of Lipid Components in Lipid Nanoparticles for Vaccines and Gene Therapy. *Adv. Drug Delivery Rev.* **2022**, *188*, 114416.
(40) Udepurkar, A.; Devos, C.; Sagmeister, P.; Destro, F.; Inguva, P.; Ahmadi, S.; Boulais, E.; Quan, Y.; Braatz, R. D.; Myerson, A. S. Structure and Morphology of Lipid Nanoparticles for Nucleic Acid Drug Delivery: A Review. *ACS Nano* **2025**, *19*, 21206.
(41) Wider, G.; Dreier, L. Measuring Protein Concentrations by NMR Spectroscopy. *J. Am. Chem. Soc.* **2006**, *128* (8), 2571−2576.
(42) Mak, J. Y. W. Determination of Samplce Concentrations by PULCON NMR Spectroscopy. *Aust. J. Chem.* **2022**, *75* (2), 160−164.
(43) Monakhova, Y. B.; Kohl-Himmelseher, M.; Kuballa, T.; Lachenmeier, D. W. Determination of the Purity of Pharmaceutical Reference Materials by 1H NMR Using the Standardless PULCON Methodology. *J. Pharm. Biomed. Anal.* **2014**, *100*, 381−386.
(44) Singh, S.; Roy, R. The Application of Absolute Quantitative 1H NMR Spectroscopy in Drug Discovery and Development. *Expet Opin. Drug Discov.* **2016**, *11* (7), 695−706.
(45) Ueda, K.; Sakagawa, Y.; Saito, T.; Fujimoto, T.; Nakamura, M.; Sakuma, F.; Kaneko, S.; Tokumoto, T.; Nishimura, K.; Takeda, J.; Arai, Y.; Yamamoto, K.; Ikeda, Y.; Higashi, K.; Moribe, K. Molecular-Level Structural Analysis of SiRNA-Loaded Lipid Nanoparticles by 1H NMR

https://doi.org/10.1021/acsomega.5c09329
ACS Omega XXXX, XXX, XXX−XXX

Relaxometry: Impact of Lipid Composition on Their Structural Properties. *Mol. Pharmaceutics* **2023**, *20* (9), 4729−4742.
(46) *The Human Metabolome Database*. https://hmdb.ca/.

Supplementary material

Supporting Information

Fast and straightforward lipid quantification in pharmaceutical compositions using NMR

Francesco Currò[a][b][c], Ander Eguskiza [c]†, Linda Cerofolini[a][b][d], Silvia Martini[c], Massimiliano Biagini[c], Daniela Stranges[c], Marco Fragai[a][b][d] and Maxime Denis[c].*

[a] Department of Chemistry Ugo Schiff (DICUS), University of Florence, via della Lastruccia 3, 50019, Sesto Fiorentino, Italy

[b] Centro di Risonanze Magnetiche (CERM), University of Florence, via Luigi Sacconi 6, 50019, Sesto Fiorentino, Italy

[c] GSK, Siena, Italy

[d] Consorzio Interuniversitario di Risonanze Magnetiche di Metalloproteine (CIRMMP), via Luigi Sacconi 6, 50019, Sesto Fiorentino, Italy

*Corresponding author: Maxime Denis. E-mail: maxime.x.denis@gsk.com . Postal address: Via Fiorentina, 1, Siena, 53100, Italy.

†Current affiliation: Asparia Glycomics, Paseo Miramón 170, Donostia-San Sebastián, Gipuzkoa, 20014, Spain

Table of Contents

Table S1. Results of Dynamic Light Scattering analysis of liposomes formulations.

Liposomes	Z-average (nm)[d]	PDI[e]
(A)	66	0.18
(B)	45	0.07
(C)	110	0.16

[d] Z-average (nm) represents the average size of particles by intensity

[e] Polidispersity Index (PDI) is a measure of particle size distribution. Liposome particles resulted to be uniform (PDI < 0.2), with no evidence of aggregation, for all formulations.

Table S2. Summary of UPLC results for lipid mix.

Lipid mix	Lipid	Theoretical (mg/mL)	Experimental (mg/mL)	Recovery %	%RSD replicates
(E) DSPC:Chol:DMPE-PEG2K (16.2:12.2:1)	DSPC	2.73	2,87	104,8%	**9.4%**
	Cholesterol	2.07	2,03	98,3%	**10.7%**
	DMPE-PEG2K	0.169	0,173	102,4%	**9.0%**

Table S3. Analysis of liposomes formulations (A), (B), (C) with UPLC-ELSD. The results obtained from liposomes solutions without and with freeze-drying and resuspension in EtOH are compared.

Liposomes	Lipid	Theoretical Concentration (mg/mL)	UPLC exp conc. solution (mg/mL)	recovery UPLC solution %	UPLC exp conc. dried (mg/mL)	recovery UPLC dried %
(A) DSPC:Chol (2:1)	DSPC	1.20	1.29	**107.5%**	1.26	**105.0%**
	Cholesterol	0.60	0.67	**111.7%**	0.66	**110.0%**
(B) DSPC:Chol:DMPE-PEG2K (10.9:14.6:1)	DSPC	1.09	1.25	**114.7%**	1.16	**106.4%**
	Cholesterol	1.47	1.43	**97.2%**	1.36	**92.5%**
	DMPE-PEG2K	0.10	0.101	**101.0%**	0.095	**95.0%**
(C) DOPC:Chol (4:1)	DOPC	3.18	3.06	**96.2%**	3.07	**96.5%**
	Cholesterol	0.79	0.76	**96.2%**	0.78	**98.7%**

Table S4. Lipid standard stocks preparation.[a]

Lipid	Molar mass (g/mol)	Weight (mg)	Volume of chloroform (mL)	Concentration (mg/mL)	Concentration in NMR tube (mg/mL)
DSPC	790.15	22.2	2	11.1	10.28
Cholesterol	386.67	12.0	2	6.0	5.56
DMG-PEG2K	2693.285	10.1	4	2.525	2.34

[a] Each lipid powder was weighed and dissolved in chloroform-d ($CDCl_3$) under rapid mixing. 500 uL of each solution was added to an NMR tube with 40 uL of DMF solution resulting in the final concentration of analysis.

Table S5. Lipid mix (A) preparation.[b]

Lipid	Molar mass (g/mol)	Stock concentration (mg/mL	Stock volume (mL)	Total volume (mL)	Final concentration (mg/mL)	Concentration in NMR tube (mg/mL)
DSPC	790.15	11.9	0.080	0.800	1.19	1.11
Cholesterol	386.67	6.0	0.0790	0.800	0.60	0.56

[b] Each lipid powder was weighed and dissolved in chloroform-d ($CDCl_3$) under rapid mixing. The stock solution was further diluted in $CDCl_3$. 500 uL of each solution was added to an NMR tube with 40 uL of DMF solution resulting in the final concentration of analysis.

Table S6. Lipid mix (B) preparation.[b]

Lipid	Molar mass (g/mol)	Stock concentration (mg/mL	Stock volume (mL)	Total volume (mL)	Final concentration (mg/mL)	Concentration in NMR tube (mg/mL)
DSPC	790.15	11.3	0.080	0.780	1.13	1.05
Cholesterol	386.67	15.9	0.070	0.780	1.53	1.42
DMPE-PEG2K	2693.285	2.925	0.030	0.780	0.11	0.104

[b] Each lipid powder was weighed and dissolved in chloroform-d ($CDCl_3$) under rapid mixing. The stock solution was further diluted in $CDCl_3$. 500 uL of each solution was added to an NMR tube with 40 uL of DMF solution resulting in the final concentration of analysis.

Table S7. Lipid mix (C) preparation.[b]

Lipid	Molar mass (g/mol)	Stock concentration (mg/mL	Stock volume (mL)	Total volume (mL)	Final concentration (mg/mL)	Concentration in NMR tube (mg/mL)
DOPC	786.13	8.0	0.320	0.800	3.20	2.96
Cholesterol	386.67	15.9	0.040	0.800	0.81	0.76

[b] Each lipid powder was weighed and dissolved in chloroform-d ($CDCl_3$) under rapid mixing. The stock solution was further diluted in $CDCl_3$. 500 uL of each solution was added to an NMR tube with 40 uL of DMF solution resulting in the final concentration of analysis.

Table S8. Lipid mix (D) preparation.[b]

Lipid	Molar mass (g/mol)	Stock concentration (mg/mL	Stock volume (mL)	Total volume (mL)	Final concentration (mg/mL)	Concentration in NMR tube (mg/mL)
DSPC	790.15	11.9	1.000	2.975	4.00	3.71
Cholesterol	386.67	15.9	1.000	2.600	6.12	5.67
DMPE-PEG2K	2693.285	2.925	0.025	1.000	0.073	0.068

[b] Each lipid powder was weighed and dissolved in chloroform-d ($CDCl_3$) under rapid mixing. The stock solution was further diluted in $CDCl_3$. 500 uL of each solution was added to an NMR tube with 40 uL of DMF solution resulting in the final concentration of analysis.

Table S9. Lipid mix (E) preparation.[c]

Lipid	Molar mass (g/mol)	Weight (mg)	Stock concentration (mg/mL	Stock volume (mL)	Volume of chloroform (mL)	Concentration (mg/mL)
DSPC	790.15	9.8	N/A	N/A	3.6	2.73
Cholesterol	386.67	12.8	N/A	N/A	6.2	2.07
DMPE-PEG2K	2693.285	9.1	1.7	0.1	1	0.17

[c] Each lipid powder was weighed and dissolved in chloroform-d ($CDCl_3$) under rapid mixing. The stock solution was further diluted in $CDCl_3$ for DMPE-PEG2K. The solutions were analyzed with UPLC-ELSD after further dilution 1:5.

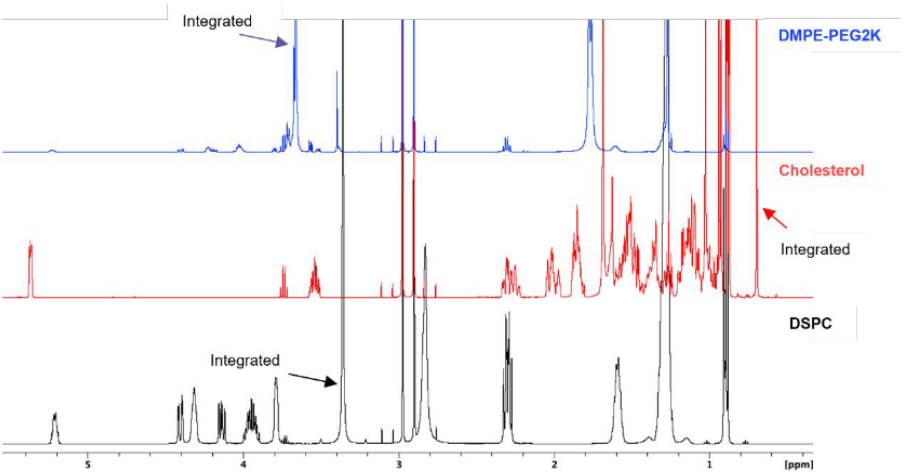

Fig. S1. 1D ^{1}H spectra of single lipid solutions in $CDCl_3$. From the bottom: DSPC solution at 10.28 mg/mL in black, with the N-methyl proton signal (9 protons) highlighted by an arrow at 3.35 ppm. In the middle, cholesterol solution at 5.56 mg/mL in red, with the methyl group signal (3 protons) highlighted at 0.69 ppm. At the top, DMPE-PEG2K solution spectrum at 2.34 mg/mL in blue, with the 180 protons from the repeating units of PEG (-[-O-CH_2-CH_2-]-) highlighted at 3.66 ppm. Each highlighted peak is well-solved and was used for integration.

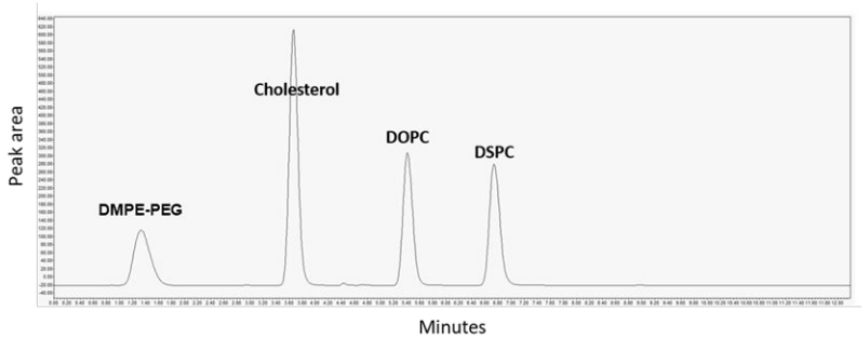

Fig. S2. Chromatogram showing the elution of lipids overtime. The standard solution contained DSPC, DOPC, cholesterol and DMPE-PEG2K. All the lipids were well separated to allow optimal analysis.

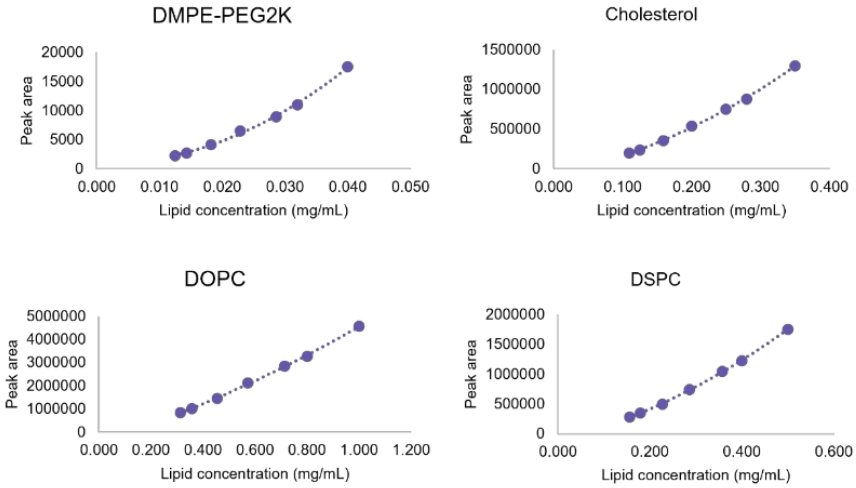

Fig. S3. Calibration curves prepared for each lipid analyzed. Seven concentration points for each curve were employed, diluting from a standard lipid stock with ethanol. The range of concentration tested was fixed according to the expected concentration in liposome samples, taking into account a 1:5 dilution factor applied to the initial liposome solutions. The curves showed a sigmoidal profile, as expected from ELSD detection and were fitted using Excel software with a quadratic equation obtaining regression values (R^2) > 0.99.

4.2 NMR Assessment of the High Order Structure of Biological Therapeutics in Erythrocytes Provides a Tool for Drug Delivery Design

This study aimed to assess the preservation of high-order structure (HOS) of pharmaceutically relevant proteins after their encapsulation within Red Blood Cells (RBCs). This is crucial to ensure the functionality of the cargo in this delivery system, whose applications have been increasing in recent years due to its biocompatibility and extended circulation. NMR characterization was used to examine the preservation of the protein native folding within the RBCs by comparing enzyme signals to those of free enzymes. Peak re-assignment helped identify residues affected by encapsulation and assess whether secondary structures were preserved. Additionally, a semi-quantitative analysis compared signal intensities of free enzyme solutions and encapsulated proteins, offering insights into encapsulation efficiency. This approach serves as a valuable analytical tool to rapidly evaluate cargo encapsulation efficiency in RBCs, facilitating optimization of the encapsulation process.

My contributions included supporting the enzyme encapsulation procedures, recording the NMR spectra, and drafting the manuscript.

The study was published in Journal of American Chemical Society and is reported in this section.

Padilla-Cortés, L., Gheorghita, G. R., Currò, F., Calamandrei, R., Susini, B., Callozzo, S., Crivello, G., Russomanno, P., Ravera, E., Cerofolini, L., & Fragai, M. NMR Assessment of the High Order Structure of Biological Therapeutics in Erythrocytes Provides a Tool for Drug Delivery Design. *Journal of the American Chemical Society*, 147(30), 26379–26388. (2025). https://doi.org/10.1021/jacs.5c05617

JACS
JOURNAL OF THE AMERICAN CHEMICAL SOCIETY
pubs.acs.org/JACS

Article

NMR Assessment of the High Order Structure of Biological Therapeutics in Erythrocytes Provides a Tool for Drug Delivery Design

Luis Padilla-Cortés, Giulia Roxana Gheorghita, Francesco Currò, Rebecca Calamandrei, Bianca Susini, Sara Callozzo, Giulia Crivello, Pasquale Russomanno, Enrico Ravera, Linda Cerofolini, and Marco Fragai*

Cite This: https://doi.org/10.1021/jacs.5c05617

ABSTRACT: An effective delivery system is crucial for ensuring the therapeutic efficacy of a drug. This is especially true for biological drugs, which possess unique physicochemical properties and complex pharmacokinetic profiles, and thus require a dedicated design. Whole erythrocytes, and more recently, nanoparticles derived from red blood cells (RBCs), have been used in preclinical studies to deliver biological therapeutics: their biocompatibility and extended circulation time help prevent immunogenicity and reduce clearance and toxicity. However, characterizing such complex systems poses challenges that complicate their development and optimization. We argue that NMR spectroscopy enables the monitoring of the preservation of the high order structure of the encapsulated proteins, as well as their concentration, thereby assisting in formulation design, development, and manufacturing.

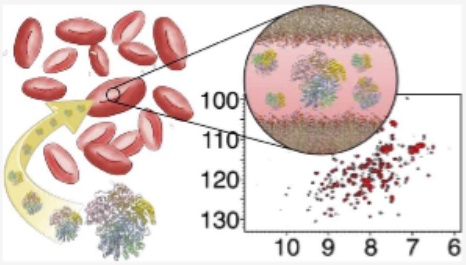

INTRODUCTION

Several enzymes are currently in clinical use to treat a number of diseases. Relevant examples include enzymatic replacement therapy for genetically deficient patients, or the clearance of essential precursors for cancer cells.[1,2] The effectiveness of these treatments is often limited due to the poor in vivo enzyme stability, immunogenicity, and the activity of inactivating antibodies. These challenges can be partially addressed by coating therapeutic proteins with biocompatible polymers such as PEG, which extend their half-life by increasing the size and shielding the enzyme from proteases and from the reticuloendothelial system.[3,4] However, even the widespread used PEGylation can cause adverse reactions: hypersensitivity, immune reactions up to anaphylaxis, and cytoplasmic vacuolation have been documented for PEGylated protein delivery.[5,6] The idea of using erythrocytes as enzyme carriers is even older than PEGylation and was first reported for beta-glucosidase and beta-galactosidase in the treatment of Gaucher's disease.[7] Erythrocytes are a promising delivery system because of their biocompatibility, biodegradability, prolonged circulation time, and ability to reduce side effects.[8,9] The reason that brought to attention the possibility of using red blood cells is their intrinsic biocompatibility, because the patient's own red blood cells can be utilized for encapsulation. Red blood cell membrane shelters therapeutic enzymes from the immune system action and plasma proteases, enhancing their therapeutic effects and enabling the safe administration of higher doses in the bloodstream.[10] Over the years, the method of encapsulation using hypotonic dialysis has been automated to enhance both the efficiency and speed of loading proteins within red blood cells directly obtained from patients on-site.[11] Additionally, various other loading techniques have been successfully implemented, such as utilizing low molecular weight protamine to facilitate the translocation of enzymes across the red blood cell membrane without causing significant disruption.[12,13] More recently, RBC membrane-derived nanoparticles have been used as new drug delivery system.[14] Several erythrocyte-encapsulated enzymes are currently under development, and one has undergone clinical evaluation.[15−17]

L-Asparaginase II was one of the first approved biologics used to treat acute lymphoblastic leukemia (ALL) and lymphoblastic lymphoma.[18,19] This enzyme, derived from various sources, is still used in patients in its unmodified and PEGylated forms, and its encapsulated erythrocyte formulation (GRASPA) has been evaluated in clinical trials against ALL

Received: April 2, 2025
Revised: July 8, 2025
Accepted: July 8, 2025

and pancreatic cancer.[20−22] Although GRASPA's approval for clinical use against ALL was discontinued, this therapeutic candidate remains a model for developing analytical tools to characterize this innovative class of biologics. To date, the characterization of erythrocyte-encapsulated enzymes has largely relied on assessing their enzymatic activity, either within the encapsulated formulation itself or after extracting the enzyme following cell lysis.[23]

The high order structure (HOS) of enzymes is a critical quality attribute because it defines the active conformation, allowing it to recognize and bind to its physiological substrates. This structural specificity is fundamental to the enzyme's function, as it determines the catalytic efficiency. Therefore, assessing the preservation of the high order structure of the enzyme is important for ensuring its biological activity and therapeutic efficacy, as well as for a comprehensive understanding of its formulations and manufacturing design and process. Moreover, the folding state of a protein, or its degraded forms can influence their immunogenicity, thus posing a risk to the safety of protein therapeutics.[24] Numerous studies have been published on the structural characterization of drug delivery systems; however, relatively few are focused on the assessment of the structural integrity of biologics inside these formulations.[25] Given the structural complexity of biologics, NMR is a powerful tool for assessing the HOS of molecules in complex matrices or pharmaceutical formulations due to its atomic resolution and versatility.[26−31] Solution NMR, with its short acquisition times and minimal sample preparation, is emerging as a crucial component in analytical workflows for biological therapeutics.[32−35] Additionally, it enables the study of entire complexes in environments that closely mimic physiological conditions, facilitating the structural characterization of internalized cargo within the intact system and correlating it with biological functionality. Moreover, NMR has been widely used to investigate the structural features of proteins, peptides and nucleic acids embedded in confined environments, such as cells.[36−40] This study demonstrates how the NMR characterization of three erythrocyte-encapsulated proteins offers insights into their HOS preservation and a semiquantitative assessment of the encapsulation yield. This represents a significant contribution to potentially optimizing encapsulation protocols, sample handling, and storage in erythrocytes and RBC membrane-derived nanoparticles.[41]

RESULTS

Analysis of the High Order Structure of Proteins Encapsulated within Erythrocytes. Three proteins differing in pharmacological relevance, function, size, and structural features were selected to investigate their encapsulation within RBC. ^{15}N-enriched human carbonic anhydrase II (CAII),[42] ^{15}N-enriched human transthyretin (TTR),[43] and ^{2}H, ^{13}C, ^{15}N-enriched *E. coli* L-Asparaginase II (ANSII)[4,44] were encapsulated in bovine red blood cells and used as models for the characterization of the preservation of the HOS of the proteins in such a delivery system. Protein encapsulation was achieved using the hypotonic dialysis method.[45] Briefly, bovine erythrocytes, mixed with concentrated protein solutions, were first dialyzed against a hypotonic solution to promote membrane permeability and protein encapsulation, then against isotonic solutions with membranes of different pore sizes to reseal the red cells and remove the nonencapsulated protein (see the details in the Materials and Methods section). During this process, we observed that a portion of the hemoglobin and likely some cytoplasmic components were released into the external buffered solution. Encapsulation and structural characterization were monitored using 2D ^{1}H−^{15}N SOFAST-HMQC NMR experiments that are optimized for increased sensitivity by using band-selective pulses for proton amide excitation, leading to shorter longitudinal relaxation and reduced recycling delay.[46]

CAII was used to assess the effectiveness of the selected methodology in encapsulating proteins within RBC. ^{15}N-filtered spectra were recorded (Figure 1) on samples prepared

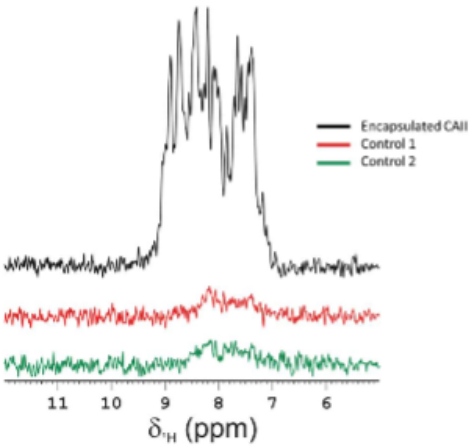

Figure 1. Evaluation of the efficacy of the encapsulation process for ^{15}N CAII. 1st FID of the 2D ^{1}H−^{15}N SOFAST-HMQC of encapsulated ^{15}N CAII in RBC (black), RBC undergoing the dialysis protocol for encapsulation in the absence of the ^{15}N-labeled CAII (Control 1, red) and RBC undergoing the encapsulation process with ^{15}N CAII without performing the hypotonic dialysis to load the protein (Control 2, green). The spectra show successful encapsulation of ^{15}N CAII in RBC using the protocol and absence of the protein in the controls. The spectra were acquired at 310 K on a spectrometer operating at 1200 MHz (^{1}H Larmor frequency).

using three different protocols: (i) the dialysis protocol for encapsulation in the presence of the ^{15}N-labeled CAII (Encapsulated CAII); (ii) the dialysis protocol for encapsulation in the absence of the ^{15}N-labeled CAII (Control 1); (iii) ^{15}N-enriched CAII added to RBC without performing the hypotonic dialysis to load the protein (Control 2). The intensity of the NMR signals from the first FID of the 2D ^{1}H−^{15}N SOFAST-HMQC spectra of Control 1 and 2 were compared with that of a sample of ^{15}N-enriched CAII encapsulated in RBC following the correct protocol described in Materials and Methods section. The spectrum recorded on the sample (Encapsulated CAII) prepared following the protocol showed intense signals in the amide proton region, while only weak background signals of HN protons were visible in the spectra of the two controls (Control 1 and Control 2). These results suggest that the background signals of HN protons, resonating in the range of 7 to 9 ppm in the spectra of the controls, originate from hemoglobin present in RBCs. Indeed, despite the low natural abundance of ^{15}N (~0.4%), the physiological concentration of hemoglobin in

https://doi.org/10.1021/jacs.5c05617

erythrocytes is high (~3 mmol dm^{-3}), therefore its signals could be detected.[47] Additionally, the supernatant of the last rinse step was always analyzed through NMR to check for the presence of residual free protein. The absence of signals in the spectra confirms that the cross-peaks observed in the 2D spectra of the samples are related to the encapsulated proteins only (Figures S1 and S2).

The 2D $^{1}H-^{15}N$ SOFAST-HMQC spectra recorded on the three proteins encapsulated within the RBCs were of relatively good quality.[48] The reduced amount of cytoplasmic components and hemoglobin, because partially released from RBCs during the hypotonic dialysis, likely accounts for the relatively good resolution of the spectra. The backbone resonances in the spectra were superimposable with those of "free" nonencapsulated proteins (Figure 2), demonstrating the preservation of the high order structure of all the proteins upon encapsulation in RBCs. Furthermore, assignment of the visible cross-peaks was easily obtained by comparing the assignment available for free CAII,[42] ANSII,[4] and TTR[43] with the 2D $^{1}H-^{15}N$ SOFAST-HMQC spectra acquired on the encapsulated enzymes (Figure 3). Almost all the residues of CAII (98% over the available assignment) could be reassigned (Figure 3, panels A and B), further confirming the preservation of the high order structure of encapsulated CAII. The 76% of the residues over the available assignment could be reassigned for ANSII (Figure 3, panels C and D). In the case of TTR, the signals in the 2D $^{1}H-^{15}N$ SOFAST-HMQC are affected by a larger line broadening due to the protein size (M_w 55 kDa) and the absence of deuteration both for the free and encapsulated protein. However, the quality of the spectra of the protein inside the cells is comparable to that of free TTR and overall, although in severe overlap, most of the signals (90% over the available assignment) could be reassigned (Figure 3, panels E and F).

In general, the spectra of the proteins encapsulated inside the RBCs and acquired immediately after sample preparation are of relatively good quality; however, broader cross-peaks were observed due to the intrinsic line-broadening effect of proteins within cells.[49−52] This could be caused by (a) a crowded and more viscous environment that causes molecules to diffuse slowly, leading to increased transverse relaxation rates (R_2); (b) weak interactions with the cytoplasmic components; (c) magnetic field inhomogeneities related to the internal heterogeneous structure of the RBCs; and primarily (d) the presence of deoxyhemoglobin, and the oxidative stress in erythrocytes over time that induces the formation of methemoglobin and hemosiderin, where Fe^{2+} is oxidized to Fe^{3+} that has a more detrimental effect on spectral quality.[53−55] This latter process contributes to a comprehensive degradation of the sample within the magnet at 310 K and to the broadening of signals over time. The broadening of CAII signals over time is shown in Figure S3. The increase of line broadening for the encapsulated protein was assessed on CAII. ^{15}N transverse relaxation rates were estimated on free CAII in PBS and CAII encapsulated in RBCs by recording the first FID of Carr−Purcell−Meiboom−Gill (CPMG) experiments. An average transverse relaxation rate (R_2) of 15 ± 1 and 22 ± 6 s^{-1} was found for free and encapsulated CAII, respectively (Figure S4). These data confirm faster decay of magnetization for the encapsulated protein.

To demonstrate the sensitivity of this method to minor structural changes in proteins, we conducted an NMR analysis. This involved mixing an aliquot of free carbonic anhydrase II

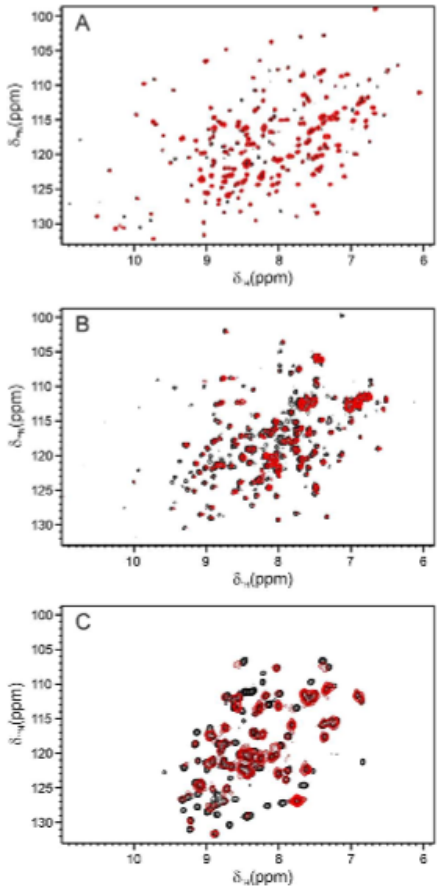

Figure 2. Comparison of the NMR spectra between free and RBC-encapsulated proteins. 2D $^{1}H-^{15}N$ SOFAST-HMQC NMR spectra of (A) CAII encapsulated in RBC (red) and free CAII (black), (B) ANSII encapsulated in RBC (red) and free ANSII (black), (C) TTR encapsulated in RBC (red) and free TTR (black). The spectra of CAII and ANSII were acquired on a spectrometer operating at 900 MHz, while the spectra of TTR were acquired on a spectrometer operating at 1200 MHz. All the experiments were recorded at 310 K in PBS buffer, pH 7.4.

(CAII) with an aliquot of CAII that had been inhibited with furosemide, both at similar protein concentrations, prior to encapsulation in red blood cells (RBCs). The free and inhibited species can be distinguished by their different chemical shifts also when the protein is encapsulated in RBCs (Figure 4). The relative amount between the two species is almost conserved during the encapsulation process (55% of free CAII: 45% of inhibited CAII).

Additional experiments on CAII were carried out using an instrument operating at 600 MHz. Although the signal-to-noise ratio is lower than the spectra recorded at high field (900 MHz), the signals of the protein are still visible and comparable (Figure S5). It is important to note that we observed variations in the quality of the spectra obtained from

https://doi.org/10.1021/jacs.5c05617

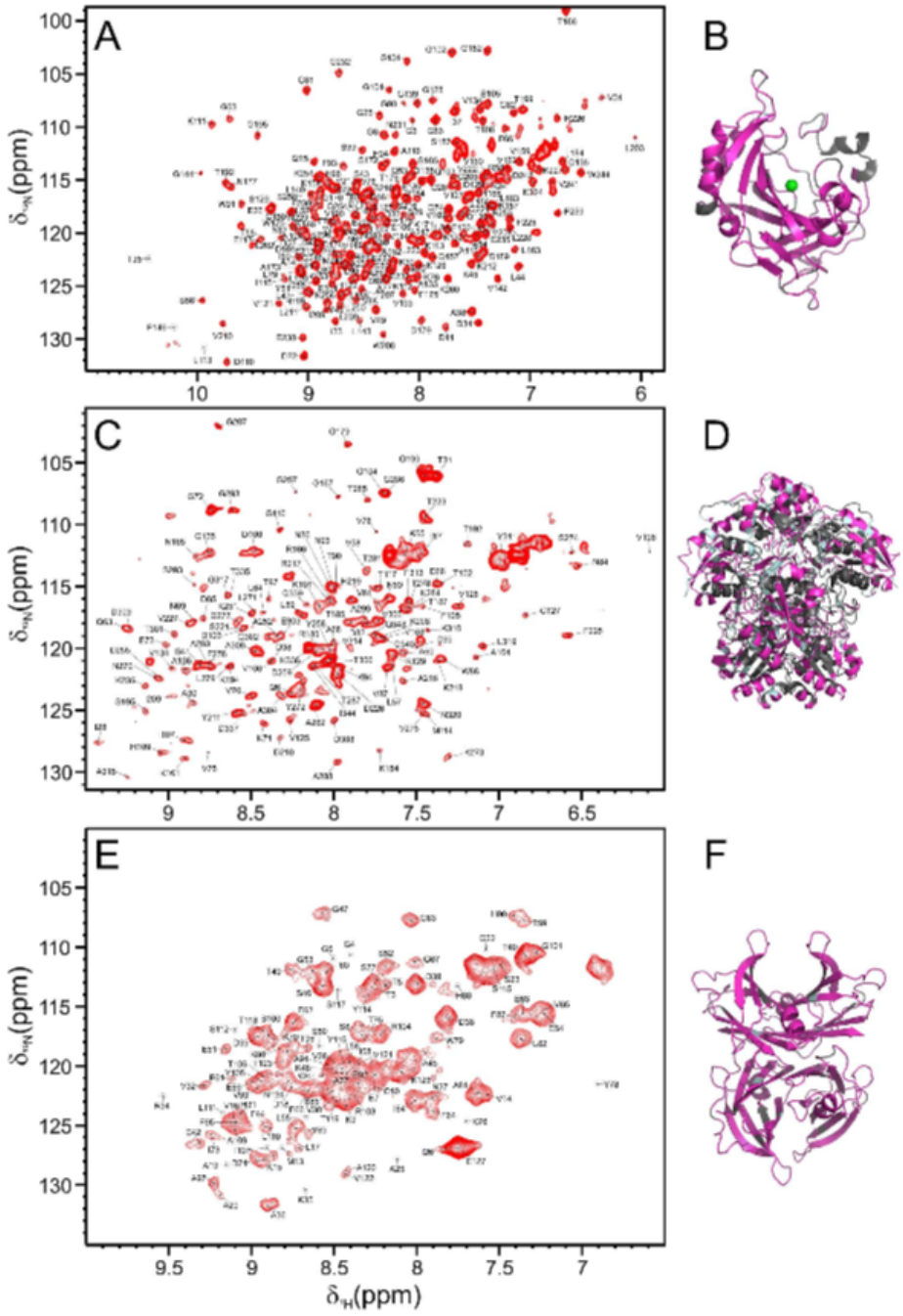

Figure 3. Assignment of RBC-encapsulated proteins and their X-ray structure highlighting the reassigned residues. (A−C−E) 2D $^{1}H-^{15}N$ SOFAST-HMQC spectrum of proteins encapsulated in red blood cells with the assignment indicated on the signals, respectively CAII (A), ANSII (C) and TTR (E). (B−D−F) X-ray structure of proteins in light blue, the residues for which the resonances have been reassigned for the protein

https://doi.org/10.1021/jacs.5c05617

Figure 3. continued

encapsulated in the red blood cells are highlighted in magenta and the residues neither assigned in the free nor in encapsulated proteins are highlighted in gray. The PDB codes for obtaining the X-ray structures were (B) 3KS3 for CAII, (D), 3ECA for ANSII and (F) 1BMZ for TTR.

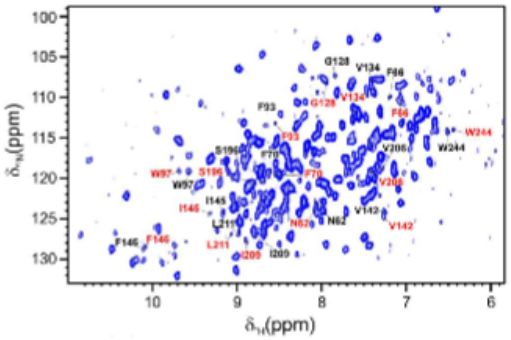

Figure 4. A 2D ^{1}H ^{15}N SOFAST HMQC spectrum was obtained for carbonic anhydrase II (CAII) encapsulated in red blood cells (RBCs), both in its free form and when inhibited by furosemide. The figure presents the assignment of shifted signals, with signals from the free protein indicated in black and those from the inhibited protein shown in red. These spectra were recorded at 310 K on a spectrometer operating at 900 MHz (^{1}H Larmor frequency).

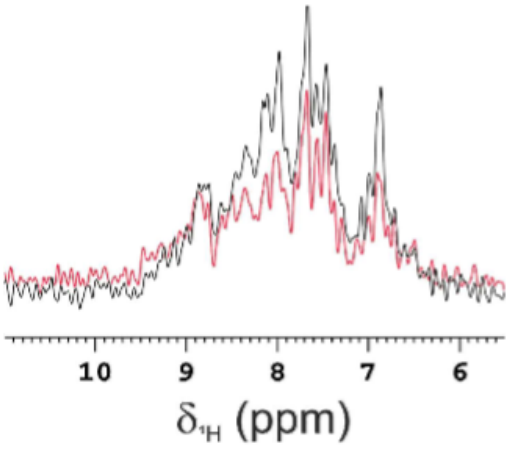

Figure 5. Estimation of ANSII content within RBC. NMR signal from the 1st FID of the $^{1}H-^{15}N$ SOFAST-HMQC of encapsulated ANSII (black), recorded immediately after sample preparation, and a solution of free ANSII 18 μmol dm^{-3} (red). The spectra were acquired at 310 K on a spectrometer operating at 1200 MHz (^{1}H Larmor frequency).

one preparation to another for the same protein. These differences are likely due to several factors, including the varying concentrations of the protein, challenges in reproducibility during the preparation process, particularly concerning the number of red blood cells treated and introduced into the NMR tube, and possibly the concentration of paramagnetic species. Tuning these parameters is an essential step to ensure the reproducibility of RBC as a delivery system, and thus its applicability in the pharmaceutical industry.

Quantification of Encapsulated Protein. An estimation of the encapsulation efficiency of enzymes within RBCs can be obtained by comparing the intensity of signals of encapsulated protein in RBCs with those of free one of known concentration in the same buffer. A solution 18 μmol dm^{-3} of free ANSII was compared with the ANSII-RBC complex. The same NMR acquisition parameters were used to compare the NMR signal from the first FID of the 2D $^{1}H-^{15}N$ SOFAST-HMQC for both spectra (Figure 5). Given the absence of severe line-broadening on the NMR signal from the encapsulated ANSII, we could assume that the different relaxation properties of ANSII within the RBC complex do not significantly affect the integral calculation. The ANSII-RBC signals were 1.4 times more intense than the free ANSII signals. Therefore, we could estimate the concentration of encapsulated ANSII to be approximately 25 μmol dm^{-3}. Considering that the initial concentration of ANSII in the solution used for encapsulation in RBC was 236 μmol dm^{-3}, we estimate an encapsulation efficiency close to 10%, which aligns with literature values.[56]

■ DISCUSSION

The analysis of NMR spectra of protein therapeutics is a widely recognized method for evaluating the preservation of their structural integrity. Biological assays can provide the amount of biologically active protein. For instance, enzymatic assays are employed to assess the quantity of encapsulated active enzyme. However, these assays do not provide information on the presence of inactive enzyme, which may result from partial unfolding, alterations in the active site, or degradation. This information is particularly relevant because the folding or degradation state of a protein significantly influences its immunogenicity.

In-cell NMR studies have demonstrated that the quality of the NMR spectra is significantly influenced by the characteristics of the proteins expressed or internalized within the cells. Considering the evident similarities between the proteins incorporated into RBCs and those examined in in-cell NMR investigations, this study identified three proteins of pharmacological significance to validate the applicability of the proposed methodology. CAII, also physiologically present in erythrocytes, served as an optimal model for the initial optimization of the encapsulation protocol due to its stability and high expression levels. Its high molecular weight and globular structure place it at the boundary of systems that can be studied without deuteration. As a metalloenzyme, it also enables us to evaluate the possible effects of the cellular environment on the protein-metal stability at the high concentrations achieved in this delivery system. The spectra recorded on CAII showed that the protein maintained its native conformation upon encapsulation, as evidenced by the superposition of the resonances in the 2D $^{1}H-^{15}N$ SOFAST-HMQC NMR spectra of the free and encapsulated proteins. Almost all the resonances on the 2D $^{1}H-^{15}N$ SOFAST-HMQC spectrum of the encapsulated protein corresponding both to secondary structure elements and loops were easily reassigned, further proving the preservation of the native HOS. CAII has also been used to show the capability of the proposed

https://doi.org/10.1021/jacs.5c05617

method to detect the minor structural alterations due to the binding of an inhibitor to the active site of enzymes. The results presented here demonstrate the effectiveness of the NMR method in identifying and quantifying the fraction of inactive enzyme present alongside the active enzyme. Notably, the analysis of the mixture reveals that the chemical shift variations caused by encapsulation are minimal compared to those observed when a ligand interacts with the active site of the enzyme, or when there is unfolding or degradation.

Transthyretin has been considered in this study for its potential applications as drug carrier and additional drug delivery system.[43] TTR, a protein with a complex quaternary structure, is composed of four identical subunits arranged as a dimer of dimers, resulting in a total mass of 55 kDa. Maintaining the tetrameric structure is crucial for its function as a carrier because it features a long channel that spans the entire molecule and contains two binding sites that can accommodate drugs and prodrugs.[44] Despite the size of the protein, which causes line broadening of the signals and somewhat compromises the quality of the spectra also, in buffer solution, the superimposition of the 2D $^{1}H-^{15}N$ SOFAST-HMQC spectra shows that the protein retains its structural integrity upon encapsulation without dissociation into the constitutive monomers. More relevant is the study carried out on L-Asparaginase II, whose RBC formulation stands as a valuable model for the analytical characterization of erythrocyte-encapsulated enzymatic therapies.[12,21] An in-depth investigation into the effects of L-Asparaginase II encapsulation on red blood cells has already been conducted: processed red blood cells (RBCs) showed dehydration, minor morphological changes, and metabolomic shifts but maintained a similar proteomic profile and improved osmotic resistance despite reduced deformability. The encapsulation process did not significantly affect RBCs half-life in a mouse model, suggesting their applicability as drug carriers for extended circulation time of drugs like asparaginase.[45] However, encapsulation effects on the structure of the enzyme have yet to be investigated. Therefore, our solution NMR analysis enabled us to complete the characterization of the complex, confirming the preservation of the high order structure of L-Asparaginase II after encapsulation. The superimposition of the NMR spectra of free enzyme and erythrocyte-encapsulated ANSII confirmed the protein structural integrity within RBCs. Moreover, the quantitative analysis of ANSII encapsulated within red blood cells highlights the efficacy of using NMR spectroscopy to estimate encapsulation efficiency. By comparing the NMR signals from encapsulated ANSII with a reference solution of known concentration, we successfully estimated the degree of encapsulation, finding an efficiency close to 10% which aligns well with existing literature. The ability to perform this analysis on the pharmaceutical formulation with minimal sample preparation and relatively short acquisition times represents a further advantage for the development and optimization of pharmaceutical formulations.

CONCLUSIONS

The development of an easily accessible methodology for the structural characterization of proteins encapsulated inside erythrocytes and red cell-derived nanoparticles represents a critical step for advancing and refining red blood cell-based drug delivery systems. Although the requirement for isotopically enriched proteins makes this methodology unsuitable for real-time monitoring of RBCs autologous preparations, this study demonstrated that NMR allows for a quick and straightforward assessment of the HOS preservation of erythrocyte-encapsulated proteins with minimal sample manipulation. Although the quality of the spectra does not allow for a detailed analysis of all the changes typically examined in comparability studies carried out in solution, this analysis still reveals any significant alterations that impact the structure of the encapsulated proteins and, consequently, their function. The analysis carried out on two enzymes and a carrier protein, different for molecular weight, structure, and function, shows that all the proteins retain their native structural features. The same NMR data can be used for fast, nondestructive quantification of the encapsulated protein unrelated to enzymatic activity and for general application. Consequently, despite the limitations still existing for labeling and size of many therapeutic proteins, this methodology is an important tool for designing, optimizing, formulating, and manufacturing novel red blood cell-based drug delivery systems.

MATERIALS AND METHODS

Materials. Luria−Bertani (LB) medium, ampicillin, kanamycin, D-glucose, sodium chloride (NaCl), sodium phosphate dibasic (Na_2HPO_4), potassium phosphate monobasic (KH_2PO_4), magnesium sulfate ($MgSO_4$), calcium chloride ($CaCl_2$), ^{15}N-amonium sulfate $(NH_4)_2SO_4$, zinc sulfate ($ZnSO_4$), Tris sulfate (Tris-SO_4), isopropil-β-D-1-tiogalattopiranoside (IPTG), sodium phosphate dibasic heptahydrate ($Na_2HPO_4{\cdot}7H_2O$), sodium phosphate monobasic monohydrate ($NaH_2PO_4{\cdot}H_2O$), Tris hydrochloride (Tris-HCl), dithiothreitol (DTT), hydrochloric acid (HCl), sodium hydroxide (NaOH), $^{2}H-^{13}C-^{15}N$-enriched medium, Coomassie blue, ethylenediaminetetraacetic acid (EDTA), sucrose, reduced glutathione and ATP were purchased from Sigma-Aldrich. Plasmids were obtained from Twist Bioscience, San Francisco, CA.

Expression and Purification of Uniformly Isotopically Enriched Carbonic Anhydrase II [U−^{15}N]. The gene encoding α-CAII into the pCAM vector was transformed into *Escherichia coli* BL21(DE3) cells, which were subsequently precultured overnight in LB medium containing ampicillin (0.1 mg cm^{-3}) and 1% glucose at 37 °C and 160 rpm. The main culture (1 dm^3) was then incubated at 37 °C, 160 rpm until it reached the optical density at 600 nm (OD_{600}) ∼0.6 and harvested for 15 min at 4000 rpm to proceed with the isotopic enrichment according to the Marley method. The cell pellet was resuspended in 1 dm^3 of M9 minimal medium (3 g dm^{-3} KH_2PO_4, 0.5 g dm^{-3} NaCl, 6.8 g dm^{-3} Na_2HPO_4) supplemented with 2 mmol dm^{-3} $MgSO_4$, 0.2 mmol dm^{-3} $CaCl_2$, 3 g dm^{-3} glucose, 1.2 g dm^{-3} ^{15}N-ammonium sulfate, 0.5 mmol dm^{-3} $ZnSO_4$ and ampicillin. The new culture was further incubated for 30 min at 37 °C and 160 rpm, before inducing with 1 mmol dm^{-3} IPTG and incubating overnight at 25 °C and 160 rpm. The cell culture was harvested at 7500 rpm for 20 min (JA-10 Beckman Coulter). The cell pellet was resuspended in 70 cm^3 of 20 mmol dm^{-3} Tris-SO_4, 500 μmol·dm^{-3} $ZnSO_4$ pH 8 and underwent 10 cycles of sonication for 30 s with a resting period of 3 min on ice, 60% power (sonicator Vibra-cell of Sonics & Materials Inc.). The lysate was ultracentrifuged at 40,000 rpm for 40 min (Beckman Optima LE-80K Ultracentrifuge, rotor F15−6 × 100y from Thermo Scientific) and the supernatant recovered is filtered with a 0.45 μm filter. The supernatant, containing crude α-CAII protein, was purified by Nickel affinity chromatography using a linear 0−0.5 mol dm^{-3} Imidazole gradient on a HisTrap 5 cm^3 (GE Healthcare). Finally, the α-CAII was subjected to a size-exclusion chromatography on a Superdex 75pg 26/60 column (Amersham Biosciences) in 50 mmol dm^{-3} sodium phosphate buffer at pH 7 (7.744 g dm^{-3} of $Na_2HPO_4{\cdot}7H_2O$, 2.913 g dm^{-3} of $NaH_2PO_4{\cdot}H_2O$, pH adjusted with HCl and NaOH).

Expression and Purification of Uniformly Isotopically Enriched TTR [U−^{15}N]. *E. coli* BL21(DE3) RIPL cells were transformed with pET-28a(+) plasmid coding for TTR gene. The

https://doi.org/10.1021/jacs.5c05617

cells were cultured in ^{15}N-enriched M9 minimal medium supplemented with kanamycin at 37 °C until OD_{600} reached 0.6−0.8 and then 1 mmol dm^{-3} IPTG was added for induction. The cells were incubated overnight at 37 °C and then harvested by centrifugation (JA-10 Beckman Coulter) at 7500 rpm for 15 min at 4 °C. The pellet was suspended in 20 mmol dm^{-3} Tris-HCl, pH 8.6 buffer supplied with 5 mmol dm^{-3} DTT (80 cm^3 per liter of culture) and sonicated at 4 °C for 10 cycles of 30 s ON and 3 min OFF, at 60% power. The suspension was centrifuged at 40,000 rpm (Beckman Optima LE-80K Ultracentrifuge, rotor F15−6 × 100y Thermo Scientific) for 40 min and the pellet was discarded. The protein was purified by anionic-exchange chromatography using a HiPrep Q FF 16/10 column (GE Healthcare Life Science), previously equilibrated with 20 mmol dm^{-3} Tris-HCl, pH 8.6. The protein was eluted in 20 mmol dm^{-3} Tris-HCl, pH 8.6 with a linear 0−1 mol dm^{-3} NaCl gradient. Fractions containing pure TTR were joined and purified by Size Exclusion Chromatography using HiLoad Superdex 75pg 26/60 in 50 mmol dm^{-3} phosphate buffer, pH 7.5.

Expression and Purification of Uniformly Isotopically Enriched L-Asparaginase II [U-^{2}D-^{13}C−^{15}N]. *E. coli* (DE3) C41 cells were transformed with pET-21a (+) plasmid with ANSII insert. The cells were cultured at 37 °C in ^{2}H−^{13}C-^{15}N-enriched medium (*E. coli*-OD2 rich growth media, Silantes) supplemented with ampicillin until OD_{600} 0.6 was reached, then 1 mmol dm^{-3} IPTG was added for induction. All reagents were previously dissolved in ^2H_2O. The culture was incubated at 37 °C overnight and then harvested by centrifugation at 6500 rpm (JA-10 Beckman Coulter) for 15 min at 4 °C. The pellet was suspended in 10 mmol dm^{-3} Tris-HCl, pH 8.0, 15 mmol dm^{-3} EDTA, 20% sucrose buffer (60 cm^3 per liter of culture) and incubated at 4 °C for 20 min under magnetic stirring. The suspension was centrifuged at 10,000 rpm (Beckman Optima LE-80K Ultracentrifuge, rotor F15−6 × 100y, Thermo Scientific) for 30 min and the supernatant was discarded. The recovered pellet was resuspended in H_2O milli-Q (60 cm^3 per liter of culture) and incubated at 4 °C for 20 min under magnetic stirring. Again, the suspension was centrifuged at 10,000 rpm for 30 min and the pellet was discarded. The supernatant was treated with ammonium sulfate to trigger the precipitation of ANSII. Under magnetic stirring, solid ammonium sulfate was added in aliquots up to 50% saturation. The precipitate was removed by centrifugation and discarded, then additional ammonium sulfate was added up to 90% saturation to trigger the precipitation of ANSII. The precipitated ANSII was redissolved in a minimal amount of 20 mmol dm^{-3} Tris-HCl, pH 8.6, and dialyzed extensively against the same buffer. ANSII was purified by anionic-exchange chromatography using a HiPrep Q FF 16/10 column (GE Healthcare Life Science). The protein was eluted in 20 mmol dm^{-3} Tris-HCl, pH 8.6 with a linear 0−1 mol dm^{-3} NaCl gradient. Fractions containing pure ANSII were identified by Coomassie staining SDS-PAGE gels, then joined and dialyzed extensively against the final buffer.

Encapsulation of ^{15}N-Labeled Proteins in Red Blood Cells. Commercially available Bovine red blood cells Packed 100% from Innovative Research were used. RBCs were washed by diluting 5 cm^3 of 100% packed RBC in 5 cm^3 of cold PBS. The sample was centrifuged at 2305 rpm (Heraeus Megafuge 16R Centrifuge, TX-400 Swinging Bucket Rotor, Thermo Scientific) for 1 min at 4 °C and the supernatant was removed. The process was repeated two more times. ^{15}N-labeled CAII, TTR and ANSII were encapsulated using a previously reported hypotonic dialysis method of encapsulation.[57] Seven parts (700 mm^3) of washed packed RBC were mixed with 3 parts (300 mm^3) of a concentrated solution of the protein (3 mmol dm^{-3} solution of CAII, 1 mmol dm^{-3} solution of TTR and 236 μmol dm^{-3} solution of ANSII). One cm^3 of this suspension was placed on a dialysis tube (12 kDa MWCO) and dialyzed against 150 cm^3 of hypotonic buffer (5 mmol dm^{-3} KH_2PO_4, 5 mmol dm^{-3} K_2HPO_4, pH 7.4) at 4 °C with a rotation of ∼20 rev/min for 180 min. The erythrocytes were then resealed by transferring the dialysis tube into a container holding 150 cm^3 of isotonic buffer (PBS 1×, 5 mmol dm^{-3} glucose, 5 mmol dm^{-3} $MgCl_2$) at 37 °C under continuous stirring for 60 min. The addition of reduced glutathione (3 mmol dm^{-3}) and ATP (2 mmol dm^{-3}) in the buffer was also evaluated (see Figure S6). An aliquot of CAII was also titrated with the active-site ligand furosemide. Then 1.95 cm^3 of a solution of free CAII at the concentration of 330 μmol dm^{-3} was mixed with 1.89 cm^3 of a solution of inhibited CAII at the concentration of 330 μmol dm^{-3}. The volume of the resulting solution was reduced to 340 mm^3. The same procedure for protein encapsulation was also performed on this sample.

In order to wash away nonencapsulated ^{15}N isotopically enriched protein or released components from the erythrocytes, the sample was transferred into a dialysis tube of 1000 kDa MWCO and dialyzed against 1 dm^3 of isotonic buffer at 4 °C for 12 h. This dialysis was repeated 2 times. The dialyzed erythrocytes were then washed with an equal volume of cold PBS three times. A first FID of 2D ^{1}H ^{15}N SOFAST-HMQC spectrum of a sample from the last wash was acquired in order to confirm the absence of any ^{15}N-labeled protein outside of the red blood cells.

Two distinct control experiments were conducted using CAII, the first protein to be studied and used to verify the efficacy of the protocol. These experiments aimed to rule out the possibility of protein adsorption on the surface of the red blood cells and to confirm the efficacy of the washing procedure.

In Control 1, the erythrocytes were subjected to hypotonic dialysis in the absence of proteins. The samples were prepared by mixing 7 parts of washed packed RBC with 3 parts of cold PBS, then 1 cm^3 of cell suspension was placed on a dialysis tube (12 kDa MWCO). The sample was dialyzed against 150 cm^3 of hypotonic buffer at 4 °C with a rotation of around ∼20 rev/min for 180 min. The dialysis tube was then transferred to a container holding 150 cm^3 of isotonic buffer at 37 °C under continuous stirring for 60 min. In order to wash away the released components from the erythrocytes, the sample was transferred into a dialysis tube of 1000 kDa MWCO and dialyzed against 1 dm^3 of isotonic buffer at 4 °C for 12 h. This dialysis was repeated two times. The dialyzed erythrocytes were then washed with an equal volume of cold PBS three times.

In Control 2, proteins were added but not encapsulated. The samples were prepared by mixing 7 parts of washed packed RBC with 3 parts of a 3 mmol dm^{-3} solution of the ^{15}N-labeled CAII, then 1 cm^3 of cell suspension was placed on a dialysis tube (12 kDa MWCO). The sample was dialyzed against 150 cm^3 of isotonic buffer at 4 °C with a rotation of around ∼20 rev/min for 180 min. The sample was then dialyzed against the same isotonic buffer at 37 °C under continuous stirring for 60 min. In order to wash away the nonencapsulated ^{15}N isotopically enriched protein, the sample was transferred into a dialysis tube of 1000 kDa MWCO and dialyzed against 1 dm^3 of isotonic buffer at 4 °C for 12 h. This dialysis was repeated two times. The dialyzed erythrocytes were then washed with an equal volume of cold PBS three times.

Sample Preparation and NMR Measurements. All NMR experiments were recorded at 310 K on Bruker Avance NEO spectrometers, operating at 900 (CAII and ANSII) and 1200 (TTR) MHz, ^{1}H Larmor frequency (21.1 and 28.2 T, respectively), equipped with triple resonance cryoprobes. Experiments on encapsulated CAII were also performed on a Bruker Avance NEO spectrometer operating at 600 MHz, ^{1}H Larmor frequency (14.1 T), and equipped with a CPQCI cryoprobe.

The NMR samples of the encapsulated proteins were prepared with 540 mm^3 of RBC suspension (in PBS buffer, pH 7.4) and 60 mm^3 of ^2H_2O, for field frequency lock purposes. The spectra of the free proteins were recorded using the same parameters and buffer composition for comparison purposes. 2D ^{1}H−^{15}N SOFAST-HMQC experiments[58] were acquired with an H_N offset of 8.1 ppm and an excitation H_N bandwidth of 4 ppm, acquisition times of 35 ms (ANSII and CAII) or 20 ms (TTR) and 14 ms (ANSII and CAII) or 10 ms (TTR) for the direct and indirect dimensions, respectively, 256 scans (for the spectra recorded at 900 and 1200 MHz) and 1024 scans (for the spectra recorded at 600 MHz), and interscan delay of 0.2 s. The lower acquisition times used to record the spectra of TTR are related to its shorter transverse relaxation time, due to its high molecular weight and absence of deuteration.

https://doi.org/10.1021/jacs.5c05617

The experiments for the determination of ^{15}N transverse relaxation rates were recorded at 310 K and 600 MHz on ^{15}N-enriched samples of free CAII in PBS and CAII encapsulated in RBCs. ^{15}N transverse relaxation rates (R_2) were measured using a Carr−Purcell−Meiboom−Gill (CPMG) sequence[59,60] with delays of 8.48, 16.96, 25.2, 33.92, 42.4, 50.88, 67.84, 84.8, 101.76, 118.72, 144.16, 169.6 ms for the free protein and 8.48, 16.96, 42.4,84.8 and 144.16 ms for the encapsulated protein, with a refocusing delay of 450 μs. Because of the low signal-to-noise ratio, the spectra for the evaluation of ^{15}N transverse relaxation rates of the encapsulated protein were acquired using 1024 scans. Transverse relaxation rates were determined by fitting the signal intensities as a function of the delay to a single-exponential decay using Dynamics Center (Bruker) software.

All the spectra were processed on a Bruker TopSpin 4.0 software package and analyzed with CARA program (ETH Zürich).

■ ASSOCIATED CONTENT

Supporting Information

The Supporting Information is available free of charge at https://pubs.acs.org/doi/10.1021/jacs.5c05617.

Additional NMR spectra for confirming the success of the washing steps; evaluation of the system stability over time and using different buffers; transverse relaxation analysis for CAII; and comparison of NMR spectra obtained at different magnetic fields (PDF)

■ AUTHOR INFORMATION

Corresponding Author

Marco Fragai − *Department of Chemistry Ugo Schiff (DICUS), University of Florence, 50019 Sesto Fiorentino, Italy; Centro di Risonanze Magnetiche (CERM), University of Florence, 50019 Sesto Fiorentino, Italy; Consorzio Interuniversitario di Risonanze Magnetiche di Metalloproteine (CIRMMP), 50019 Sesto Fiorentino, Italy;* orcid.org/0000-0002-8440-1690; Email: marco.fragai@unifi.it

Authors

Luis Padilla-Cortés − *Department of Chemistry Ugo Schiff (DICUS), University of Florence, 50019 Sesto Fiorentino, Italy; Centro di Risonanze Magnetiche (CERM), University of Florence, 50019 Sesto Fiorentino, Italy*

Giulia Roxana Gheorghita − *Department of Chemistry Ugo Schiff (DICUS), University of Florence, 50019 Sesto Fiorentino, Italy; Centro di Risonanze Magnetiche (CERM), University of Florence, 50019 Sesto Fiorentino, Italy; Giotto Biotech, 50129 Firenze, Italy*

Francesco Currò − *Department of Chemistry Ugo Schiff (DICUS), University of Florence, 50019 Sesto Fiorentino, Italy; Centro di Risonanze Magnetiche (CERM), University of Florence, 50019 Sesto Fiorentino, Italy*

Rebecca Calamandrei − *Department of Chemistry Ugo Schiff (DICUS), University of Florence, 50019 Sesto Fiorentino, Italy; Centro di Risonanze Magnetiche (CERM), University of Florence, 50019 Sesto Fiorentino, Italy; Consorzio Interuniversitario di Risonanze Magnetiche di Metalloproteine (CIRMMP), 50019 Sesto Fiorentino, Italy*

Bianca Susini − *Department of Chemistry Ugo Schiff (DICUS), University of Florence, 50019 Sesto Fiorentino, Italy; Centro di Risonanze Magnetiche (CERM), University of Florence, 50019 Sesto Fiorentino, Italy; Consorzio Interuniversitario di Risonanze Magnetiche di Metalloproteine (CIRMMP), 50019 Sesto Fiorentino, Italy*

Sara Callozzo − *Department of Chemistry Ugo Schiff (DICUS), University of Florence, 50019 Sesto Fiorentino, Italy; Centro di Risonanze Magnetiche (CERM), University of Florence, 50019 Sesto Fiorentino, Italy; Consorzio Interuniversitario di Risonanze Magnetiche di Metalloproteine (CIRMMP), 50019 Sesto Fiorentino, Italy*

Giulia Crivello − *Consorzio Interuniversitario di Risonanze Magnetiche di Metalloproteine (CIRMMP), 50019 Sesto Fiorentino, Italy; Department of Agricultural and Food Sciences (DISTAL), University of Bologna, 475121 Cesena, Italy*

Pasquale Russomanno − *Department of Chemistry Ugo Schiff (DICUS), University of Florence, 50019 Sesto Fiorentino, Italy; Centro di Risonanze Magnetiche (CERM), University of Florence, 50019 Sesto Fiorentino, Italy*

Enrico Ravera − *Department of Chemistry Ugo Schiff (DICUS), University of Florence, 50019 Sesto Fiorentino, Italy; Centro di Risonanze Magnetiche (CERM), University of Florence, 50019 Sesto Fiorentino, Italy; Consorzio Interuniversitario di Risonanze Magnetiche di Metalloproteine (CIRMMP), 50019 Sesto Fiorentino, Italy;* orcid.org/0000-0001-7708-9208

Linda Cerofolini − *Department of Chemistry Ugo Schiff (DICUS), University of Florence, 50019 Sesto Fiorentino, Italy; Centro di Risonanze Magnetiche (CERM), University of Florence, 50019 Sesto Fiorentino, Italy; Consorzio Interuniversitario di Risonanze Magnetiche di Metalloproteine (CIRMMP), 50019 Sesto Fiorentino, Italy*

Complete contact information is available at: https://pubs.acs.org/10.1021/jacs.5c05617

Author Contributions

The manuscript was written through contributions of all authors./All authors have given approval to the final version of the manuscript./L.P.-C. and G.R.G. contributed equally.

Notes

The authors declare no competing financial interest.

■ ACKNOWLEDGMENTS

This paper is adapted from a Ph.D. thesis. The authors acknowledge the support and the use of resources of Instruct-ERIC, a landmark ESFRI project, and specifically the CERM/CIRMMP Italy centre, Res4Priopath Joint Research Activities Consortium (ID Number: ISID_JRA_s8mf), "Progetto Dipartimenti di Eccellenza 2023-2027" to the Department of Chemistry "Ugo Schiff" of the University of Florence. "Finanziato dall'Unione europea- Next Generation EU, Missione 4 Componente 1 CUP B53D23015790006 - PRIN 2022 2022ZEZS45 - Molecular recognition of Fusobacterium envelope glycans by Siglecs − GLYDOME; PRIN 2022 DD 104−02-02-2022 (2022WANFH5 CUP: B53D23013990006); MSCA-ITN "Glytunes" (contract n° 956758); Progetto Finalizzato GR-2021-12372019, PNRR-MCNT2-2023-12377336 "Disease biosignatures in ALS/FTD spectrum: new impactful biological perspectives beyond clinical approaches", the Recombinant Proteins JOYNLAB laboratory and the project "Potentiating the Italian Capacity for Structural Biology Services in Instruct Eric (ITACA.SB)" (Project n° IR0000009) within the call MUR 3264/2021 PNRR M4/C2/L3.1.1, funded by the European Union NextGenerationEU. This study was also supported by the European Union - NextGenerationEU programme in the context of the National

Recovery and Resilience Plan, Mission 4, Component 2, Investment 1.4, CN00000041, CN3 "National Center for Gene Therapy and Drugs based on RNA Technology" - Spoke 5 "Inflammatory and Infectious Diseases", CUP: B13C22001010001, and by Italian Ministry of Health project "Hub multidisciplinare e interregionale di ricerca e sperimentazione clinica per il contrasto alle pandemie ed all'antibiotico resistenza" (PAN-HUB 2021-T4-AN-07).

REFERENCES

(1) Schiffmann, R.; Kopp, J. B.; Austin, H. A., III; Sabnis, S.; Moore, D. F.; Weibel, T.; Balow, J. E.; Brady, R. O. Enzyme Replacement Therapy in Fabry DiseaseA Randomized Controlled Trial. *JAMA* **2001**, *285* (21), 2743−2749.

(2) Kakkis, E. D.; Muenzer, J.; Tiller, G. E.; Waber, L.; Belmont, J.; Passage, M.; Izykowski, B.; Phillips, J.; Doroshow, R.; Walot, I.; Hoft, R.; Yu, K. T.; Okazaki, S.; Lewis, D.; Lachman, R.; Thompson, J. N.; Neufeld, E. F. Enzyme-Replacement Therapy in Mucopolysaccharidosis I. *New England Journal of Medicine* **2001**, *344* (3), 182−188.

(3) Veronese, F. M.; Mero, A. The Impact of PEGylation on Biological Therapies. *BioDrugs* **2008**, *22* (5), 315−329.

(4) Cerofolini, L.; Giuntini, S.; Carlon, A.; Ravera, E.; Calderone, V.; Fragai, M.; Parigi, G.; Luchinat, C. Characterization of PEGylated Asparaginase: New Opportunities from NMR Analysis of Large PEGylated Therapeutics. *Chem.—Eur. J.* **2019**, *25* (8), 1984−1991.

(5) Sellaturay, P.; Nasser, S.; Islam, S.; Gurugama, P.; Ewan, P. W. Polyethylene Glycol (PEG) Is a Cause of Anaphylaxis to the Pfizer/BioNTech mRNA COVID-19 Vaccine. *Clin. Exp. Allergy* **2021**, *51* (6), 861−863.

(6) Lee, S. H.; Cha, J. M.; Lee, J. I.; Joo, K. R.; Shin, H. P.; Baek, I. H.; Jeon, J. W.; Lim, J. U.; Lee, J. L.; Lee, H. M.; Cho, Y.-H. Anaphylactic Shock Caused by Ingestion of Polyethylene Glycol. *Intest Res.* **2015**, *13* (1), 90.

(7) Ihler, G. M.; Glew, R. H.; Schnure, F. W. Enzyme Loading of Erythrocytes. *Proc. Natl. Acad. Sci. U.S.A.* **1973**, *70* (9), 2663−2666.

(8) Biagiotti, S.; Paoletti, M. F.; Fraternale, A.; Rossi, L.; Magnani, M. Drug Delivery by Red Blood Cells. *IUBMB Life* **2011**, *63* (8), 621−631.

(9) Muzykantov, V. R. Drug Delivery by Red Blood Cells: Vascular Carriers Designed by Mother Nature. *Expert Opinion on Drug Delivery* **2010**, *7* (4), 403−427.

(10) Koleva, L.; Bovt, E.; Ataullakhanov, F.; Sinauridze, E. Erythrocytes as Carriers: From Drug Delivery to Biosensors. *Pharmaceutics* **2020**, *12* (3), 276.

(11) Mambrini, G.; Mandolini, M.; Rossi, L.; Pierigè, F.; Capogrossi, G.; Salvati, P.; Serafini, S.; Benatti, L.; Magnani, M. Ex Vivo Encapsulation of Dexamethasone Sodium Phosphate into Human Autologous Erythrocytes Using Fully Automated Biomedical Equipment. *Int. J. Pharm.* **2017**, *517* (1), 175−184.

(12) Kwon, Y. M.; Chung, H. S.; Moon, C.; Yockman, J.; Park, Y. J.; Gitlin, S. D.; David, A. E.; Yang, V. C. L-Asparaginase Encapsulated Intact Erythrocytes for Treatment of Acute Lymphoblastic Leukemia (ALL). *J. Controlled Release* **2009**, *139* (3), 182−189.

(13) He, H.; Ye, J.; Wang, Y.; Liu, Q.; Chung, H. S.; Kwon, Y. M.; Shin, M. C.; Lee, K.; Yang, V. C. Cell-Penetrating Peptides Meditated Encapsulation of Protein Therapeutics into Intact Red Blood Cells and Its Application. *J. Controlled Release* **2014**, *176*, 123−132.

(14) Nguyen, P. H. D.; Jayasinghe, M. K.; Le, A. H.; Peng, B.; Le, M. T. N. Advances in Drug Delivery Systems Based on Red Blood Cells and Their Membrane-Derived Nanoparticles. *ACS Nano* **2023**, *17* (6), 5187−5210.

(15) Bianchi, M.; Rossi, L.; Pierigè, F.; Biagiotti, S.; Bregalda, A.; Tasini, F.; Magnani, M. Preclinical and Clinical Developments in Enzyme-Loaded Red Blood Cells: An Update. *Expert Opinion on Drug Delivery* **2023**, *20* (7), 921−935.

(16) Li, Y.; Raza, F.; Liu, Y.; Wei, Y.; Rong, R.; Zheng, M.; Yuan, W.; Su, J.; Qiu, M.; Li, Y.; Raza, F.; Liu, Y.; Wei, Y.; Rong, R.; Zheng, M.; Yuan, W.; Su, J.; Qiu, M. Clinical Progress and Advanced Research of Red Blood Cells Based Drug Delivery System. *Biomaterials* **2021**, *279*, No. 121202.

(17) Jiang, Y.; Yuan, Y.; Peng, F.; Deng, Y.; Ren, C.; Liu, C.; Dong, H.; Tu, T. Erythrocyte-Based Drug Delivery: How Far from Clinical Application? *Curr. Drug Delivery* **2024**, *21* (1), 52−64.

(18) Dolowy, W. C.; Henson, D.; Cornet, J.; Sellin, H. Toxic and Antineoplastic Effects of L-Asparaginase: Study of Mice with Lymphoma and Normal Monkeys and Report on a Child with Leukemia. *Cancer* **1966**, *19* (12), 1813−1819.

(19) Hill, J. M.; Roberts, J.; Loeb, E.; Khan, A.; MacLellan, A.; Hill, R. W. L-Asparaginase Therapy for Leukemia and Other Malignant Neoplasms: Remission in Human Leukemia. *JAMA* **1967**, *202* (9), 882−888.

(20) Bertrand, Y.; Thomas, X.; Baruchel, A.; Mazingue, F.; Auvrignon, A.; Corm, S.; Dombret, H.; Chevallier, P.; Galambrun, C.; Huguet, F.; Legrand, F.; Mechinaud, F.; Vey, N.; Chabaud, S.; Baron, F. N.; Philip, I.; Liens, D.; Godfrin, Y. GRASPALL 2005.01 Clinical Study: L-Asparaginase Loaded into Red Blood Cells Is Effective at Depleting Serum Asparagine in Children and Adults with Relapsed Acute Lymphoblastic Leukaemia (ALL). *Blood* **2008**, *112* (11), 306.

(21) Domenech, C.; Thomas, X.; Chabaud, S.; Baruchel, A.; Gueyffier, F.; Mazingue, F.; Auvrignon, A.; Corm, S.; Dombret, H.; Chevallier, P.; Galambrun, C.; Huguet, F.; Legrand, F.; Mechinaud, F.; Vey, N.; Philip, I.; Liens, D.; Godfrin, Y.; Rigal, D.; Bertrand, Y. L-Asparaginase Loaded Red Blood Cells in Refractory or Relapsing Acute Lymphoblastic Leukaemia in Children and Adults: Results of the GRASPALL 2005−01 Randomized Trial. *Br. J. Hamaetol.* **2011**, *153* (1), 58−65.

(22) Thomas, X.; Le Jeune, C. Erythrocyte Encapsulated L-Asparaginase (Graspa) in Acute Leukemia. *International Journal of Hematologic Oncology* **2016**, *5* (1), 11−25.

(23) Bax, B. E. Erythrocytes as Carriers of Therapeutic Enzymes. *Pharmaceutics* **2020**, *12* (5), 435.

(24) van Beers, M. M. C.; Bardor, M. Minimizing Immunogenicity of Biopharmaceuticals by Controlling Critical Quality Attributes of Proteins. *Biotechnol J.* **2012**, *7* (12), 1473−1484.

(25) Zarrin, A.; Foroozesh, M.; Hamidi, M. Carrier Erythrocytes: Recent Advances, Present Status, Current Trends and Future Horizons. *Expert Opinion on Drug Delivery* **2014**, *11* (3), 433−447.

(26) Rizzo, D.; Cerofolini, L.; Pérez-Rafols, A.; Giuntini, S.; Baroni, F.; Ravera, E.; Luchinat, C.; Fragai, M. Evaluation of the Higher Order Structure of Biotherapeutics Embedded in Hydrogels for Bioprinting and Drug Release. *Anal. Chem.* **2021**, *93* (32), 11208−11214.

(27) Perodeau, J.; Arbogast, L. W.; Nieuwkoop, A. J. Solid-State NMR Characterization of Lyophilized Formulations of Monoclonal Antibody Therapeutics. *Mol. Pharmaceutics* **2023**, *20* (3), 1480−1489.

(28) Cerofolini, L.; Giuntini, S.; Ravera, E.; Luchinat, C.; Berti, F.; Fragai, M. Structural Characterization of a Protein Adsorbed on Aluminum Hydroxide Adjuvant in Vaccine Formulation. *npj Vaccines* **2019**, *4* (1), 20.

(29) Li, M.; Xu, W.; Su, Y. Solid-State NMR Spectroscopy in Pharmaceutical Sciences. *TrAC Trends in Analytical Chemistry* **2021**, *135*, No. 116152.

(30) Brinson, R. G.; Marino, J. P.; Delaglio, F.; Arbogast, L. W.; Evans, R. M.; Kearsley, A.; Gingras, G.; Ghasriani, H.; Aubin, Y.; Pierens, G. K.; Jia, X.; Mobli, M.; Grant, H. G.; Keizer, D. W.; Schweimer, K.; Ståhle, J.; Widmalm, G.; Zartler, E. R.; Lawrence, C. W.; Reardon, P. N.; Cort, J. R.; Xu, P.; Ni, F.; Yanaka, S.; Kato, K.; Parnham, S. R.; Tsao, D.; Blomgren, A.; Rundlöf, T.; Trieloff, N.; Schmieder, P.; Ross, A.; Skidmore, K.; Chen, K.; Keire, D.; Freedberg, D. I.; Suter-Stahel, T.; Wider, G.; Ilc, G.; Plavec, J.; Bradley, S. A.; Baldisseri, D. M.; Sforça, M. L.; Zeri, A. C. de M.; Wei, J. Y.; Szabo, C. M.; Amezcua, C. A.; Jordan, J. B.; Wikström, M. Enabling Adoption of 2D-NMR for the Higher Order Structure Assessment of Monoclonal Antibody Therapeutics. *MAbs* **2019**, *11* (1), 94−105.

(31) Phyo, P.; Zhao, X.; Templeton, A. C.; Xu, W.; Cheung, J. K.; Su, Y. Understanding Molecular Mechanisms of Biologics Drug

https://doi.org/10.1021/jacs.5c05617

Delivery and Stability from NMR Spectroscopy. *Adv. Drug Delivery Rev.* **2021**, *174*, 1−29.
(32) Rößler, P.; Mathieu, D.; Gossert, A. D. Enabling NMR Studies of High Molecular Weight Systems Without the Need for Deuteration: The XL-ALSOFAST Experiment with Delayed Decoupling. *Angew. Chem., Int. Ed.* **2020**, *59* (43), 19329−19337.
(33) Cerofolini, L.; Ravera, E.; Fischer, C.; Trovato, A.; Sacco, F.; Palinsky, W.; Angiuoni, G.; Fragai, M.; Baroni, F. Integration of NMR Spectroscopy in an Analytical Workflow to Evaluate the Effects of Oxidative Stress on Abituzumab: Beyond the Fingerprint of mAbs. *Anal. Chem.* **2023**, *95* (24), 9199−9206.
(34) Song, J.; Taraban, M.; Yu, Y. B.; Lu, L.; Biswas, P. G.; Xu, W.; Xi, H.; Bhambhani, A.; Hu, G.; Su, Y. In-Situ Biophysical Characterization of High-Concentration Protein Formulations Using wNMR. *mAbs* **2024**, *16* (1), No. 2304624.
(35) Du, Y.; Song, J.; Lu, L.; Yeung, E.; Givand, J.; Procopio, A.; Su, Y.; Hu, G. Design of a Reciprocal Injection Device for Stability Studies of Parenteral Biological Drug Products. *J. Pharm. Sci.* **2024**, *113* (5), 1330−1338.
(36) Müntener, T.; Häussinger, D.; Selenko, P.; Theillet, F.-X. In-Cell Protein Structures from 2D NMR Experiments. *J. Phys. Chem. Lett.* **2016**, *7* (14), 2821−2825.
(37) Siegal, G.; Selenko, P. Cells, Drugs and NMR. *J. Magn. Reson.* **2019**, *306*, 202−212.
(38) Dzatko, S.; Krafcikova, M.; Hänsel-Hertsch, R.; Fessl, T.; Fiala, R.; Loja, T.; Krafcik, D.; Mergny, J.-L.; Foldynova-Trantirkova, S.; Trantirek, L. Evaluation of the Stability of DNA I-Motifs in the Nuclei of Living Mammalian Cells. *Angew. Chem., Int. Ed.* **2018**, *57* (8), 2165−2169.
(39) Luchinat, E.; Barbieri, L.; Cremonini, M.; Banci, L. Protein In-Cell NMR Spectroscopy at 1.2 GHz. *J. Biomol NMR* **2021**, *75* (2−3), 97−107.
(40) Luchinat, E.; Banci, L. In-Cell NMR: Recent Progresses and Future Challenges. *Rend. Fis. Acc. Lincei* **2023**, *34* (3), 653−661.
(41) Lu, T.; Lee, C.-H.; Anvari, B. Morphological Characteristics, Hemoglobin Content, and Membrane Mechanical Properties of Red Blood Cell Delivery Systems. *ACS Appl. Mater. Interfaces* **2022**, *14* (16), 18219−18232.
(42) Cerofolini, L.; Staderini, T.; Giuntini, S.; Ravera, E.; Fragai, M.; Parigi, G.; Pierattelli, R.; Luchinat, C. Long-Range Paramagnetic NMR Data Can Provide a Closer Look on Metal Coordination in Metalloproteins. *J. Biol. Inorg. Chem.* **2017**, *23*, 71−80.
(43) Cerofolini, L.; Vasa, K.; Bianconi, E.; Salobehaj, M.; Cappelli, G.; Bonciani, A.; Licciardi, G.; Pérez-Râfols, A.; Padilla-Cortés, L.; Antonacci, S.; Rizzo, D.; Ravera, E.; Viglianisi, C.; Calderone, V.; Parigi, G.; Luchinat, C.; Macchiarulo, A.; Menichetti, S.; Fragai, M. Combining Solid-State NMR with Structural and Biophysical Techniques to Design Challenging Protein-Drug Conjugates. *Angew. Chem., Int. Ed.* **2023**, *62* (31), No. e202303202.
(44) Ravera, E.; Ciambellotti, S.; Cerofolini, L.; Martelli, T.; Kozyreva, T.; Bernacchioni, C.; Giuntini, S.; Fragai, M.; Turano, P.; Luchinat, C. Solid-State NMR of PEGylated Proteins. *Angew. Chem., Int. Ed. Engl.* **2016**, *55* (7), 2446−2449.
(45) Robert, M.; Laperrousaz, B.; Piedrahita, D.; Gautier, E.-F.; Nemkov, T.; Dupuy, F.; Nader, E.; Salnot, V.; Mayeux, P.; D'Alessandro, A.; Lavazec, C.; Joly, P.; Scheer, A.; Connes, P.; Cibiel, A. Multiparametric Characterization of Red Blood Cell Physiology after Hypotonic Dialysis Based Drug Encapsulation Process. *Acta Pharmaceutica Sinica B* **2022**, *12* (4), 2089−2102.
(46) Schanda, P.; Kupče, Ē.; Brutscher, B. SOFAST-HMQC Experiments for Recording Two-Dimensional Deteronuclear Correlation Spectra of Proteins within a Few Seconds. *J. Biomol. NMR* **2005**, *33* (4), 199−211.
(47) Lodemann, P.; Schorer, G.; Frey, B. M. Wrong Molar Hemoglobin Reference Values—a Longstanding Error That Should Be Corrected. *Ann. Hematol* **2010**, *89* (2), 209−209.
(48) Luchinat, E.; Barbieri, L.; Cremonini, M.; Nocentini, A.; Supuran, C. T.; Banci, L. Drug Screening in Human Cells by NMR Spectroscopy Allows the Early Assessment of Drug Potency. *Angew. Chem., Int. Ed. Engl.* **2020**, *59* (16), 6535−6539.
(49) Luchinat, E.; Banci, L. A Unique Tool for Cellular Structural Biology: In-Cell NMR *. *J. Biol. Chem.* **2016**, *291* (8), 3776−3784.
(50) Luchinat, E.; Banci, L. In-Cell NMR: A Topical Review. *IUCrJ.* **2017**, *4* (2), 108−118.
(51) Theillet, F.-X.; Binolfi, A.; Frembgen-Kesner, T.; Hingorani, K.; Sarkar, M.; Kyne, C.; Li, C.; Crowley, P. B.; Gierasch, L.; Pielak, G. J.; Elcock, A. H.; Gershenson, A.; Selenko, P. Physicochemical Properties of Cells and Their Effects on Intrinsically Disordered Proteins (IDPs). *Chem. Rev.* **2014**, *114* (13), 6661−6714.
(52) Wang, Y.; Li, C.; Pielak, G. J. Effects of Proteins on Protein Diffusion. *J. Am. Chem. Soc.* **2010**, *132* (27), 9392−9397.
(53) Kanias, T.; Acker, J. P. Biopreservation of Red Blood Cells−the Struggle with Hemoglobin Oxidation. *FEBS J.* **2010**, *277* (2), 343−356.
(54) Bertini, I. *Biological Inorganic Chemistry: Structure and Reactivity*; University Science Books, **2007**.
(55) Bertini, I.; Luchinat, C.; Parigi, G.; Ravera, E. Chapter 7 - Transition Metal Ions: Shift and Relaxation. In *NMR of Paramagnetic Molecules (Second ed.)*; Bertini, I.; Luchinat, C.; Parigi, G.; Ravera, E., Eds.; Elsevier: Boston, 2017; 175−253.
(56) Borsakova, D. V.; Plakhotnik, M. E.; Koleva, L. D.; Bovt, E. A.; Alexandrovich, Y. G.; Ataullakhanov, F. I.; Sinauridze, E. I. Comparative methodological studies of L-asparaginase encapsulation into erythrocytes. *Oncohematology* **2018**, *13* (3), 91−101.
(57) Bax, B. E.; Bain, M. D.; Talbot, P. J.; John Parker-Williams, E.; Chalmers, R. A. Survival of Human Carrier Erythrocytes in Vivo. *Clinical Science* **1999**, *96* (2), 171−178.
(58) Schanda, P.; Brutscher, B. Very Fast Two-Dimensional NMR Spectroscopy for Real-Time Investigation of Dynamic Events in Proteins on the Time Scale of Seconds. *J. Am. Chem. Soc.* **2005**, *127* (22), 8014−8015.
(59) Kay, L. E.; Nicholson, L. K.; Delaglio, F.; Bax, A.; Torchia, D. A. Pulse Sequences for Removal of the Effects of Cross Correlation between Dipolar and Chemical-Shift Anisotropy Relaxation Mechanisms on the Measurement of Heteronuclear T1 and T2 Values in Proteins. *Journal of Magnetic Resonance (1969)* **1992**, *97* (2), 359−375.
(60) Peng, J. W.; Wagner, G. Investigation of Protein Motions via Relaxation Measurements. *Meth. Enzymol.* **1994**, *239*, 563−596.

https://doi.org/10.1021/jacs.5c05617

SUPPORTING INFORMATION

NMR Assessment of the High Order Structure of Biological Therapeutics in Erythrocytes Provides a Tool for Drug Delivery Design

Luis Padilla-Cortés [‡[a][b]], Giulia Roxana Gheorghita [‡[a][b][c]], Francesco Currò[a][b], Rebecca Calamandrei[a][b][d], Bianca Susini[a][b][d], Sara Callozzo[a][b][d], Giulia Crivello[d][e], Pasquale Russomanno[a][b], Enrico Ravera[a][b][d], Linda Cerofolini[a][b][d], and Marco Fragai*[a][b][d]

[a] Department of Chemistry Ugo Schiff (DICUS), University of Florence, Via della Lastruccia 3, 50019, Sesto Fiorentino, Italy.
[b] Centro di Risonanze Magnetiche (CERM), University of Florence, Via Luigi Sacconi 6, 50019, Sesto Fiorentino, Italy.
[c] Giotto Biotech, s.r.l. Via Francesco Crispi 6, 50129Firenze, Italy
[d] Consorzio Interuniversitario di Risonanze Magnetiche di Metalloproteine (CIRMMP), Via Luigi Sacconi 6, 50019, Sesto Fiorentino, Italy.
[e] Department of Agricultural and Food Sciences (DISTAL), University of Bologna, Piazza Goidanich 60, 475121, Cesena, Italy

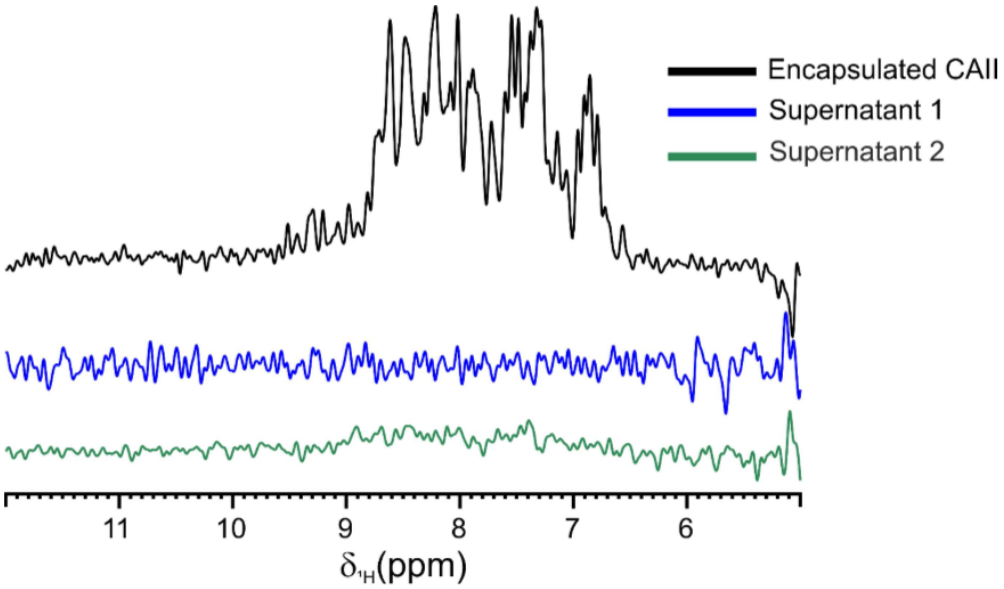

Figure S1. 1st FIDs of the 2D ^{1}H-^{15}N SOFAST-HMQC spectra of a) encapsulated ^{15}N CAII in RBC (black), b) supernatant of the last rinse step (blue, supernatant 1), and c) supernatant recovered from the NMR tube after the acquisition of the set of NMR experiments (lasting 17 h) on CAII encapsulated in RBCs (green, supernatant 2). The data prove that the observed signal in the 2D ^{1}H-^{15}N SOFAST-HMQC spectrum is related to the encapsulated protein only and that the protein is not released from RBCs during the acquisition of the NMR spectra.

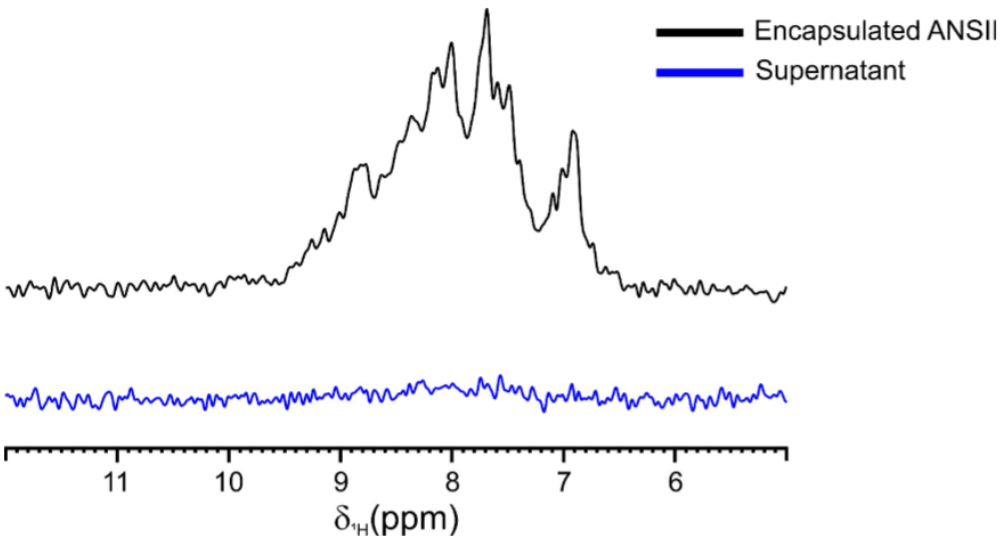

Figure S2. 1st FIDs of the 2D ^{1}H-^{15}N SOFAST-HMQC spectra of encapsulated ^{2}H-^{13}C-^{15}N ANSII in RBCs (black) and supernatant of the last rinse step (blue, supernatant 1).

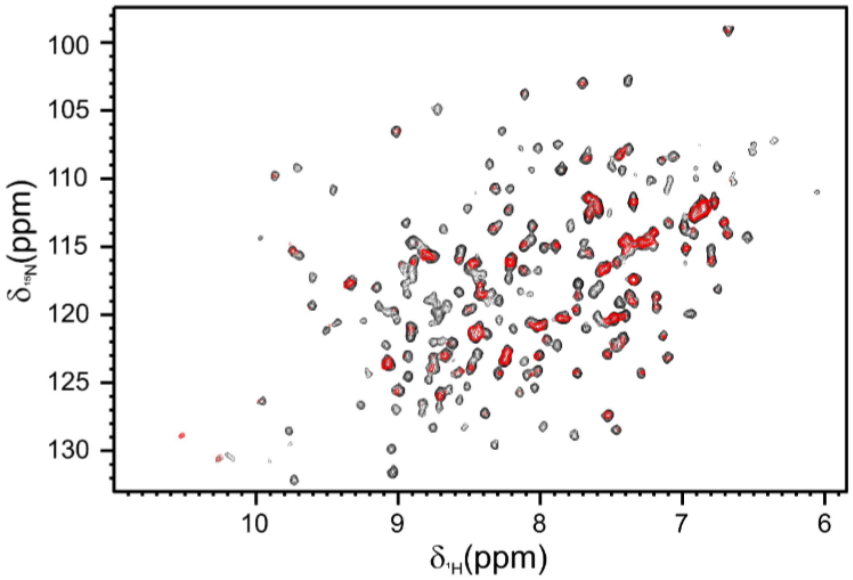

Figure S3. Broadening of NMR signals for CAII encapsulated in RBC over time at 310K. Overlay of 2D ^{1}H-^{15}N SOFAST-HMQC spectra of CAII encapsulated in RBC, acquired immediately after sample preparation (black) and after 2 h of permanence within the magnet at 310 K (red). The spectra were acquired at 310 K on a spectrometer operating at 900 MHz (^{1}H Larmor frequency).

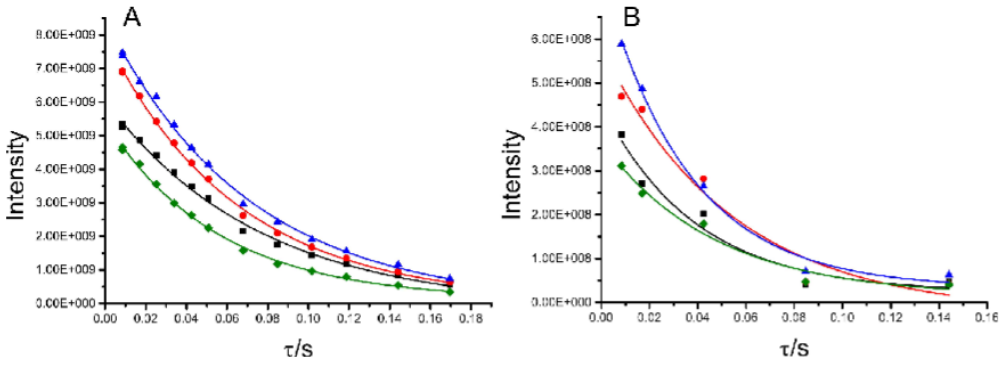

Figure S4. Curves of ^{15}N transverse relaxation. The curves were obtained fitting the signal intensity of the 1st FID of 2D ^{1}H-^{15}N HSQC-type CPMG experiments in Dynamic Center (Bruker) software for (A) free CAII and (B) CAII encapsulated in RBCs.

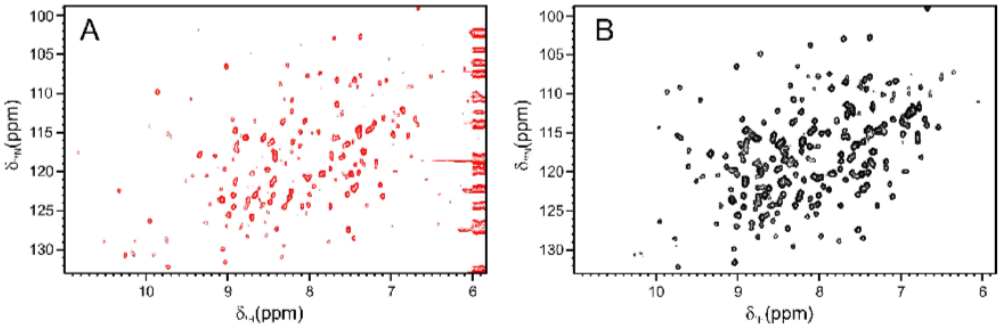

Figure S5. Comparison of 2D ^{1}H-^{15}N SOFAST HMQC spectra recorded on samples of CAII encapsulated in RBCs at (A) 600 MHz (red) and (B) 900 MHz (black). The same acquisition times on the direct and indirect dimensions were used. The spectra were recorded using 1024 and 256 scans for the instrument operating at 600 and 900 MHz, respectively.

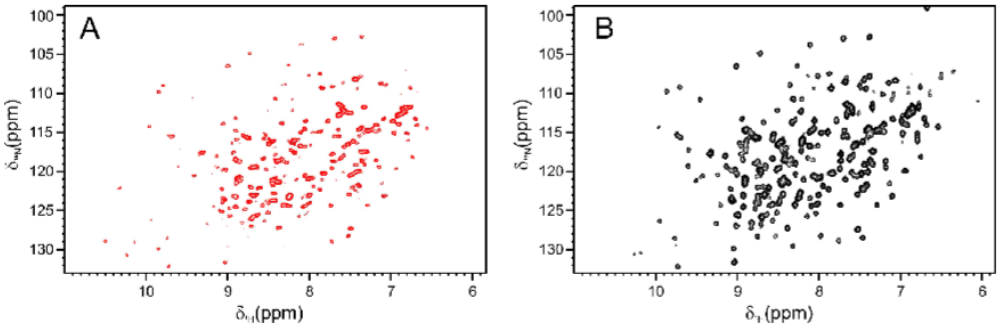

Figure S6. Comparison of 2D ^{1}H-^{15}N SOFAST HMQC spectra recorded on samples of CAII encapsulated in RBCs with (A) or without (B) reduced glutathione (3 mmol·dm^{-3}) and ATP (2 mmol·dm^{-3}) in the buffer. Spectrum (A) was acquired on a spectrometer operating at 950 MHz, while spectrum (B) on a spectrometer operating at 900 MHz. The same acquisition times on the direct and indirect dimensions were used.

4.3 Monitoring PEG Shedding with NMR: Molecular Insight into LNP Stability

In this section the draft of the latest paper prepared in the frame of this PhD project is reported.

In this study we explored the phenomenon of PEG shedding from LNPs using Pulsed Gradient Spin-Echo (PGSE) NMR to assess formulation stability under various conditions and increase the knowledge of which factors influence the release in vivo. The rate of PEG shedding influences LNP biodistribution and should be considered in formulation design and as quality control to ensure LNP efficacy. Complementary analyses with Dynamic Light Scattering (DLS), Nanoparticle Tracking Analysis (NTA), and Cryo-Electron Microscopy (Cryo-EM) were conducted to assess shed PEG and changes in particle size and morphology.

Monitoring PEG Shedding with NMR: Molecular Insight into LNP Stability

Francesco Currò[a][b][c], Linda Cerofolini[a][b][e], Gaëtan Dias Mirandela[d], Silvia Martini[c], Frédéric Fontaine[d], Francesco Berti[c], Milos Erak[d], Massimiliano Biagini[c], Daniela Stranges[c], Marco Fragai[a][b][e], Maxime Denis[c]

[a] Department of Chemistry Ugo Schiff (DICUS), University of Florence, Via della Lastruccia, 3, 50019, Sesto Fiorentino, Italy

[b] Centro di Risonanze Magnetiche (CERM), University of Florence,Via Luigi Sacconi 6, 50019, Sesto Fiorentino, Italy

[c] GSK, Siena, Italy

[d] GSK, Rixensart, Belgium

[e] Consorzio Interuniversitario di Risonanze Magnetiche di Metalloproteine (CIRMMP) Via Luigi Sacconi 6, 50019, Sesto Fiorentino, Italy

KEYWORDS: LNP, NMR, PEG, stability, analytics

ABSTRACT: Lipid nanoparticles (LNPs) are essential carriers for nucleic acid therapeutics. They are coated with a pegylated lipid that prevents particle aggregation and rapid clearance by the immune system. However, PEG shedding in serum is necessary to facilitate cellular uptake, making the rate of PEG detachment a critical factor in modulating LNP biodistribution and activity. In this study, we investigated PEG shedding from LNPs using Pulsed Gradient Spin-Echo (PGSE) NMR to provide insights into the stability and behavior of PEG-LNP under various conditions. PEG release was detected over incubation of formulations at 25°C, demonstrating that shedding can occur also outside serum environment, raising a concern of stability for the whole manufacturing process and storage time. Conversely, we assessed the impact of a freeze-thaw cycle at -80°C and lyophilization, which showed no significant increase in free PEG content, demonstrating PEG attachment stability under these long-term storage conditions. Moreover, we showed how PEG shedding rate of different formulations in serum can be predicted just by adding albumin in the NMR tubes with the LNP solution. Shorter PEG chains (14-C DMPE-PEG2K) exhibited faster shedding rates compared to longer chains (18-C DSPE-PEG2K), as already reported in serum. Complementary analyses using Dynamic Light Scattering (DLS), Nanoparticle Tracking Analysis (NTA), and Cryo-Electron Microscopy (Cryo-EM) were performed to assess the potential of these techniques to detect shed PEG and to investigate any concomitant changes in particle size and morphology, highlighting the unique NMR capability of directly assessing this phenomenon.

Introduction

Lipid nanoparticles (LNPs) are spherical vesicles composed of multilayer cores dispersed between lipid layers, where positively charged lipids interplay with negatively charged nucleic acid cargo. These nanoparticles have gained prominence for their ability to enhance bioavailability, therapeutic efficacy, target specificity, safety, and stability[1,2]. Originally crafted for small molecule delivery, LNPs have transitioned into essential vehicles for nucleic acids, marking a significant milestone with the approval of ONPATTRO (Patisiran), a pioneering LNP delivering small interfering RNA for treating transthyretin-mediated hereditary amyloidosis[1]. LNPs garnered widespread attention following their successful deployment in mRNA vaccines against SARS-CoV-2, such as Moderna's mRNA-1273 and Pfizer/BioNTech's BNT162b2, underscoring their pivotal role in modern therapeutic strategies[2,3]. Integral to LNP functionality is the incorporation of a pegylated lipid, which enhances particle solubility and prevents aggregation. The PEG coating creates a steric barrier that diminishes the adhesion of plasma proteins and immune cells to the surface of nanoparticles, the so-called “stealth effect”. By doing so, it increases the circulation time of nanoparticles within the vascular system, enhancing the likelihood of reaching the target site before being sequestered by the mononuclear phagocyte system[4]. However, PEG is known to shed from particles in serum overtime, allowing the fusion of nanoparticles with cellular membranes, and the release of the therapeutic payload into the cytoplasm[5]. Research by Chen et al. demonstrated significant variations in cellular uptake and transfection efficiency across four types of LNP formulations, which differed in both polyethylene glycol lipid chain lengths (carbon 14 vs. carbon 18) and molar ratios (6% vs. 3%)[6].

Therefore, the choice of pegylated lipid should be made carefully, according to the intended application, achieving a delicate balance between extended circulation time and effective cellular delivery.

The stability of formulations is also a concern, as it remains unclear whether PEG shedding can occur during storage, or throughout all the manufacturing processes that involve handling, mixing, shaking, that might stress the particles. A recent study suggested that shaking with air entrainment creates air-liquid interfacial forces, which can strip away PEGylated lipids from the outer surface of LNPs [7]. This reduction in steric hindrance among neighboring LNPs leads to the merging of particles, with some mRNA strands removed from the LNP. Consequently, the final product consists of stable LNPs with larger sizes but reduced mRNA payloads.

Despite its importance, current quality control measures often overlook PEG dissociation due to the complexity and scarcity of reliable analytical techniques. Monitoring PEG shedding would provide insights into the mechanisms behind the phenomenon, functional to predict the LNP behavior in vivo and guide a rational design of formulations accordingly the intended application.

Wilson et al. presented a simple, quantitative, label-free, and real-time approach for directly measuring PEG shedding using conventional NMR equipment under conditions closed to physiological environment[8]. Since PEG associated with lipid nanoparticles diffuses much slower than free PEG, PGSE NMR can be used to distinguish the relative populations over time and quantify them, thereby determining the PEG shedding rate profile.

This method was refined for our applications and applied to investigate several LNP formulations under different stress/storage conditions.

We monitored the stability of DMPE-PEG2K after incubation at 25°C up to one month, to observe if PEG detachment could occur during LNP storage time. Moreover, we examined the impact of a freeze-thaw at -80° and lyophilization and resuspension that are processes known to alter the morphological/structural features of LNPs even in presence of a cryoprotectant but that are essential for a long effective storage of the formulations.

Moreover, the differences in PEG shedding rate of LNP formulations containing 14-C DMPE-PEG2K and 18-C DSPE-PEG2K were monitored on intact particle samples within their formulation buffer following the addition of albumin, to mimic the serum environment and predict how different LNP formulations behave in vivo.

In addition, we used Dynamic Light Scattering (DLS), Nanoparticle Tracking Analysis (NTA), and Cryo-Electron Microscopy (Cryo-EM) to determine if the formation of PEG micelles after shedding was detectable with other techniques, and to examine any changes in particle size and morphology following PEG release.

Experimental section

Materials

All reagents were purchased from common commercial sources and were used without additional purification. Dlin-MC3-DMA was purchased from Cayman Chemical. Distearoylphosphatidylcholine (DSPC), cholesterol and sucrose were purchased from Sigma Aldrich. DMPE-PEG2K was purchased from Avanti Polar. EZCap EGFP mRNA was purchased from ApeX Bio. Ethanol was purchased from Merck. HyPure WFI quality water was purchased from Cytiva. Tris-HCl 1 M pH 8 and 10x PBS buffer pH 7.4 were purchased from Invitrogen.

PD-10 desalting columns were purchased from Cytiva (cat. 17085101). Float-A-Lyzer G2 Dialysis Devices, Spectra/Por, MWCO: 100kDa were purchased from Repligen. 5 mm NMR tubes were purchased from Bruker. Anotop 25 filters 0.02 um were purchased from Whatman.

Formulation

Lipid nanoparticles were prepared through microfluidics using NanoAssemblr Ignite. The lipid compositions of the formulations analyzed, detailed in Table 1, were selected to replicate the formulation of Onpattro, the first approved RNA-LNP based drug, with slight modifications in lipid ratio due to further optimizations[11]. The lipid solution was prepared by dissolving the lipids in ethanol, which was then mixed with the aqueous phase containing eGFP mRNA in a 75 mM citrate buffer at pH 4 to form the LNPs. A total flow rate of 12 mL/min and an organic to aqueous phase flow rate ratio of 1:2 were applied for the mixing. The resulting solutions were exchanged in the final formulation buffer that was either Tris-HCl 20 mM pH 8 with variable sucrose concentrations as cryoprotectant and PBS1x pH 7.4 through PD-10 desalting columns.

Preliminary analyses were performed in each sample to assess particle size distribution using Dynamic Light Scattering as the evaluation of the average particle size and their homogeneity is an indicator of a successful formulation.

Table 1: Lipid composition of tested LNP formulations

Lipid	% mol
Dlin-MC3-DMA	40%
DSPC	10%
Cholesterol	48%
Pegylated Lipid*	2%

*Specified for each experiment

1% (w/w) DMPE-PEG2K solutions were prepared dissolving the powder in Tris-HCl 20 mM pH 8 buffer.

Dialysis of the LNP formulation was conducted to exchange the buffer from 20 mM Tris-HCl at pH 8 with 7.5% sucrose to PBS 1x at pH 7.4. This was achieved using a Float-A-Lyzer G2 Dialysis Device (Spectra/Por) with a molecular weight cut-off (MWCO) of 100 kDa. The process involved placing 1 mL of the formulation within the dialysis membrane and allowing it to float in 500 mL of PBS 1x at pH 7.4, agitated for 24 hours, with the buffer being exchanged three times.

For lyophilization, 600 µL of the LNP solution was loaded into 3 mL lyophilization vials (Muller) and dried using an Epsilon Martin Christ 2-10d LSC Plus lyophilizer. The lyophilized samples were then resuspended in the initial volume of 600 µL per vial with 20 mM Tris and varying amounts of sucrose.

PGSE NMR

^{1}H diffusion experiments were employed to monitor real time PEG forms in LNP formulations, exploiting the different diffusion rate of free PEG and LNP linked PEG. The method was based on the work of Wilson et al.[8] and refined for our purposes. The technique employed in our study is based on pulsed gradient spin-echo NMR, which enables the differentiation of signals from different species based on their diffusion coefficients. As shown in Figure 1, ranging from the minimum strength of gradient (2%) to the maximum (98%) signals are filtered according to their diffusion rate. The signals close to the one arising from the PEG chain (3.60 ppm), indeed, disappeared because they belong to the fast diffusion excipients.

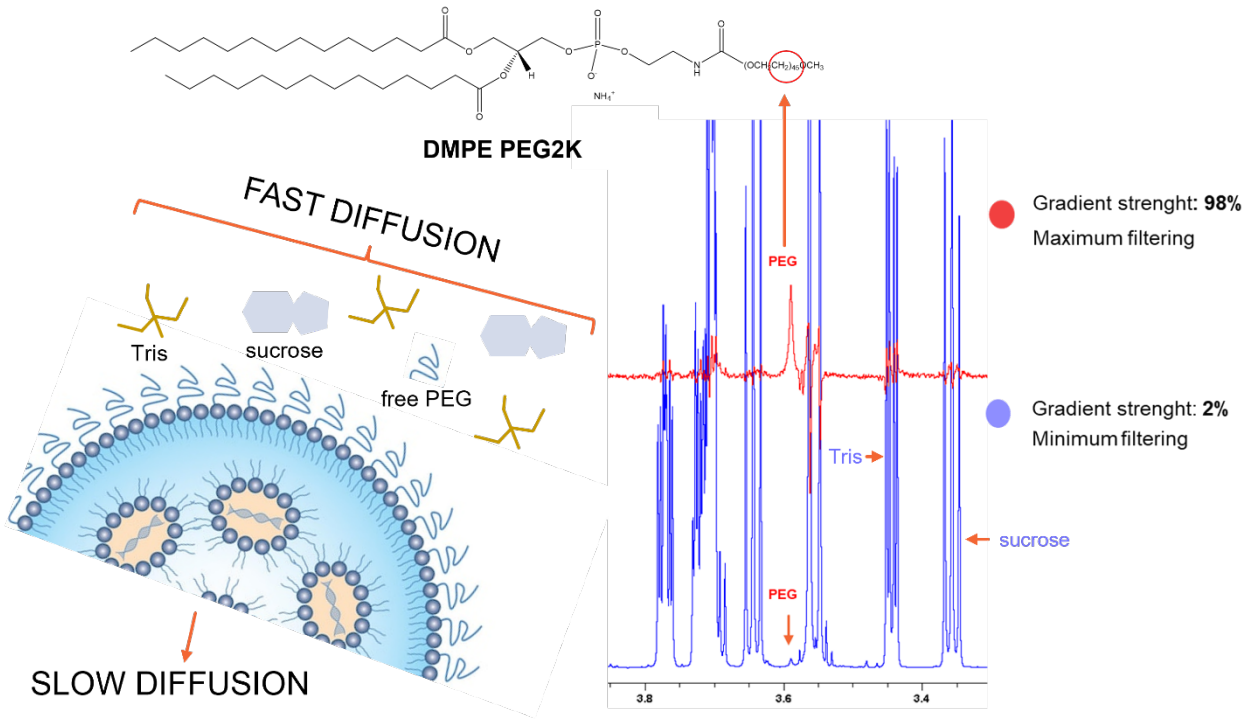

Figure 1. Application of diffusion filter to LNP full formulation. The signals associated with the small excipients are filtered out using the maximum gradient strength due to their rapid diffusion. The signals related to the slow-diffusing LNP, such as the PEG chain signal at 3.60 ppm, are minimally affected by the diffusion filter.

Specifically, the PEG signal is a combination of PEG linked to the LNP and potential freely dissociated PEG in solution. By applying selective pseudo 2D DOSY on this signal, we calibrated the diffusion pulse length and the gradient strength to obtain a decay of PEG integral signal at least up to 10% of the initial value to be representative of the whole population. Elaboration of data with Dynamics Center software provided the integral of PEG signal at each point of the gradient acquired (TD = 32, from 2% to 98%). Then GraphPad Prism software was employed to fit the curves depicting the decay of the integral of the signal, using Stejskal-Tanner equation[9] (Figure 2).

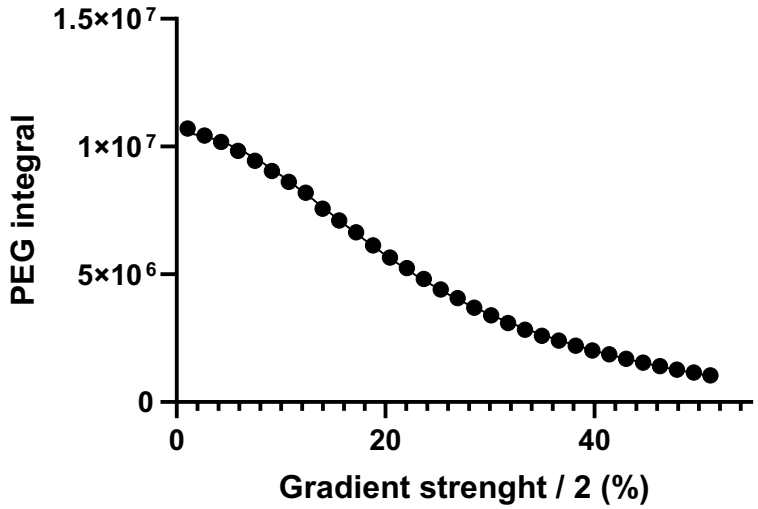

Figure 2. PEG integral curve decay under gradient diffusion filtering. For each sample, the acquisition parameters were set to reduce the PEG signal to at least 10% of its initial value, ensuring a complete decay profile. The integrals from 32 gradient points were calculated using Dynamics Center, and the resulting curves were plotted in GraphPad Prism for fitting.

Each sample was first analyzed using a one-component equation to verify if all the PEG was still linked to LNP, with a unique diffusion coefficient describing effectively the system. If the fitting resulted incomplete, two-component equation was employed. The two-component equation takes in account the PEG bound to PEG and the free PEG fraction.

Stejskal-Tanner equation (one-component):

$$I = I_0 \exp(-\gamma^2 G^2 \delta^2 D(\Delta - \delta/3))$$

Stejskal-Tanner equation (two-components):

$$I = I_0 [w1\exp(-\gamma^2 G^2 \delta^2 D1(\Delta - \delta/3)) + w2\exp(-\gamma^2 G^2 \delta^2 D2(\Delta - \delta/3))]$$

where:

- I = signal intensity with a gradient
- I_0 = signal intensity without a gradient
- γ = gyromagnetic ratio of the nucleus
- G = gradient strength
- δ = duration of the gradient pulse (little delta)

- D = diffusion coefficient
- Δ = the diffusion time (big delta)
- w = PEG form fraction

In this way it's possible to calculate the proportions of various PEG species, along with their corresponding diffusion coefficients, according to the best curve fit.

NMR experiments were recorded on a Bruker Avance III spectrometer operating at 900 MHz 1H Larmor frequency at 298 K. 50 µL of D_2O were added to 500 µL of each sample for the preparation of NMR tubes for field frequency lock purposes. To induce PEG shedding, an additional 50 µL of a BSA solution at 4.4 mM, prepared by dissolving 60 mg in 200 µL (MW = 68,000), was added to achieve a final concentration of 366 µM in the tube, comparable to serum levels.

Pseudo2D NMR experiments were acquired with the following parameters:

ledbpgppr2s; B° = 900 MHz; NS = 32 TD (F2) = 32768; TD (F1) = 32; P1 = 7.10 us; D1 = 3.75 s; RG = 101; T = 298 K Δ = 700 ms; δ = 4 ms

Processing with QSINE function, SSB = 3 to minimize line width and consequently PEG signal overlap.

DLS analysis

Free DMPE-PEG2K solutions were prepared at different concentrations to assess if PEG micelles were detectable and assess the size of free PEG. Solutions of DMPE-PEG2K 1% (w/w) and DMPE-PEG2K 10% (w/w) were prepared by dissolving the powder in water. The exact Critical Micellar Concentration for this lipid was not found in literature but for the homologous DSPE-PEG 2000 is reported to be between 0.5–1 µM, way far below a concentration of 1% (w/w) which

corresponds to 3.5 mM (MW = 2790 Da)[10]. So, we believe it's reasonable that the pegylated lipid forms micelle at the analyzed concentration.

Then an LNP formulation containing DMPE-PEG2K was analyzed before and after 13 hours since the addition of BSA, reproducing the NMR conditions, with a final concentration of BSA 366 μM. LNP samples were diluted 100x in HyPure WFI quality water previously filtered with Anotop 25 filters 0.02 μm for analysis. Experiments were recorded using DLS Zetasizer ULTRA Malvern, loading 80μL of each sample in the BRAND™ UV Disposable Cuvettes. Measurements were performed in triplicate, with a controlled temperature of 25°C and equilibration time of 120 s.

NTA analysis

The same 1% PEG solution and LNP formulations before and after addition of BSA tested with DLS were analyzed.

LNP samples were diluted 1:5000 with HyPure WFI quality water previously filtered with Anotop 25 filters 0.02 μm for analysis.

The analysis was performed in three replicates on NanoSight NS300. The samples were measured for 60 s at 20 °C (RT) using a blue laser (488 nm), sCMOS camera and under a constant syringe pump speed of 50 (arbitrary units). Data were analyzed using NTA 3.4 Build 3.4.4 software, with a detection threshold of 5 or 6 depending on the sample. The capillary was cleaned after each sample by injecting 1 mL of HyPure WFI-quality water and removing any bubbles by introducing air.

Cryo-EM analysis

The same LNP formulations were analyzed before and after 13 hours from the addition of BSA as done with the other techniques, using 4 µL of samples for each analysis.

A solution of 4 uL of LNPs (total lipid concentration = 2 mg/mL) was applied on Quantifoil Cu R2/2 300 mesh carbon grids (Quantifoil) previously glow discharged at 15 mA for 10 seconds using a PELCO easiGlow™ system (Ted Pella Inc.). Excess of LNP solution was blotted out for 5 seconds and grid was plunged-frozen in liquid ethane at -180°C using EM-GP (Leica Microsystems). Subsequentially, grids were transferred to a Simple Origins Dual Grid Cryo Transfer Holder Model 205 (Simple Origins) maintained at -180°C and inserted into a Talos L120C (ThermoFisher Scientific) with an accelerating voltage of 120 kV. Images were recorded at 22,000X and 45,000X magnification using a Ceta M 4k camera (ThermoFisher Scientific) with a dose rate of ~22 e-/A^2 under a defocus ranging from -4 to -7 µm.

Results and discussion

DMPE-PEG2K stability in storage conditions

The stability of the DMPE-PEG2K linkage to LNPs was evaluated under various storage conditions to determine potential concerns regarding PEG shedding and to identify conditions that might induce PEG release. An incubation at 25°C for up to one month served as an accelerated stress test to assess the possibility of PEG shedding outside serum environment. Additionally, a freeze-thaw cycle at -80°C followed by lyophilization and resuspension in the initial buffer was performed. These processes, commonly used in long-term LNP storage, are known to induce stress due to phase transitions that may potentially include PEG stability. A

cryoprotectant is usually added to formulations to mitigate these effects, we chose sucrose as it is one of the most commonly employed[11].

Analysis of fresh samples

The fresh samples presented a percentage around of 10% of a species with higher diffusion coefficient respect to the low diffusion predominant form which reasonably belongs to the PEG attached to LNP. A possible explanation could be the existence of a small fraction of free-PEG even in the fresh LNP or it could be explained with the partial overlap of sucrose/Tris signals which own a fast diffusion coefficient. The 2D display of the experiment failed to solve graphically if this fraction was aligned to sucrose row or resolved, belonging to PEG. The excipients signals, such as Tris and sucrose, are well separated by the LNP signals, except for PEG one which appears as a stripe, with undefined diffusion coefficient, confirming the co-existence of different diffusion rate forms resonating at the same chemical shift (Figure 3).

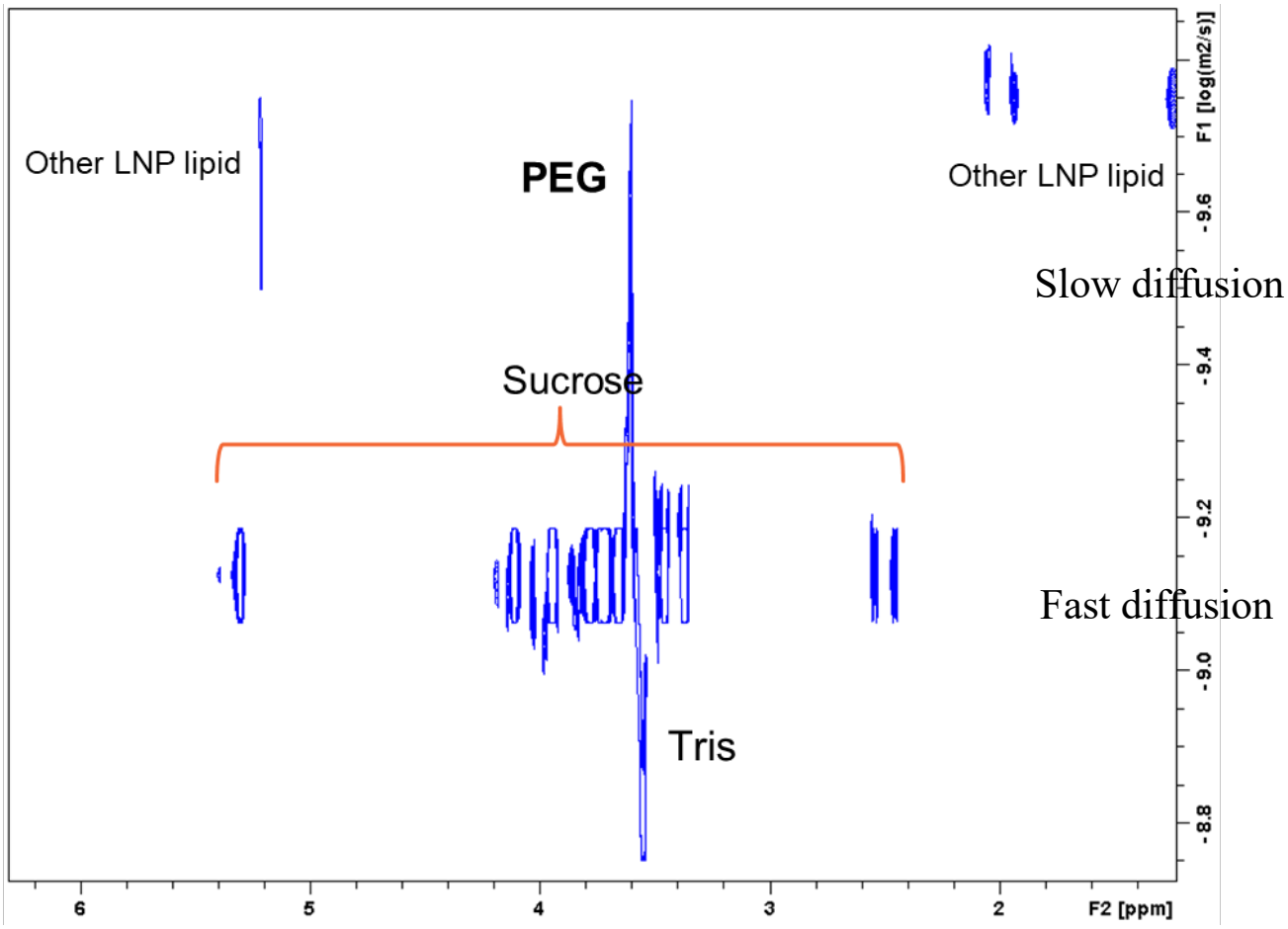

Figure 3: 2D DOSY of LNP sample. The spectrum displays chemical shifts along the F2 axis and diffusion coefficients (log(m²/s)) along the F1 axis, effectively separating the signals of fast-diffusing sucrose and Tris molecules from the slower-diffusing LNP lipid signals. The PEG signal, which partially overlaps with sucrose and Tris signals, appears as an unresolved stripe. ledbpgppr2s; B° = 900 MHz; NS = 32 TD = 32; T = 298K big DELTA = 700 ms little DELTA = 4 ms.

To clarify this point an analogous LNP formulation in Tris 20 mM without sucrose was put in dialysis (membrane with cut-off 100kDa) against PBS 1x. The ^{1}H spectra of the resulting solution showed the absence of excipients signals (Figure 4). However, the analysis of the well-solved PEG signal still indicated a percentage between 6-10% of a fast diffusion form. This suggested that a small fraction of the PEG-lipid may already exist in the free PEG-lipid state in fresh samples.

Schroder et al. used a diffusion NMR sequence with a T2 filter that showed the presence of minor components with lower molecular weight than LNPs, likely attributable to PEG micelles, even

whether the single-component decay seemed to fit to describe the PEG integral. These results can suggest that LNPs exhibit a dynamic distribution, potentially resulting from an equilibrium between PEG micelles and LNPs[11].

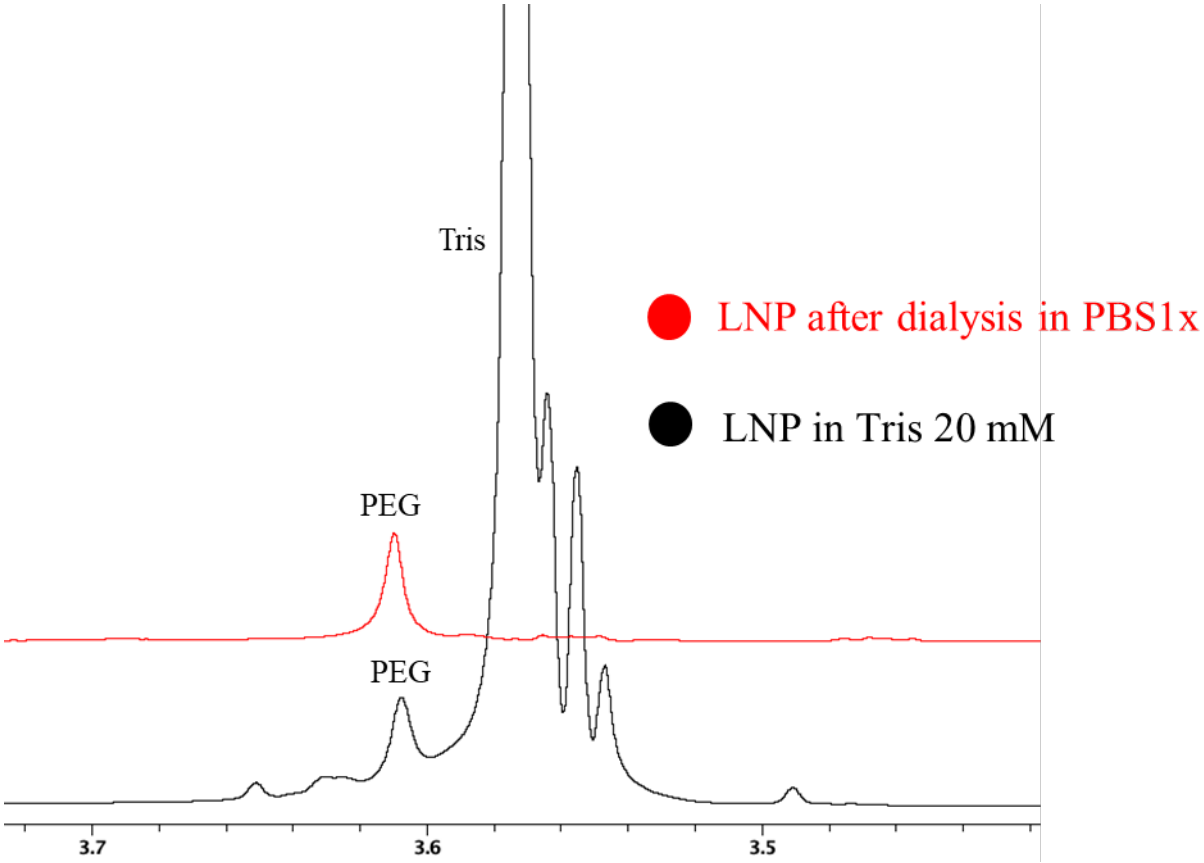

Figure 4: 1D ^{1}H spectra of LNP formulation in Tris 20 mM (in black) and after buffer exchange via dialysis in PBS 1x (in red). The modest overlap affecting the PEG signal with the Tris signal is eliminated after dialysis in PBS 1x, allowing for complete resolution of the PEG signal.

Incubation at 298K

The analysis conducted after 6 and 30 days of incubation at 25°C revealed a slight increase in faster diffusion forms of PEG, from 10% initially to 17% after 6 days and 22% after 30 days (Table 2). These results documented for the first time that PEG can shed from LNPs outside serum, raising a stability concern that should be taken into consideration. However, it's also fair to specify that the amount of dissociated PEG remains very low, even after a month under these accelerated conditions, which are unlikely to occur for LNP batches typically stored frozen at -

20°C or -80°C, or kept in liquid form for shorter periods. Therefore, this data is not particularly concerning by itself, but it does confirm the need to analyze this attribute in batches as part of quality control.

Sample	PEG form	Fresh	6 days at 25°	30 days at 25°	Freeze and thaw -80°	Lyophilization and reconstitution
LNP DMPE-PEG2K sucrose 7.5%	Free	**10%** $D=6.5*10^{-10}$	**17%** $D=5.2*10^{-10}$	**22%** $D=1.2*10^{-10}$	**0%**	**0%**
	LNP	**90%** $D=1.1*10^{-11}$	**83%** $D=1.1*10^{-11}$	**78%** $D=8.0*10^{-12}$	**100%** D=1.0*10-11	**100%** $D=5.5*10^{-12}$

D = Diffusion coefficient (m^2/s)

Freeze-thaw and lyophilization

LNP formulations are typically frozen or lyophilized for long storage, so we assessed whether the attachment of PEG to the particles could be altered by freeze-thaw cycles or lyophilization (followed by resuspension). Both freeze-thaw and lyophilization treatments did not result in an increase in free PEG in either sample, demonstrating the stability of PEG attachment under these conditions (Table 2). An equivalent formulation containing a lower concentration of sucrose (3% w/w) as a cryoprotectant was also tested to determine whether the outcome was dependent on a specific sucrose concentration. The results were comparable, with no significant release of PEG observed.

In-vivo simulation (BSA-induced PEG Shedding)

In addition to evaluating the stability of formulations under storage conditions, we aimed to refine a method for predicting the PEG shedding rate from LNPs once injected. This is crucial

because the rate at which PEG detaches can impact particle targeting in various regions of the body, allowing for the tailored design of formulations[12]. We started our investigation by studying an LNP formulation with DMPE-PEG2K, before and after addition of BSA. We expected that the protein could trigger the release of PEG simulating the serum environment (Figure 5).

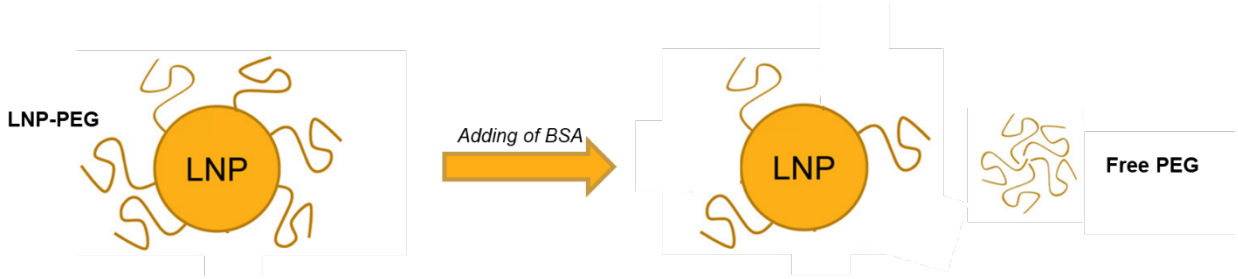

Figure 5: Scheme of PEG release from LNP after BSA addition. The addition of BSA to an LNP solution can simulate in vivo conditions by inducing PEG release from the particles. This interaction mirrors the formation of a protein corona around LNPs in the presence of serum proteins, thereby promoting PEG shedding.

When analysed alone the LNP formulation exhibited a one-component decay of the PEG integral as the gradient strength was applied. However, after the addition of BSA, the decay of the curve could be described with a two-component equation, indicating the contribution of another faster diffusion species (Figure 6). The resulting diffusion coefficients of the two populations differed from one order of magnitude fraction. These two fractions respectively correspond to the LNP bound fraction and the free micelles, whose diffusion coefficients are in agreement with the values reported in literature ($5*10^{-12}$ m^2/s for the LNP fraction, $5*10^{-11}$ m^2/s for the micelles) and our experiment on a solution of PEG 1% in formulation buffer which gave D=$5*10^{-11}$ m^2/s[9,12,13].

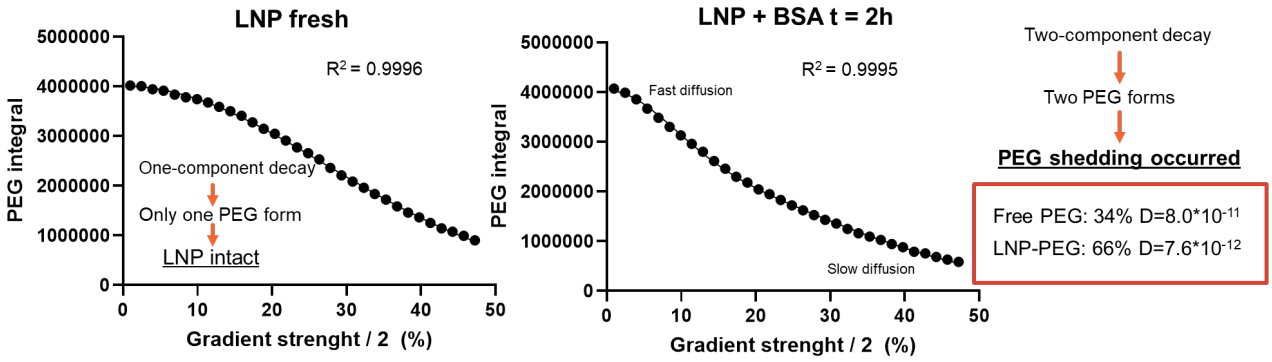

Figure 6. Fitting analysis of PEG integral along diffusion gradient, before and after addition of BSA. When analyzed fresh, the LNP with DMPE-PEG2K exhibited a one-component decay of the PEG integral as the gradient strength was applied, with a diffusion coefficient (D) = $7.6*10^{-12}$. However, after the addition of BSA, the decay of the curve could be described with a two-component equation, indicating the contribution of one faster diffusion species. Specifically, 34% with a of $8.0*10^{-11}$, attributable to the released PEG, and 66% with D= $7.6*10^{-12}$, originated from the remaining pegylated lipid attached to the LNP.

Afterwards, we performed a comparison of the tested LNP solution with another formulation that differed only in the length of the pegylated lipid chain: 18-C 1,2-distearoyl-sn-glycero-3-phosphoethanolamine-N-[amino(polyethylene glycol)-2000] (DSPE-PEG2K). We monitored the PEG release after the addition of BSA up to 13 hours. The DMPE-PEG LNP showed appearance of a faster diffusion form which progressively increased up to remaining the only one after 13 hours, indicating complete PEG shedding, while the DSPE-PEG2K LNP remained stable (Figure 7).

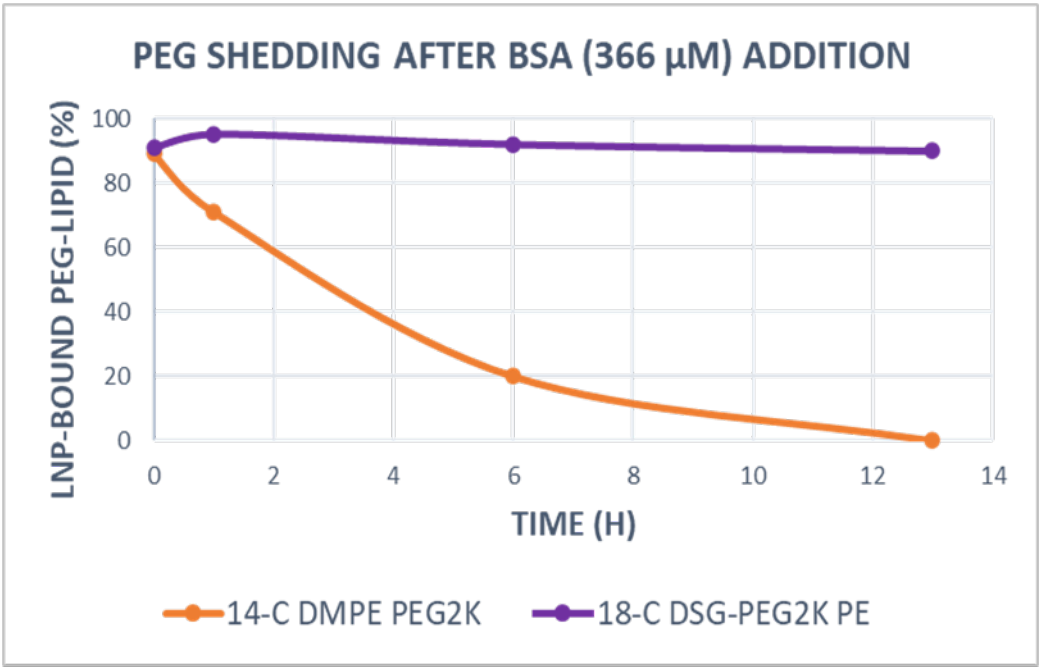

Figure 7: Percentage of PEG bound to LNP overtime in 14-C DMPE-PEG2K and 18-C DSPE-PEG2K LNPs after addition of BSA. Two LNP formulations, differing only in the length of the pegylated lipid chain, 14-C DMPE-PEG2K and 18-C DSPE-PEG2K, were analysed both fresh and following the addition of 366 µM BSA. These samples were evaluated at intervals of 0, 1, 6, and 13 hours after BSA addition. For the 18-C DSPE-PEG2K formulation, the percentage of PEG linked to the LNP remained stable around 90%, with minor fluctuations likely attributed to experimental variability. In contrast, the 14-C DMPE-PEG2K formulation exhibited a gradual decrease in PEG retention, dropping from 90% to 72% after 1 hour, down to 20% after 6 hours, eventually resulting in complete PEG release after 13 hours.

These results are in accordance with previous works that underlined the different PEG release for formulations with different lipid chain length in serum. Difference on shedding kinetics between 14-C and 18-C pegylated lipids could be explained with the stronger hydrophobic interactions which link the longer aliphatic chain to LNP. This should be taken in consideration in the LNP formulation design considering the importance of a correct PEG shedding timing in the serum for an effective delivery of the cargo.

We demonstrated compared to the other studies performed so far that it's not strictly necessary to perform the studies in serum, to simulate in-vivo conditions, but it's possible to gain insights into the behavior of the pegylated lipid, just adding to the LNP solution one of the main

components of serum and responsible of the corona formation which is albumin. This can be helpful to accelerate the analyses allowing to study LNPs directly in their formulation buffer and avoiding the use of serum which can give availability, regulatory and variability issues.

DLS and NTA analysis

DLS and NTA analyses were employed to evaluate whether these techniques could serve to assess PEG shedding by either directly detecting free PEG micelles or indirectly inferring PEG release through measuring changes in particle size. First, free standard PEG solutions (1% and 10% w/w) were initially analyzed to detect if the polymer micelles were detectable with DLS and NTA.

The DLS analysis revealed a principal peak between 1 and 10 nm for both 1% PEG and 10% PEG solutions, with secondary peaks ranging from 10 to 1000 nm for 1% PEG, and from 100 to 10000 nm for 10% PEG. The low intensity of these secondary peaks, even when analyzing data by intensity which is biased toward larger particles, suggests that these larger populations are negligible. In elaboration by number, these larger peaks disappear, showing only the main peaks of the smaller populations (Supplementary material).

NTA analysis was not feasible for PEG solutions, as no particles were detected by the camera, likely due to the PEG average size being below the NTA detection limit of 10 nm.

LNP formulations were analyzed both before and after 13 hours since the addition of BSA (final concentration = 366 μM), replicating NMR conditions that induced complete PEG shedding. No free PEG was detected in the LNP samples using DLS (Figure 8A) and in NTA neither (Figure 8B), possibly due to the low concentration and small size relative to the larger LNPs, taking into consideration DLS bias towards larger particles when measuring heterogeneous populations.

Both DLS and NTA analysis showed the inability to detect DMPE-PEG2K micelles after PEG shedding from LNPs. Nevertheless, a significant increase in the average particle size was observed with both techniques (Table 2). This finding aligns with Berger et al. work using NTA, which attributed the increased sizing to protein adsorption on LNPs, causing PEG release and leading to particle aggregation[14].

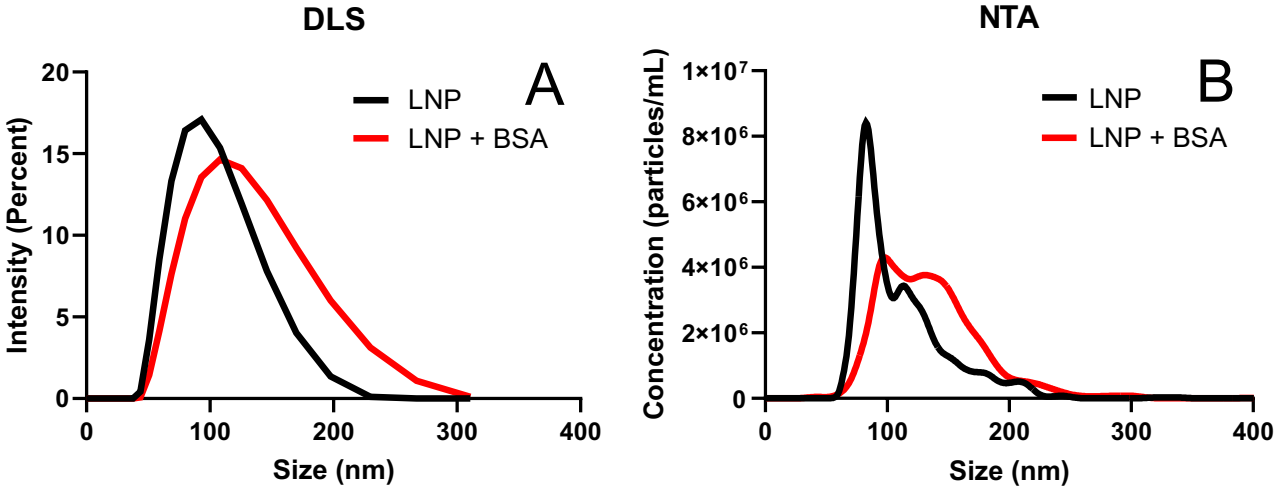

Figure 8: DLS (A) and NTA (B) analysis of LNP size distribution before and after 13 hours since the addition of BSA. The size profiles suggested that some particle aggregation occurred after the addition of BSA, likely due to the release of PEG. No PEG micelles are detected with both techniques.

Table 2: LNP size before and after 13 hours since BSA addition (366 μM), using DLS and NTA.

	Average Size (nm)	
	LNP	LNP + BSA
DLS	90	104
NTA	112	136

Cryo-EM

To determine whether PEG shedding alters particle morphology, we analyzed samples previously studied using NMR with Cryo-EM. Initially, the LNP formulation was examined alone, revealing, as expected a mixed population of particles, some with "blebs" and some without[15] (Figure 9A). After adding BSA at the same concentration used in the NMR study (366 μM) and incubating

overnight, PEG should be nearly completely shed from the LNPs based on NMR results. No macroscopic morphological changes are detectable through visual analysis (Figure 9B). We might expect to observe PEG micelles, but the acquired images make it challenging to distinguish different populations. The presence of black dots caused by the protein is clearly visible, dispersed within the matrix. Thus, this technique is not suitable for detecting PEG shedding.

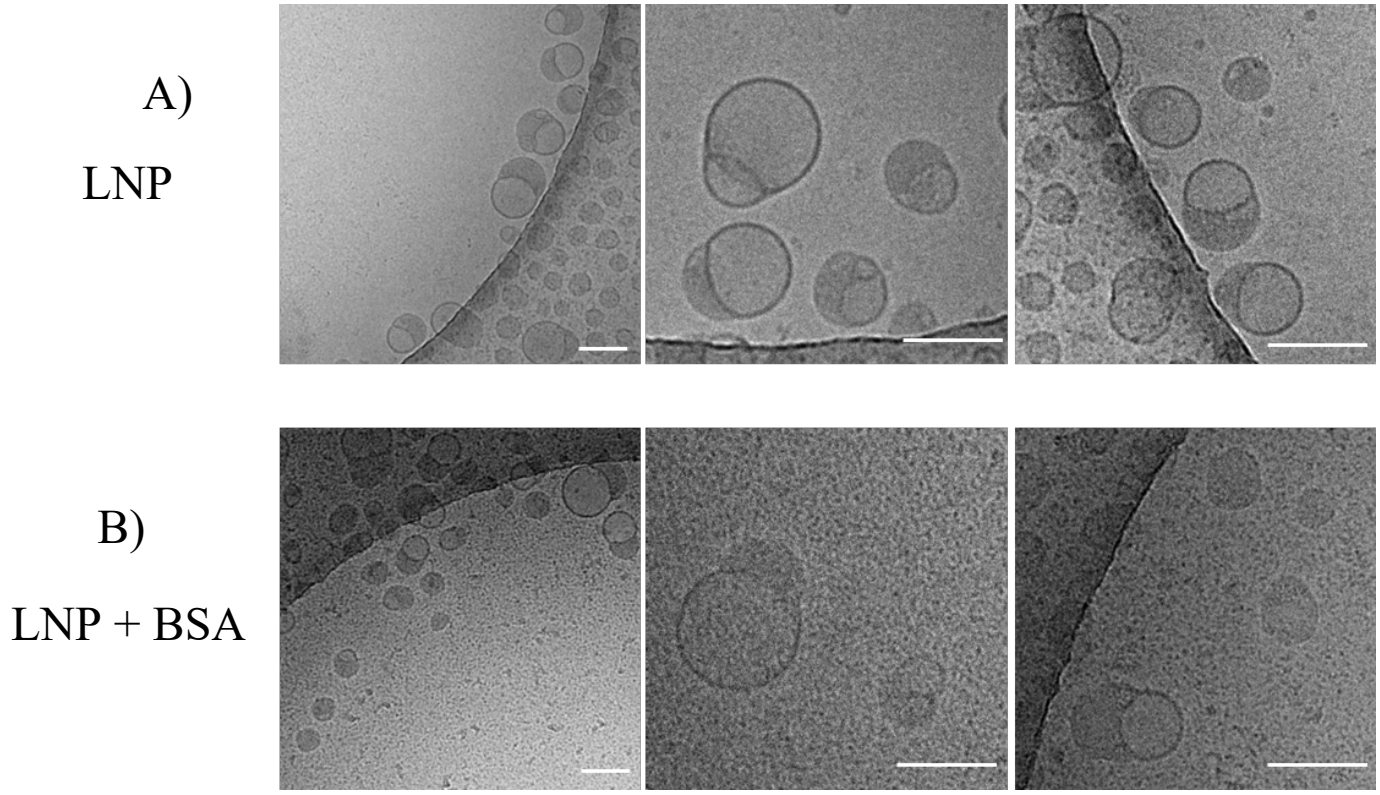

Figure 9: Cryo-EM image panel of LNP formulation with DMPE-PEG2K in absence and after 13 hours of incubation (+BSA) with BSA. The granularity aspect (black dots) observed in LNP PEG shed + BSA row represents the free BSA. The white scale bar is 100 nm

Conclusions

This research has provided important insights into the phenomenon of PEG shedding in lipid nanoparticles. By refining a PGSE NMR method, we were able to precisely quantify PEG release under a variety of conditions. We evaluated PEG stability under different storage conditions,

observing modest PEG shedding at 25°C over the span of one month. This finding raises concerns about the stability of PEG throughout the entire drug product manufacturing process, as shedding can occur even in the absence of serum or protein interactions. In contrast, PEG attachment remained stable following freeze-thaw cycles and lyophilization, indicating that these long-term storage methods for LNPs do not compromise PEG linkage. In addition, we confirmed that PEG shedding rates are significantly influenced by the chain length of the PEGylated lipids, through the addition of BSA to LNPs in their formulation buffers, providing a quick and easy method to predict behavior of LNPs in serum, which can support a rational design of formulations. Conventional methods such as DLS, Nanoparticle Tracking Analysis (NTA), and Cryo-EM did not detect PEG release, highlighting the unique sensitivity of NMR in monitoring this process. These findings underscore the importance of integrating PEG shedding assessments into standard quality control protocols to ensure consistent batch performance and stability. Future studies should explore how various formulation parameters, including lipid composition and buffer characteristics, influence PEG release under different storage or stress conditions, thereby advancing our understanding and enabling the rational design of LNPs.

ACKNOWLEDGMENTS

This work was sponsored by GlaxoSmithKline Biologicals SA. The authors acknowledge also the support and the use of resources of Instruct-ERIC, a landmark ESFRI project, and specifically the CERM/CIRMMP Italy centre, “Progetto Dipartimenti di Eccellenza 2023-2027” to the Department of Chemistry “Ugo Schiff” of the University of Florence, the Recombinant Proteins JOYNLAB laboratory and the project. Fondazione CR Firenze, Bando Grandi Attrezzature 2024 - progetto n. 58348.

REFERENCES

(1) Akinc, A.; Maier, M. A.; Manoharan, M.; Fitzgerald, K.; Jayaraman, M.; Barros, S.; Ansell, S.; Du, X.; Hope, M. J.; Madden, T. D.; Mui, B. L.; Semple, S. C.; Tam, Y. K.; Ciufolini, M.; Witzigmann, D.; Kulkarni, J. A.; van der Meel, R.; Cullis, P. R. The Onpattro Story and the Clinical Translation of Nanomedicines Containing Nucleic Acid-Based Drugs. *Nat Nanotechnol* **2019**, *14* (12), 1084–1087. https://doi.org/10.1038/s41565-019-0591-y.

(2) Qassem, S.; Breier, D.; Naidu, G. S.; Hazan-Halevy, I.; Peer, D. Unlocking the Therapeutic Potential of Locked Nucleic Acids through Lipid Nanoparticle Delivery. *Mol Ther Nucleic Acids* **2024**, *35* (2), 102224. https://doi.org/10.1016/j.omtn.2024.102224.

(3) Hou, X.; Zaks, T.; Langer, R.; Dong, Y. Lipid Nanoparticles for MRNA Delivery. *Nat Rev Mater* **2021**, *6* (12), 1078–1094. https://doi.org/10.1038/s41578-021-00358-0.

(4) Waggoner, L. E.; Miyasaki, K. F.; Kwon, E. J. Analysis of PEG-Lipid Anchor Length on Lipid Nanoparticle Pharmacokinetics and Activity in a Mouse Model of Traumatic Brain Injury. *Biomater Sci* **2023**, *11* (12), 4238–4253. https://doi.org/10.1039/d2bm01846b.

(5) Kumar, V.; Qin, J.; Jiang, Y.; Duncan, R. G.; Brigham, B.; Fishman, S.; Nair, J. K.; Akinc, A.; Barros, S. A.; Kasperkovitz, P. V. Shielding of Lipid Nanoparticles for SiRNA Delivery: Impact on Physicochemical Properties, Cytokine Induction, and Efficacy. *Mol Ther Nucleic Acids* **2014**, *3* (September), e210. https://doi.org/10.1038/mtna.2014.61.

(6) Chen, D.; Ganesh, S.; Wang, W.; Amiji, M. The Role of Surface Chemistry in Serum Protein Corona-Mediated Cellular Delivery and Gene Silencing with Lipid Nanoparticles. *Nanoscale* **2019**, *11* (18), 8760–8775. https://doi.org/10.1039/c8nr09855g.

(7) Matthessen, R.; Van Pottelberge, R.; Goffin, B.; De Winter, G. Impact of Mixing and Shaking on MRNA-LNP Drug Product Quality Characteristics. *Sci Rep* **2024**, *14* (1), 1–11. https://doi.org/10.1038/s41598-024-70680-4.

(8) Wilson, S. C.; Baryza, J. L.; Reynolds, A. J.; Bowman, K.; Keegan, M. E.; Standley, S. M.; Gardner, N. P.; Parmar, P.; Agir, V. O.; Yadav, S.; Zunic, A.; Vargeese, C.; Lee, C. C.; Rajan, S. Real Time Measurement of PEG Shedding from Lipid Nanoparticles in Serum via NMR Spectroscopy. *Mol Pharm* **2015**, *12* (2), 386–392. https://doi.org/10.1021/mp500400k.

(9) Wilson, S. C.; Baryza, J. L.; Reynolds, A. J.; Bowman, K.; Keegan, M. E.; Standley, S. M.; Gardner, N. P.; Parmar, P.; Agir, V. O.; Yadav, S.; Zunic, A.; Vargeese, C.; Lee, C. C.; Rajan, S. Real Time Measurement of PEG Shedding from Lipid Nanoparticles in Serum via NMR Spectroscopy. *Mol Pharm* **2015**, *12* (2), 386–392. https://doi.org/10.1021/mp500400k.

(10) Ashok, B.; Arleth, L.; Hjelm, R. P.; Rubinstein, I.; Önyüksel, H. In Vitro Characterization of PEGylated Phospholipid Micelles for Improved Drug Solubilization: Effects of PEG Chain Length and PC Incorporation. *J Pharm Sci* **2004**, *93* (10), 2476–2487. https://doi.org/10.1002/jps.20150.

(11) Kon, E.; Elia, U.; Peer, D. Principles for Designing an Optimal MRNA Lipid Nanoparticle Vaccine. *Curr Opin Biotechnol* **2022**, *73*, 329–336. https://doi.org/10.1016/j.copbio.2021.09.016.

(12) Suzuki, T.; Suzuki, Y.; Hihara, T.; Kubara, K.; Kondo, K.; Hyodo, K.; Yamazaki, K.; Ishida, T.; Ishihara, H. PEG Shedding-Rate-Dependent Blood Clearance of PEGylated Lipid Nanoparticles in Mice: Faster PEG Shedding Attenuates Anti-PEG IgM Production. *Int J Pharm* **2020**, *588* (August), 119792. https://doi.org/10.1016/j.ijpharm.2020.119792.

(13) Schroder, R.; Ozuguzel, U.; Du, Y.; Corts, T. M.; Liu, Y.; Mittal, S.; Templeton, A. C.; Chaudhuri, B.; Gindy, M.; Wagner, A.; Su, Y. Molecular Dynamics of Lipid Nanoparticles Explored through Solution and Solid-State NMR Spectroscopy and MD Simulations. *Journal of Physical Chemistry B* **2025**. https://doi.org/10.1021/acs.jpcb.5c01399.

(14) Berger, M.; Degey, M.; Leblond Chain, J.; Maquoi, E.; Evrard, B.; Lechanteur, A.; Piel, G. Effect of PEG Anchor and Serum on Lipid Nanoparticles: Development of a Nanoparticles Tracking Method. *Pharmaceutics* **2023**, *15* (2). https://doi.org/10.3390/pharmaceutics15020597.

(15) Cheng, M. H. Y.; Leung, J.; Zhang, Y.; Strong, C.; Basha, G.; Momeni, A.; Chen, Y.; Jan, E.; Abdolahzadeh, A.; Wang, X.; Kulkarni, J. A.; Witzigmann, D.; Cullis, P. R. Induction of Bleb Structures in Lipid Nanoparticle Formulations of MRNA Leads to Improved Transfection Potency. *Advanced Materials* **2023**, *35* (31), 1–11. https://doi.org/10.1002/adma.202303370.

Supporting information

Monitoring PEG Shedding with NMR: Molecular Insight into LNP Stability

Francesco Currò[a][b][c], Linda Cerofolini[a][b][e], Gaëtan Dias Mirandela[d] , Silvia Martini[c], Frédéric Fontaine[d], Francesco Berti[c], Milos Erak[d], Massimiliano Biagini[c], Daniela Stranges[c], Marco Fragai[a][b][e], Maxime Denis[c]

[a] Department of Chemistry Ugo Schiff (DICUS), University of Florence, Via della Lastruccia, 3, 50019, Sesto Fiorentino, Italy

[b] Centro di Risonanze Magnetiche (CERM), University of Florence,Via Luigi Sacconi 6, 50019, Sesto Fiorentino, Italy

[c] GSK, Siena, Italy

[d] GSK, Rixensart, Belgium

[e] Consorzio Interuniversitario di Risonanze Magnetiche di Metalloproteine (CIRMMP) Via Luigi Sacconi 6, 50019, Sesto Fiorentino, Italy

KEYWORDS: LNP, NMR, PEG shedding, stability, analytics

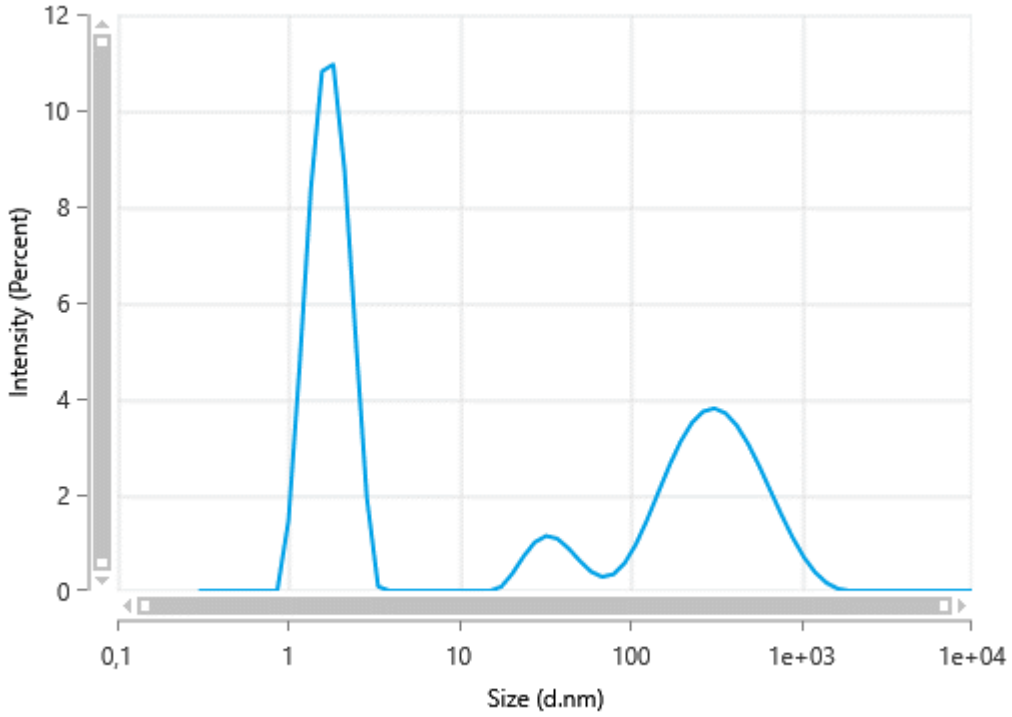

Figure S1: DLS profile by intensity of PEG 1% solution in water. The main population appears between 1 and 5 nm, with secondary peaks at approximately 50 nm and 500 nm. The low intensity of these secondary peaks, considering the bias of DLS toward larger particles, suggests that these larger populations are negligible.

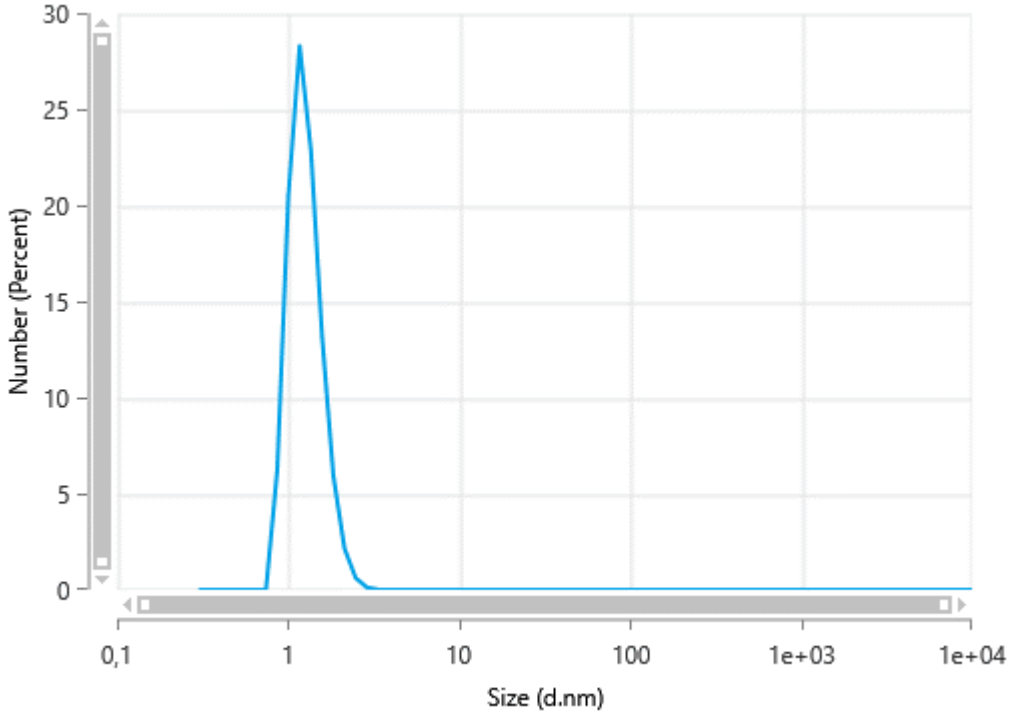

Figure S2: DLS profile by number of PEG 1% solution in water. The secondary peaks visible by intensity are not observed, confirming that the effective size of particles ranged between 1 and 5 nm.

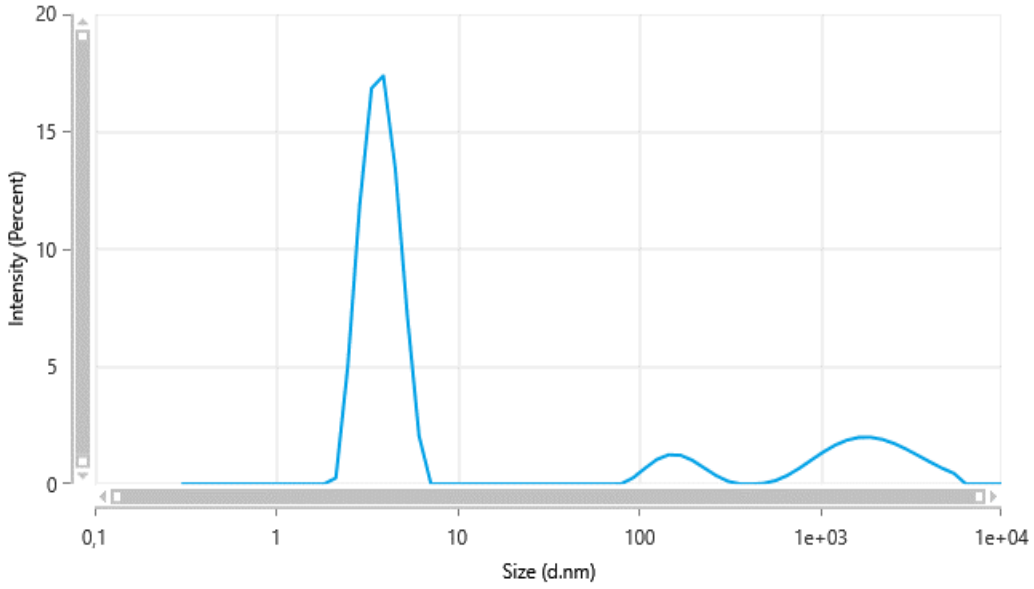

Figure S3: DLS profile by number of PEG 10% solution in water. The main population appears between 1 and 10 nm, with secondary peaks between 100 nm and 10000 nm. The low intensity of these secondary peaks, considering the bias of DLS toward larger particles, suggests that these larger populations are negligible. The general increase in size for this PEG concentration compared to 1% could be due to the formation of more and larger PEG micelles.

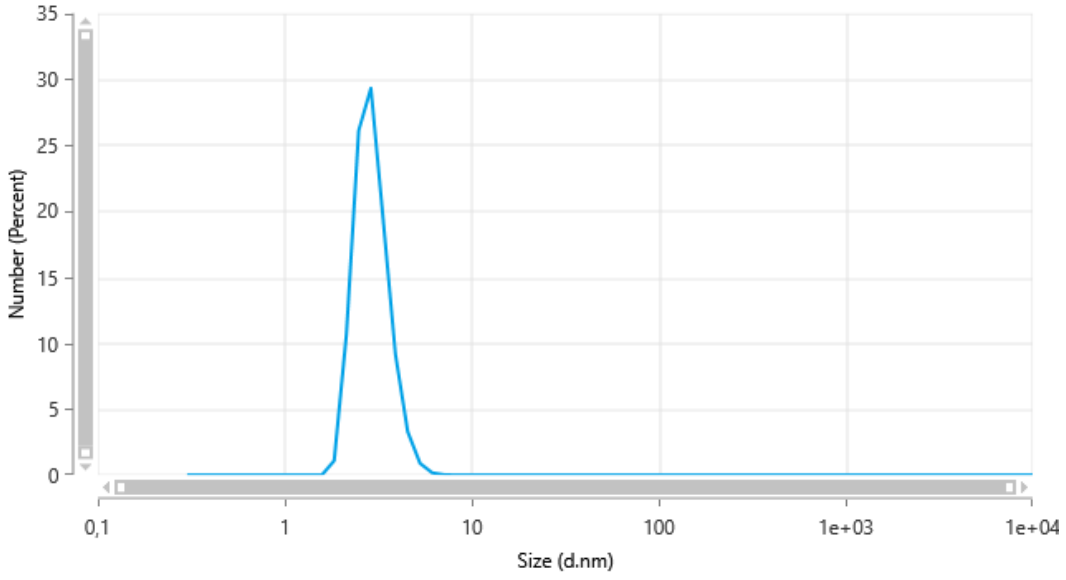

Figure S4: DLS profile by number of PEG 10% solution in water. The secondary peaks visible by intensity are not observed, confirming that the effective size of particles ranged between 1 and 10 nm.

5 Conclusions and future perspectives

Throughout this research project, we contributed to advancing characterization of pharmaceutical delivery systems, with a particular focus on liposomes, lipid nanoparticles (LNPs), and red blood cells (RBCs).

In the first study, we developed and refined NMR-based methods for quantifying lipids in liposome formulations. Using DMF as an internal standard provided high accuracy and precision when analyzing standard mixtures that reproduce the complex liposome environment. Additionally, the PULCON NMR method, which is based on an external standard, was adapted for lipid quantification to improve reproducibility and consistency. This is particularly beneficial for industrial applications that require the analysis of numerous samples. Liposome solutions were also evaluated using UPLC-ELSD, which showed comparable results to NMR, thereby validating NMR as a viable and efficient alternative for lipid quantification. NMR emerged as a robust, efficient, and reproducible technique, offering significant advantages, including speed of analysis. This approach does not require the construction of calibration curves and relies on a single reference, simplifying the analysis process. It provides a streamlined solution to assess and optimize lipid compositions throughout the manufacturing process.

Next, we demonstrated the preservation of the protein HOS upon erythrocyte encapsulation. The analysis carried out on two enzymes and a carrier protein, different for molecular weight, structure, and function, shows that all the proteins retain their native structural features. This finding is crucial for ensuring stability and biological effectiveness, guiding the optimization of encapsulation protocols. Additionally, a semi-quantitative analysis of ANSII was conducted by comparing the intensity of enzyme signals from a free standard solution with the spectrum of the encapsulated enzyme. This approach has the potential to be applied to other cargos, including small molecules and nucleic acids, allowing for in-situ rapid characterization of complexes typically formed from patient blood through automated dialysis. This study supports the development of red blood cells as novel smart delivery systems and underscores the suitability of NMR to study biologics in complex environments that resemble physiological conditions.

Additionally, this research shed light on the phenomenon of PEG shedding in lipid nanoparticles. Through the refinement of PGSE NMR techniques, the study successfully quantified PEG release under various conditions. Notably, we confirmed that PEG shedding rates vary substantially based on PEGylated lipid chain length, underscoring the necessity for careful consideration in LNP

formulation design to balance circulation stability with effective cellular delivery. We also explored PEG stability under various storage conditions, noting slight PEG shedding at 25°C over a month novel finding that indicates shedding can occur outside serum environments. However, PEG attachment remained stable after freeze-thaw and lyophilization processes. Complementary techniques such as DLS, Nanoparticle Tracking Analysis (NTA), and Cryo-EM were unable to detect PEG release, underscoring NMR unique capability to reliably observe this phenomenon. These insights suggest the necessity of integrating PEG shedding assessments into routine quality control to ensure consistent batch efficacy and stability. Future research should focus on examining various formulation parameters that affect PEG release, including lipid composition and buffer type, under different storage or stress conditions. This will enable us to understand the factors that influence this phenomenon and provide new insights for the rational design of LNP.

Our findings highlighted several strengths of NMR when studying pharmaceutical delivery systems compared to other analytical methods. One major advantage is its atomic resolution, which is essential for obtaining detailed information on specific components within complex formulations. This was evidenced by NMR ability to resolve individual peaks for quantifying each component in liposomes and for the specific analysis of PEG in LNPs. Another key strength is that NMR is a non-destructive technique capable of examining encapsulated cargo under full formulation conditions; it can even mimic the physiological environments in which a biomolecule is meant to function, as demonstrated in our study of enzymes encapsulated in red blood cells. Additionally, the versatility of NMR allows for a comprehensive analysis of diverse delivery systems. The abundance of information that NMR can provide is wide, ranging from the quantitative information on individual components to insights into architecture, structural features, and dynamic aspects related to functional performance, as illustrated by our research. However, it’s always advisable to integrate into the analytical workflow complementary techniques to validate data and address certain intrinsic limitations, such as sensitivity.

Overall, advanced NMR techniques were successfully applied to explore relevant delivery systems in depth, optimizing analytical tools for quality control and enhancing our understanding of their structural and morphological properties. Continuing to enhance NMR methodologies in the future could profoundly shape the rational design and quality control of next-generation delivery systems for biologic drugs.

6 References

1. Vargason, A. M., Anselmo, A. C. & Mitragotri, S. The evolution of commercial drug delivery technologies. *Nature Biomedical Engineering* vol. 5 951–967 Preprint at https://doi.org/10.1038/s41551-021-00698-w (2021).
2. Ezike, T. C. *et al.* Advances in drug delivery systems, challenges and future directions. *Heliyon* vol. 9 Preprint at https://doi.org/10.1016/j.heliyon.2023.e17488 (2023).
3. Ko, H. J. & Kim, Y. J. Antigen Delivery Systems: Past, Present, and Future. *Biomol Ther (Seoul)* 31, 370–387 (2023).
4. Adepu, S. & Ramakrishna, S. Controlled drug delivery systems: Current status and future directions. *Molecules* 26, (2021).
5. Sultana, A., Zare, M., Thomas, V., Kumar, T. S. S. & Ramakrishna, S. Medicine in Drug Discovery Nano-based drug delivery systems : Conventional drug delivery routes , recent developments and future prospects. *Med Drug Discov* 15, 100134 (2022).
6. Losada-Barreiro, S., Celik, S., Sezgin-Bayindir, Z., Bravo-Fernández, S. & Bravo-Díaz, C. Carrier Systems for Advanced Drug Delivery: Improving Drug Solubility/Bioavailability and Administration Routes. *Pharmaceutics* vol. 16 Preprint at https://doi.org/10.3390/pharmaceutics16070852 (2024).
7. Trucillo, P. Drug carriers: Classification, administration, release profiles, and industrial approach. *Processes* vol. 9 Preprint at https://doi.org/10.3390/pr9030470 (2021).
8. Ko, H. J. & Kim, Y. J. Antigen Delivery Systems: Past, Present, and Future. *Biomol Ther (Seoul)* 31, 370–387 (2023).
9. Adepu, S. & Ramakrishna, S. Controlled drug delivery systems: Current status and future directions. *Molecules* 26, (2021).
10. Sultana, A., Zare, M., Thomas, V., Kumar, T. S. S. & Ramakrishna, S. Medicine in Drug Discovery Nano-based drug delivery systems : Conventional drug delivery routes , recent developments and future prospects. *Med Drug Discov* 15, 100134 (2022).
11. Nitish Bhatia, P. M. & S. S. *Characterization Tools for Current Drug Delivery Systems*. vols 978-981-97-2596–0_2 (Springer, Sungapore, 2024).
12. Kulkarni, S., Haghi, A. K. & Manwatkar, S. *Characterization, Restoration and Optimization*.
13. Markova, N. *et al.* Biophysical Characterization of Viral and Lipid-Based Vectors for Vaccines and Therapeutics with Light Scattering and Calorimetric Techniques. *Vaccines (Basel)* 10, (2022).
14. Chiari-, B. G. & Silva, B. L. Physicochemical characterization of drug nanocarriers. 4991–5011 (2017).
15. Ramos, T. I. *et al.* The Hitchhiker ' s Guide to Human Therapeutic Nanoparticle Development. 1–49 (2022).
16. Alshawwa, S. Z., Kassem, A. A., Farid, R. M. & Mostafa, S. K. Nanocarrier Drug Delivery Systems : Characterization , Limitations , Future Perspectives and Implementation of Artificial Intelligence. (2022).
17. Nsairat, H. *et al.* Liposomes: structure, composition, types, and clinical applications. *Heliyon* 8, e09394 (2022).
18. Large, D. E., Abdelmessih, R. G., Fink, E. A. & Auguste, D. T. Liposome composition in drug delivery design, synthesis, characterization, and clinical application. *Adv Drug Deliv Rev* 176, 113851 (2021).
19. Jash, A., Ubeyitogullari, A. & Rizvi, S. S. H. Liposomes for oral delivery of protein and peptide-based therapeutics: challenges, formulation strategies, and advances. *J Mater Chem B* 9, 4773–4792 (2021).
20. Bulbake, U., Doppalapudi, S., Kommineni, N. & Khan, W. Liposomal formulations in clinical use: An updated review. *Pharmaceutics* 9, 1–33 (2017).

21. Sharma, V. K. & Agrawal, M. K. A historical perspective of liposomes-a bio nanomaterial. *Mater Today Proc* 45, 2963–2966 (2021).
22. Sharma, V. K. & Agrawal, M. K. A historical perspective of liposomes-a bio nanomaterial. *Mater Today Proc* 45, 2963–2966 (2021).
23. Nsairat, H. *et al.* Liposomes: structure, composition, types, and clinical applications. *Heliyon* 8, e09394 (2022).
24. Liu, P., Chen, G. & Zhang, J. A Review of Liposomes as a Drug Delivery System : Current. *Molecules* 27, 1372 (2022).
25. Allen, T. M. & Cullis, P. R. Liposomal drug delivery systems: From concept to clinical applications. *Advanced Drug Delivery Reviews* vol. 65 36–48 Preprint at https://doi.org/10.1016/j.addr.2012.09.037 (2013).
26. Agrawal, S. S., Baliga, V. & Londhe, V. Y. Liposomal Formulations: A Recent Update. *Pharmaceutics* 17, 1–24 (2025).
27. Gbian, D. L. & Omri, A. Lipid-Based Drug Delivery Systems for Diseases Managements. *Biomedicines* 10, (2022).
28. Nikolova, M. P., Kumar, E. M. & Chavali, M. S. Updates on Responsive Drug Delivery Based on Liposome Vehicles for Cancer Treatment. *Pharmaceutics* 14, 1–51 (2022).
29. Barenholz, Y. Doxil® - The first FDA-approved nano-drug: Lessons learned. *Journal of Controlled Release* 160, 117–134 (2012).
30. Zhang, K. P., Fang, X., Zhang, Y. & Chao, M. The prognosis of cancer patients undergoing liposomal doxorubicin-based chemotherapy A systematic review and meta-analysis. *Medicine (United States)* 100, E26690 (2021).
31. Rivankar, S. An overview of doxorubicin formulations in cancer therapy. *J Cancer Res Ther* 10, 853–858 (2014).
32. Hamill, R. J. Amphotericin B formulations: A comparative review of efficacy and toxicity. *Drugs* 73, 919–934 (2013).
33. Pemán, J. & Quindós, G. Liposomal amphotericin B: thirty years of a highly effective therapy for the treatment of invasive mycoses. *Rev Iberoam Micol* 38, 39–41 (2021).
34. Herrada, J. *et al.* In vitro and in vivo antifungal activity of ambisome compared to conventional amphotericin B and fluconazole against Candida auris. *Antimicrob Agents Chemother* 65, (2021).
35. Roman, F. *et al.* Adjuvant system AS01: from mode of action to effective vaccines. *Expert Rev Vaccines* 23, 715–729 (2024).
36. Didierlaurent, A. M. *et al.* The Development of the Adjuvant System AS01: A Combination of Two Immunostimulants MPL and QS-21 in Liposomes. *Immunopotentiators in Modern Vaccines: Second Edition* 265–285 (2017) doi:10.1016/B978-0-12-804019-5.00014-1.
37. Syed, Y. Y. RTS,S/AS01 malaria vaccine (Mosquirix®): a profile of its use. *Drugs and Therapy Perspectives* 38, 373–381 (2022).
38. Bergstrand, N., Arfvidsson, M. C., Kim, J. M., Thompson, D. H. & Edwards, K. Interactions between pH-sensitive liposomes and model membranes. *Biophys Chem* 104, 361–379 (2003).
39. Izadiyan, Z. *et al.* Advancements in Liposomal Nanomedicines: Innovative Formulations, Therapeutic Applications, and Future Directions in Precision Medicine. *Int J Nanomedicine* 20, 1213–1262 (2025).
40. Balouch, M., Storchmannová, K., Štěpánek, F. & Berka, K. Computational Prodrug Design Methodology for Liposome Formulability Enhancement of Small-Molecule APIs. *Mol Pharm* 20, 2119–2127 (2023).
41. Akinc, A. *et al.* The Onpattro story and the clinical translation of nanomedicines containing nucleic acid-based drugs. *Nat Nanotechnol* 14, 1084–1087 (2019).
42. Qassem, S., Breier, D., Naidu, G. S., Hazan-Halevy, I. & Peer, D. Unlocking the therapeutic potential of locked nucleic acids through lipid nanoparticle delivery. *Mol Ther Nucleic Acids* 35, 102224 (2024).

43. Hou, X., Zaks, T., Langer, R. & Dong, Y. Lipid nanoparticles for mRNA delivery. *Nat Rev Mater* 6, 1078–1094 (2021).
44. Larson, N. R. *et al.* pH-Dependent Phase Behavior and Stability of Cationic Lipid–mRNA Nanoparticles. *J Pharm Sci* 111, 690–698 (2022).
45. Ickenstein, L. M. & Garidel, P. Lipid-based nanoparticle formulations for small molecules and RNA drugs. *Expert Opin Drug Deliv* 16, 1205–1226 (2019).
46. Waggoner, L. E., Miyasaki, K. F. & Kwon, E. J. Analysis of PEG-lipid anchor length on lipid nanoparticle pharmacokinetics and activity in a mouse model of traumatic brain injury. *Biomater Sci* 11, 4238–4253 (2023).
47. Kumar, V. *et al.* Shielding of lipid nanoparticles for siRNA delivery: Impact on physicochemical properties, cytokine induction, and efficacy. *Mol Ther Nucleic Acids* 3, e210 (2014).
48. Shi, L. *et al.* Effects of polyethylene glycol on the surface of nanoparticles for targeted drug delivery. *Nanoscale* 13, 10748–10764 (2021).
49. Chen, D., Ganesh, S., Wang, W. & Amiji, M. The role of surface chemistry in serum protein corona-mediated cellular delivery and gene silencing with lipid nanoparticles. *Nanoscale* 11, 8760–8775 (2019).
50. Suzuki, T. *et al.* PEG shedding-rate-dependent blood clearance of PEGylated lipid nanoparticles in mice: Faster PEG shedding attenuates anti-PEG IgM production. *Int J Pharm* 588, 119792 (2020).
51. Estapé Senti, M. *et al.* Anti-PEG antibodies compromise the integrity of PEGylated lipid-based nanoparticles via complement. *Journal of Controlled Release* 341, 475–486 (2022).
52. Matthessen, R., Van Pottelberge, R., Goffin, B. & De Winter, G. Impact of mixing and shaking on mRNA-LNP drug product quality characteristics. *Sci Rep* 14, 1–11 (2024).
53. Gallud, A. *et al.* Time evolution of PEG-shedding and serum protein coronation determines the cell uptake kinetics and delivery of lipid nanoparticle formulated mRNA. *bioRxiv* (2021) doi:10.1101/2021.08.20.457104.
54. Gao, W., Langer, R. & Farokhzad, O. C. Poly(ethylene glycol) with observable shedding. *Angewandte Chemie - International Edition* 49, 6567–6571 (2010).
55. Wilson, S. C. *et al.* Real time measurement of PEG shedding from lipid nanoparticles in serum via NMR spectroscopy. *Mol Pharm* 12, 386–392 (2015).
56. Muzykantov, V. R. Drug delivery by red blood cells: Vascular carriers designed by mother nature. *Expert Opin Drug Deliv* 7, 403–427 (2010).
57. Villa, C. H., Anselmo, A. C., Mitragotri, S. & Muzykantov, V. Red blood cells: Supercarriers for drugs, biologicals, and nanoparticles and inspiration for advanced delivery systems. *Adv Drug Deliv Rev* 106, 88–103 (2016).
58. Hou, K. *et al.* A Multifunctional Magnetic Red Blood Cell-Mimetic Micromotor for Drug Delivery and Image-Guided Therapy. *ACS Appl Mater Interfaces* 14, 3825–3837 (2022).
59. Dai, J. *et al.* Red blood cell membrane-camouflaged nanoparticles loaded with AIEgen and Poly(I: C) for enhanced tumoral photodynamic-immunotherapy. *Natl Sci Rev* 8, (2021).
60. Wang, C., Wang, M., Zhang, Y., Jia, H. & Chen, B. Cyclic arginine-glycine-aspartic acid-modified red blood cells for drug delivery: Synthesis and in vitro evaluation. *J Pharm Anal* 12, 324–331 (2022).
61. Zhang, X. *et al.* Engineered red blood cells as an off-the-shelf allogeneic anti-tumor therapeutic. *Nat Commun* 12, 1–14 (2021).
62. Biagiotti, S., Perla, E. & Magnani, M. Drug transport by red blood cells. 1–10 (2023) doi:10.3389/fphys.2023.1308632.
63. Thomas, X. & Le Jeune, C. Erythrocyte Encapsulated L -Asparaginase (Graspa) in Acute Leukemia . *Int J Hematol Oncol* 5, 11–25 (2016).
64. Bax, B. E. Erythrocytes as carriers of therapeutic enzymes. *Pharmaceutics* 12, (2020).

65. Berikkhanova, K. *et al.* Drug-loaded erythrocytes: Modern approaches for advanced drug delivery for clinical use. *Heliyon* 10, e23451 (2024).
66. Lynggaard, L. S. *et al.* Asparaginase encapsulated in erythrocytes as second-line treatment in hypersensitive patients with acute lymphoblastic leukaemia. *Br J Haematol* 197, 745–754 (2022).
67. Koleva, L., Bovt, E., Ataullakhanov, F. & Sinauridze, E. Erythrocytes as carriers: From drug delivery to biosensors. *Pharmaceutics* 12, 1–44 (2020).
68. Bianchi, M. *et al.* Preclinical and clinical developments in enzyme-loaded red blood cells: an update. *Expert Opin Drug Deliv* 20, 921–935 (2023).
69. Shi, J. *et al.* Engineered red blood cells as carriers for systemic delivery of a wide array of functional probes. *Proc Natl Acad Sci U S A* 111, 10131–10136 (2014).
70. Benga, G. & Cox, G. Light and Scanning Electron Microscopy of Red Blood Cells From Humans and Animal Species Providing Insights into Molecular Cell Biology. *Front Physiol* 13, 1–13 (2022).
71. Simmler, C., Napolitano, J. G., McAlpine, J. B., Chen, S. N. & Pauli, G. F. Universal quantitative NMR analysis of complex natural samples. *Current Opinion in Biotechnology* vol. 25 51–59 Preprint at https://doi.org/10.1016/j.copbio.2013.08.004 (2014).
72. Bharti, S. K. & Roy, R. Quantitative 1H NMR spectroscopy. *TrAC - Trends in Analytical Chemistry* vol. 35 5–26 Preprint at https://doi.org/10.1016/j.trac.2012.02.007 (2012).
73. Wong, Y. T. A., Aspers, R. L. E. G., Uusi-Penttilä, M. & Kentgens, A. P. M. Rapid Quantification of Pharmaceuticals via 1H Solid-State NMR Spectroscopy. *Anal Chem* 94, 16667–16674 (2022).
74. Holzgrabe, U. Quantitative NMR spectroscopy in pharmaceutical applications. *Progress in Nuclear Magnetic Resonance Spectroscopy* vol. 57 229–240 Preprint at https://doi.org/10.1016/j.pnmrs.2010.05.001 (2010).
75. Wu, Q., Yuan, H., Zhang, L. & Zhang, Y. Recent advances on multidimensional liquid chromatography-mass spectrometry for proteomics: From qualitative to quantitative analysis-A review. *Analytica Chimica Acta* vol. 731 1–10 Preprint at https://doi.org/10.1016/j.aca.2012.04.010 (2012).
76. Qu, M. *et al.* Qualitative and quantitative characterization of protein biotherapeutics with liquid chromatography mass spectrometry. *Mass Spectrometry Reviews* vol. 36 734–754 Preprint at https://doi.org/10.1002/mas.21500 (2017).
77. Miura, T. *et al.* Collaborative Study to Validate Purity Determination by 1 H Quantitative NMR Spectroscopy by Using Internal Calibration Methodology. 68, 868–878 (2020).
78. Wider, G. & Dreier, L. Measuring protein concentrations by NMR spectroscopy. *J Am Chem Soc* 128, 2571–2576 (2006).
79. Mak, J. Y. W. Pulcon. 75, 160–164 (2022).
80. Singh, S. & Roy, R. The application of absolute quantitative 1H NMR spectroscopy in drug discovery and development. *Expert Opin Drug Discov* 11, 695–706 (2016).
81. Lagerquist, L., Rahkila, J. & Eklund, P. Utilization of 31 P PULCON for Quantitative Hydroxyl Group Determination in Lignin by NMR Spectroscopy. 5–9 (2019) doi:10.1021/acssuschemeng.9b01269.
82. Monakhova, Y. B., Kohl-Himmelseher, M., Kuballa, T. & Lachenmeier, D. W. Determination of the purity of pharmaceutical reference materials by 1H NMR using the standardless PULCON methodology. *J Pharm Biomed Anal* 100, 381–386 (2014).
83. Pauli, G. F., Gödecke, T., Jaki, B. U. & Lankin, D. C. Quantitative 1H NMR. Development and potential of an analytical method: An update. *Journal of Natural Products* vol. 75 834–851 Preprint at https://doi.org/10.1021/np200993k (2012).
84. Mulard, E. D., Gilard, V. & Balayssac, S. Quantitative Nuclear Magnetic Resonance for Small Biological Molecules in Complex Mixtures : Practical Guidelines and Key Considerations for Non-Specialists. 1–21 (2025).

85. Webster, G. K. & Kumar, S. Expanding the analytical toolbox: Pharmaceutical application of quantitative NMR. *Anal Chem* 86, 11474–11480 (2014).
86. Tang, Q. *et al.* Applications of quantitative 13C NMR in pharmaceutical analysis: From small molecule drugs to biopolymers. *J Pharm Anal* 101346 (2025) doi:10.1016/j.jpha.2025.101346.
87. Bingol, K. & Brüschweiler, R. Multidimensional APPROACHES to NMR-based metabolomics. *Analytical Chemistry* vol. 86 47–57 Preprint at https://doi.org/10.1021/ac403520j (2014).
88. Crook, A. A. & Powers, R. Quantitative NMR-Based Biomedical Metabolomics: Current Status and Applications. *Molecules* vol. 25 Preprint at https://doi.org/10.3390/molecules25215128 (2020).
89. Simmler, C., Napolitano, J. G., McAlpine, J. B., Chen, S. N. & Pauli, G. F. Universal quantitative NMR analysis of complex natural samples. *Curr Opin Biotechnol* 25, 51–59 (2014).
90. Giraudeau, P. Quantitative NMR spectroscopy of complex mixtures. *Chemical Communications* 10 doi:10.1039/D3CC01455Jï.
91. Sobolev, A. P., Ingallina, C., Spano, M., Di Matteo, G. & Mannina, L. NMR-Based Approaches in the Study of Foods. *Molecules* vol. 27 Preprint at https://doi.org/10.3390/molecules27227906 (2022).
92. Buya, A. B., Mahlangu, P. & Witika, B. A. From lab to industrial development of lipid nanocarriers using quality by design approach. *Int J Pharm X* 8, 100266 (2024).
93. Alshaer, W. *et al.* Quality by Design Approach in Liposomal Formulations: Robust Product Development. *Molecules* 28, (2023).
94. Giordani, S., Marassi, V., Zattoni, A., Roda, B. & Reschiglian, P. Liposomes characterization for market approval as pharmaceutical products: Analytical methods, guidelines and standardized protocols. *J Pharm Biomed Anal* 236, 115751 (2023).
95. Sercombe, L. *et al.* Advances and challenges of liposome assisted drug delivery. *Front Pharmacol* 6, 1–13 (2015).
96. Fan, Y., Marioli, M. & Zhang, K. Analytical characterization of liposomes and other lipid nanoparticles for drug delivery. *J Pharm Biomed Anal* 192, 113642 (2021).
97. Yan, Q. *et al.* Defining the required critical quality attributes (CQAs) and phase requirements for mRNA/ LNP product development and manufacture. *Biophorum* (2023).
98. Mosca, M., Ceglie, A. & Ambrosone, L. Effect of membrane composition on lipid oxidation in liposomes. *Chem Phys Lipids* 164, 158–165 (2011).
99. Wang, C., Gamage, P. L., Jiang, W. & Mudalige, T. Excipient-related impurities in liposome drug products. *Int J Pharm* 657, 124164 (2024).
100. Zuidam, N. J., Gouw, H. K. M. E., Barenholz, Y. & Crommelin, D. J. A. Physical (in) stability of liposomes upon chemical hydrolysis: the role of lysophospholipids and fatty acids. *BBA - Biomembranes* 1240, 101–110 (1995).
101. Ickenstein, L. M., Sandström, M. C., Mayer, L. D. & Edwards, K. Effects of phospholipid hydrolysis on the aggregate structure in DPPC/DSPE-PEG2000 liposome preparations after gel to liquid crystalline phase transition. *Biochim Biophys Acta Biomembr* 1758, 171–180 (2006).
102. Simmler, C., Napolitano, J. G., McAlpine, J. B., Chen, S. N. & Pauli, G. F. Universal quantitative NMR analysis of complex natural samples. *Curr Opin Biotechnol* 25, 51–59 (2014).
103. Li, M., Xu, W. & Su, Y. Solid-state NMR spectroscopy in pharmaceutical sciences. *TrAC - Trends in Analytical Chemistry* 135, (2021).
104. Malet-Martino, M. & Holzgrabe, U. NMR techniques in biomedical and pharmaceutical analysis. *J Pharm Biomed Anal* 55, 1–15 (2011).
105. Schlattmann, D., Weber, B., Wyszynski, L., Schönhoff, M. & Haas, H. Molecular localization and exchange kinetics in pharmaceutical liposome and mRNA lipoplex nanoparticle products

determined by small angle X-ray scattering and pulsed field gradient NMR diffusion measurements. *European Journal of Pharmaceutics and Biopharmaceutics* 201, (2024).
106. Brecht, V. & Peschka-su, R. Parameters influencing the determination of liposome lamellarity by 31 P-NMR Margret Fro. 109, 103–112 (2001).
107. Franz, A. H., Samoshina, N. M. & Samoshin, V. V. A convenient method for the relative and absolute quantification of lipid components in liposomes by 1H- and 31P NMR-spectroscopy. *Chem Phys Lipids* 261, 105395 (2024).
108. Endo, N., Aoki, C., Sugiki, T. & Sakai-Kato, K. Quantitative lipid composition characterization of intact liposomes via 31P nuclear magnetic resonance spectroscopy. *Analytical Sciences* 40, 871–879 (2024).
109. Farhadi, F. *et al.* Journal of Pharmaceutical and Biomedical Analysis A validated 1 H-NMR method for quantitative analysis of DOTAP lipid in nanoliposomes containing soluble Leishmania antigen. *J Pharm Biomed Anal* 194, 113809 (2021).
110. Cansell, M. *et al.* Phospholipid Profiles of Oleaginous Pressed Cakes Using NMR and Gas Chromatography. *JAOCS, Journal of the American Oil Chemists' Society* 94, 1219–1223 (2017).
111. Shoolery, J. N. A Basic Guide to NMR, 3rd Edition. *Stan's Library* (2008) doi:10.3247/sl2nmr08.012.
112. Schwalbe, H. Applied NMR Spectroscopy for Chemists and Life Scientists. By Oliver Zerbe and Simon Jurt. *Angewandte Chemie International Edition* vol. 53 (2014).
113. Emeline Barbet-Massin and Guido Pintacuda. Biomolecular Solid-State NMR/Basics. (2012).
114. Zheng, Z., Chen, K., Liu, Y., Munson, E. J. & Su, Y. Quantitative Solid-State NMR Spectroscopy (qSSNMR) in Pharmaceutical Analysis. *Magnetic Resonance in Chemistry* Preprint at https://doi.org/10.1002/mrc.5536 (2025).
115. Seifert, A. C., Li, C., Wilhelm, M. J., Wehrli, S. L. & Wehrli, F. W. Towards quantification of myelin by solid-state MRI of the lipid matrix protons. *Neuroimage* 163, 358–367 (2017).
116. Rizzo, D. *et al.* Evaluation of the Higher Order Structure of Biotherapeutics Embedded in Hydrogels for Bioprinting and Drug Release. *Anal Chem* 93, 11208–11214 (2021).
117. Berkowitz, S. A., Engen, J. R., Mazzeo, J. R. & Jones, G. B. Analytical tools for characterizing biopharmaceuticals and the implications for biosimilars. *Nature Reviews Drug Discovery* vol. 11 527–540 Preprint at https://doi.org/10.1038/nrd3746 (2012).
118. Kloczewiak, M., Banks, J. M., Jin, L. & Brader, M. L. A Biopharmaceutical Perspective on Higher-Order Structure and Thermal Stability of mRNA Vaccines. *Mol Pharm* 19, 2022–2031 (2022).
119. Aubin, Y., Jones, C. & All, V. Using NMR Spectroscopy to Obtain the Higher Order *Structure of Biopharmaceutical Products*. https://www.biopharminternational.com/view/ (2010).
120. Wang, D. *et al.* Nmr spectroscopy for protein higher order structure similarity assessment in formulated drug products. *Molecules* 26, (2021).
121. Brinson, R. G. *et al.* Enabling adoption of 2D-NMR for the higher order structure assessment of monoclonal antibody therapeutics. *MAbs* 11, 94–105 (2018).
122. Zubkov, M. *et al.* Physical characterization using diffusion NMR spectroscopy. *Magnetic Resonance in Chemistry* 55, 414–424 (2017).
123. Lindon, J. C., Liu, M. & Nicholson, J. K. Diffusion Coefficient Measurement by High Resolution NMR Spectroscopy: Biochemical and Pharmaceutical Applications. *Rev Anal Chem* 18, 23–66 (1999).
124. Grimaldi, M. *et al.* A New Approach to Supramolecular Structure Determination in Pharmaceutical Preparation of Self-Assembling Peptides: A Case Study of Lanreotide Autogel. *Pharmaceutics* 14, (2022).
125. Monnery, B. D., Jerca, V. V., Hoogenboom, R. & Swift, T. Polymer conformation determination by NMR spectroscopy: comparative diffusion ordered 1H-NMR spectroscopy

of poly(2-ethyl-2-oxazoline)s and poly(ethylene glycol) in D2O. *Polym Chem* 15, 3077–3085 (2024).
126. Ruzicka, E., Pellechia, P. & Benicewicz, B. C. Polymer Molecular Weights via DOSY NMR. *Anal Chem* 95, 7849–7854 (2023).
127. Libánská, A. *et al.* Using surface plasmon resonance, capillary electrophoresis and diffusion-ordered NMR spectroscopy to study drug release kinetics. *Commun Chem* 6, (2023).
128. Doyen, C. *et al.* Nuclear Magnetic Resonance Spectroscopy: A Multifaceted Toolbox to Probe Structure, Dynamics, Interactions, and Real-TimeIn SituRelease Kinetics in Peptide-Liposome Formulations. *Mol Pharm* 18, 2521–2539 (2021).
129. Fiorati, A. *et al.* TEMPO-nanocellulose/Ca2+ hydrogels: Ibuprofen drug diffusion and in vitro cytocompatibility. *Materials* 13, 183 (2020).
130. Canzi, G., Mrse, A. A. & Kubiak, C. P. Diffusion-ordered NMR spectroscopy as a reliable alternative to TEM for determining the size of gold nanoparticles in organic solutions. *Journal of Physical Chemistry C* 115, 7972–7978 (2011).
131. Valentini, M. *et al.* Diffusion NMR Spectroscopy for the Characterization of the Size and Interactions of Colloidal Matter: The Case of Vesicles and Nanoparticles. *J Am Chem Soc* 126, 2142–2147 (2004).
132. Patil, S. M., Keire, D. A. & Chen, K. Comparison of NMR and Dynamic Light Scattering for Measuring Diffusion Coefficients of Formulated Insulin: Implications for Particle Size Distribution Measurements in Drug Products. *AAPS Journal* 19, 1760–1766 (2017).
133. Schlattmann, D., Weber, B., Wyszynski, L., Schönhoff, M. & Haas, H. Molecular localization and exchange kinetics in pharmaceutical liposome and mRNA lipoplex nanoparticle products determined by small angle X-ray scattering and pulsed field gradient NMR diffusion measurements. *European Journal of Pharmaceutics and Biopharmaceutics* 201, (2024).
134. Demco, D. E. & Pich, A. Structure and Dynamics of Temperature-Responsive Microgels and Hydrogels by NMR Spectroscopy, Relaxometry, and Diffusometry. *Macromolecular Chemistry and Physics* vol. 224 Preprint at https://doi.org/10.1002/macp.202200410 (2023).
135. Rothbauer, G. A. *et al.* Nuclear Magnetic Resonance Investigation of the Effect of pH on Micelle Formation by the Amino Acid-Based Surfactant Undecyl l-Phenylalaninate. *J Surfactants Deterg* 21, 139–153 (2018).
136. Sabatino, P. *et al.* NMR study of the influence of pH on phenol sorption in cationic CTAB micellar solutions. *Colloids Surf A Physicochem Eng Asp* 370, 42–48 (2010).

7 Ringraziamenti

E’ stato un percorso tosto, che mi ha messo di più alla prova in tutta la mia carriera da studente e lavoratore, ma che per questo è stato anche il più gratificante. Ho raggiunto tanti traguardi e la crescita professionale e umana è stata esponenziale. Dato che per l’appunto considero questi 3 anni non solo come il tempo necessario per il raggiungimento del titolo ma nella loro interezza di periodo di vita vissuta, sono state tante le persone che hanno avuto un ruolo significativo e che colgo l’occasione per ringraziare.

In primis devo partire da Maxime che ha preso sotto la sua ala dal primo giorno di dottorato il ragazzo timido e impacciato con la mano che tremava in laboratorio e lo ha accompagnato ogni giorno in un processo costante di miglioramento, puntando sempre a non accontentarsi e a essere minuzioso e accurato in ogni cosa. Non mi hai mai fatto sentire solo, ma anzi, in ogni passo mi sono sempre potuto appoggiare alla tua guida che è la migliore che potessi desiderare. Poi devo dire un enorme grazie a Linda e Silvia che indubbiamente sono state le migliori maestre di NMR possibili e che mi hanno anche sempre fatto sentire in un’ambiente amico. Avete infatti accompagnato i miei primi passi al CERM e GSK rispettivamente, due posti che mi spaventavano per il livello scientifico altisonante, di cui temevo di non essere all’altezza, ma a cui voi mi avete introdotto con gentilezza e premura. Ringrazio poi Daniela, Marco e Massimiliano che mi hanno permesso di lavorare in modo mirato verso gli obiettivi, non facendomi mai mancare nulla. In particolare Daniela, per essersi impegnata in modo sostanziale a portare il mio lavoro a un livello superiore, attraverso visibilità, risorse e direzione scientifica; Marco per essere sempre stato estremamente pragmatico, sbrogliando dinamiche complesse, mettendo al primo posto il bene per me e Massimiliano, che mi ha scelto per la prima volta, senza il quale questo percorso splendido non sarebbe mai iniziato, e che c’è sempre stato per accompagnarmi al traguardo in maniera sicura.

Infine un enorme grazie a tutti i membri dei team di BPS e Physico-Chem a GSK Siena, Size&Morphology in GSK Belgio e al gruppo di ricerca del prof. Fragai per avermi accolto insieme a voi, dove ho conosciuto persone meravigliose e scienziati eccellenti (+ menzione d’onore per il prof. Lelli e il suo supporto nelle 2 settimane in Svizzera).

Transitiamo progressivamente verso la vita fuori dal lavoro, ma rimanendo dentro all’ambiente lavorativo, ringraziando tutta la cerchia di amici di GSK e affiliati per aver ricreato nei pranzi a mensa quella pausa dolce da ricreazione a scuola e naturalmente per tutte le “grandi opportunità” che abbiamo condiviso in azienda, ma soprattutto anche per il tempo fuori, che ha permesso di staccare dalle fatiche del dottorato, godendosi la più piacevole delle compagnie. Menziono in particolare il Francesco che mi ha preceduto, il number 1, che oltre a motivo di confusione per tutti i colleghi per

gli ovvi motivi, è stato come un fratello maggiore durante il percorso, “absolutely” garanzia di risate costanti, ma anche capace di una parola di conforto nel momento del bisogno.
Poi naturalmente c’è Marta, che mi ha conosciuto all’inizio di questo percorso, che non ha mai capito bene esattamente cosa stessi facendo a livello scientifico, ma che sono sicuro abbia capito tante cose su di me. Mi hai fatto crescere tanto durante questo lasso di tempo, condividendo la quotidianità di questo percorso e bellissime esperienze. Meglio di tutti sai quanto sono pigro e quanta fatica facessi la mattina a venire tutti i giorni a lavoro, grazie per avermi svegliato, letteralmente e in senso figurato.

Rimaniamo a Siena, ma usciamo dal lavoro, ci trasferiamo a casa dalla mia famiglia acquisita in via dei Rossi. Lorenzino, il mio bro, che è arrivato in concomitanza all’inizio di questo percorso e mi ha fatto provare come è avere il fratellino che non ho mai avuto. Grazie per tutte le risate che ci siamo fatti, la tua saggezza da giovane vecchio e va detto, anche per avermi sempre fatto trovare un ambiente confortevole al ritorno da lavoro, senza di te la casa non sarebbe sopravvissuta a questi anni di dottorato. Ora aspetto il tuo momento il prossimo anno, mi raccomando. Grazie anche ai dirimpettai Giuseppe e Francesco, per aver costruito insieme questo senso di famiglia allargata, che trova il momento di massima espressione nell’impazzimento davanti le partite. Peppino, continua a cucinare i tuoi manicaretti e quello che sappiamo noi, pentola sempre accesa.

Passiamo poi invece al “vecchio”, alle persone che ci sono da prima che questo percorso iniziasse, e che mi fanno pensare da tempo di essere realizzato nell’amicizia, di non poter chiedere di più: gli SBIRULONI. Siete una costante da tanti anni, il rifugio sicuro quando serve supporto e i primi destinatari di qualsiasi stupidaggine passi per la mente. In rigoroso ordine alfabetico, altrimenti vi offendete: Alessio che è il primo per lettera ma il primo in senso assoluto, dal primo giorno delle medie, semplicemente una garanzia, ci siamo plasmati l’un l’altro, sai già tutto. Giovanni, comandante nerazzurro, nonostante stiamo riuscendo a vederci meno ultimamente, so sempre di poter contare sulla tua sensibilità. Leonardo, quanti ricordi insieme, quante avventure terribili e per questo favolose, continuiamo a scrivere la Storia tra una riflessione antropologica e l’altra. Lorenzo o dovrei dire Parenzo o forse Dylan, da coinquilino senese a punto di riferimento dei weekend viterbesi, quante battute insieme che è meglio non riportare… ma anche un’altra persona con cui so di potermi confidare. Mario, il GOAT della viterbesità, semplicemente la mascotte di Sbirulandia, nonché dotato di grande vena attoriale. Pierluigi, il CEO del milanismo, dei fornelli e del drip, semplicemente l’essere perfetto. Tyson, il più puro, la persona su cui puoi sempre fare affidamento, la spalla su cui piangere, lo sbirulone con il quale gasarsi.

Infine, il ringraziamento più sentito a mamma e papà per avermi reso la persona che sono e indicato con il vostro esempio la strada da seguire. Grazie per avermi sempre supportato nelle scelte e fornito gli strumenti per raggiungere i miei obiettivi. So di poter contare sempre su di voi.

Francesco